Bio-inspired polydopamine-hybrid-films for the self-regulatory photocatalytic water splitting

Master Thesis

For obtaining the academic degree

Master of Science (M.Sc.)

Submitted in January 2020

by

Marcel Boecker

Faculty of Chemistry, Pharmaceutical Science, Geography and Geosciences

of the

Johannes Gutenberg University Mainz

Max-Planck-Institute for Polymer Research Mainz

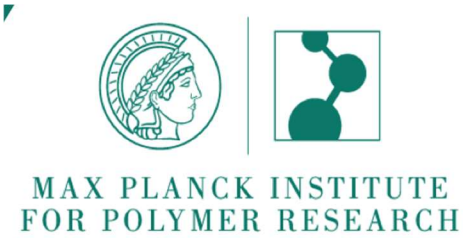

1. Reviewer: Prof. Dr. Tanja Weil

2. Reviewer: Prof. Dr. Holger Frey

Projectleader: Katrin Wunderlich

Supervisor: Tommaso Marchesi D'Alvise

Ich, Marcel Boecker, Matrikelnummer 2706675 versichere, dass ich meine Masterarbeit selbstständig verfasst und keine anderen als die angegebenen schriftlichen und elektronischen Quellen sowie andere Hilfsmittel benutzt habe. Alle Ausführungen, die anderen Schriften wörtlich oder sinngemäß entnommen wurden, habe ich kenntlich gemacht.

I, Marcel Boecker, matriculation number 2706675, assure that I wrote my master's thesis independently and that I did not use any other written and electronic sources other than those specified, as well as other aids. I have made all statements that have been taken literally or analogously from other writings.

_____ _____

(Place, Date) (Signature)

Acknowledgment

First of all, I would like to thank Prof. Dr. Tanja Weil from the Max Planck Institute for Polymer Research for the opportunity to do my master's thesis in her group, as well as for her expertise and suggestions during the group meetings. I also thank Dr. Katrin Wunderlich for her support and guidance in this work. I would also like to thank Tommaso Marchesi and Sean Harvey for the knowledge they conveyed, technical advice, constructive discussions and the good working atmosphere. I would also like to thank Tilmann Herberger, Julia and Ahmed for the great atmosphere in the lab and the interesting discussions. I would also like to thank all of the MPIP technicians and employees for the training to operate several instruments, as well as for various measurements without this work would not have been possible. Not to forget all of the MPIP colleagues for informative discussions and the general good working atmosphere at the institute. I would also like to thank the cooperation partners Maria Wächtler from the Leibniz Institute of photonic technology, Alexander Mengele from the University of Ulm and Christof Neumann from the University of Jena for the good cooperation. Finally, I would like to thank my family for all the support and motivation that went beyond this work.

Zusammenfassung

Diese Arbeit ist Teil eines Projekts zur Wasserspaltung an photokatalytisch aktiven Filmen in Zusammenarbeit mit Dr. Maria Wächtler (Leibniz-Institut für Photonische Technologien, Jena), CATALIGHT (Projekt der Universitäten Jena und Ulm) und AK Weil (MPIP Mainz). Die Wasserspaltung gewinnt in Zeiten des Klimawandels und der daraus folgenden Bedeutung von Erneuerbarenenergie, sowie Möglichkeiten diese effektiv speichern zu können, immer mehr an Bedeutung. In dieser Arbeit wurden die Grundlagen für den Aufbau eines solchen Systems untersucht. Hierfür wurde zum einen die mögliche kovalente Anbindung eines Katalysators an einen ultradünnen Polydopaminfilm untersucht. Die Anbindung des Katalysators erfolgte mittels Michael-Addition und Schiffsche Basen Reaktion. Die optimale Aufarbeitung wurde mittels MALDI-Imaging untersucht. Mittels ToF-SIMS konnte die homogene Verteilung des Katalysators und der Einfluss der Aufarbeitung überprüft werden. Die kovalente Anbindung des Katalysators wurde mittels XPS Messungen bestätigt. Außerdem konnte über die Reduktion von Nicotinamidadenindinukleotid die katalytische Aktivität des gebundenen Katalysators am Polydopaminfilm nachgewiesen werden.

Zur Untersuchung des gesamten Systems, bestehend aus CdSe/CdS Nanorods als Lichtsammelsystem, Polydopamin und eines Katalysators, wurden die Nanorods mit Polydopamin durch die Selbstoxidation von Dopamin im Basischen ummantelt. In einem weiteren Schritt wurden die ummantelten Nanorods mit dem Katalysator funktionalisiert. Die Funktionalisierung der Partikel erfolgte auf gleiche Weise wie die Funktionalisierung der Polydopaminfilme. Für eine bessere Stabilität in Lösung musste das System zusätzlich mit Polyethylenglykol funktionalisiert werden. Mittels Absorptionsmessungen wurde der Einfluss des Polydopamins auf die Lichtsammeleigenschaften des Systems untersucht. Des Weiteren wurde mit verschiedensten Methoden (DLS, TEM, EDX und DOSY) versucht den genauen Aufbau des Systems zu charakterisieren. Außerdem wurde auch für das System in Lösung die katalytische Aktivität durch die Reduktion von Nicotinamidadenindinukleotid durch thermische und photokatalytische Reduktion überprüft. Hierdurch konnte das grundlegende Konzept des System, die Verwendung der erzeugten Photoelektronen für eine nachfolgende Katalyse, bewiesen werden. Abschließend wurde der Einfluss der Nanorods auf den Photostrom des Systems untersucht.

Abstract

This work is part of a project on water splitting on photocatalytically active films in collaboration with Dr. Maria Wächtler (Leibniz Institute for Photonic Technologies, Jena), CATALIGHT (project of the universities of Jena and Ulm) and AK Weil (MPIP Mainz). Water splitting is becoming increasingly important in times of climate change and the resulting importance of renewable energy, as well as ways to store it effectively. In this work the basics for the construction of such a water splitting system were examined. For this, the possible covalent connection of a catalyst to an ultra-thin polydopamine film was examined. The catalyst was connected by means of Michael addition and Schiff base reaction. The optimal processing was examined using MALDI imaging. ToF-SIMS was used to check the homogeneous distribution of the catalyst and the influence of the workup. The covalent connection of the catalyst was confirmed by XPS measurements. In addition, the reduction of nicotinamide adenine dinucleotide was able to demonstrate the catalytic activity of the bound catalyst on the polydopamine film.

To investigate the entire system, consisting of CdSe/CdS nanorods as a light collection system, polydopamine and a catalyst, the nanorods were coated with polydopamine through the self-oxidation of dopamine in the basic. In a further step, the coated nanorods were functionalized with the catalyst. The particles were functionalized in the same way as the functionalization of the polydopamine films. For better stability in solution, the system also had to be functionalized with polyethylene glycol. The influence of polydopamine on the light collection properties of the system was examined by means of absorption measurements. Furthermore, various methods (DLS, TEM, EDX and DOSY) were used to try to characterize the exact structure of the system. In addition, the catalytic activity was checked for the system in solution by the reduction of nicotinamide adenine dinucleotide by thermal and photocatalytic reduction. This proved the basic concept of the system, the use of the generated photoelectrons for subsequent catalysis. Finally, the influence of the nanorods on the photocurrent of the system was examined.

Table of Contents

1. Motivation

Due to climate change, green energies that do not require fossil fuels and therefore do not generate harmful emissions are becoming increasingly important. Hydrogen has been shown to be a good alternative to fossil fuels acting as a chemical energy storage. Because of its high fuel value ($H_2 + 0.5\ O_2 \rightarrow H_2O + 56.7\ \mathrm{kcal/mol}$)[1] and its non-harmful and emission-free combustion product, water, which is also the raw material for the production. Electricity can thus be obtained relatively easily using a reagent that is available in large quantities all over the world. Since electricity is still being produced in large quantities from non-renewable energies and is therefore not "green", the hydrogen obtained from this electricity is also not emission-free. To solve this problem, a system should be developed that enables hydrogen to be obtained directly from sunlight since it is also available all over the world. CdSe/Cds core shell rods are a good choice as light collectors, since they show a strong photo response across the entire visible light spectrum. In addition, the rod shape and the combination of CdSe with CdS improve the charge separation after the excitation, which means that the photoelectrons generated can be made available more easily for water splitting. Furthermore, the combination of CdS with polydopamine (PDA) has shown that PDA improves charge separation due to the fact that it can act as an electron donor.[2] It was also possible to pass the free electrons from the CdS core through the PDA shell to another semiconductor.[2] Furthermore, due to its optical properties, PDA should expand the accesible wavelength range. In the conceived system, instead of another semiconductor, a catalyst (shown in theory) is to be used which, for reasons of simpler detection, is initially suitable for NADH production by reducing NAD^+. The catalytically active center of the catalyst shown (RhCp) can also be used for hydrogen generation, however the effectiveness of Pt-based catalysts is higher, which is why it should be switched to such a catalyst for hydrogen production.

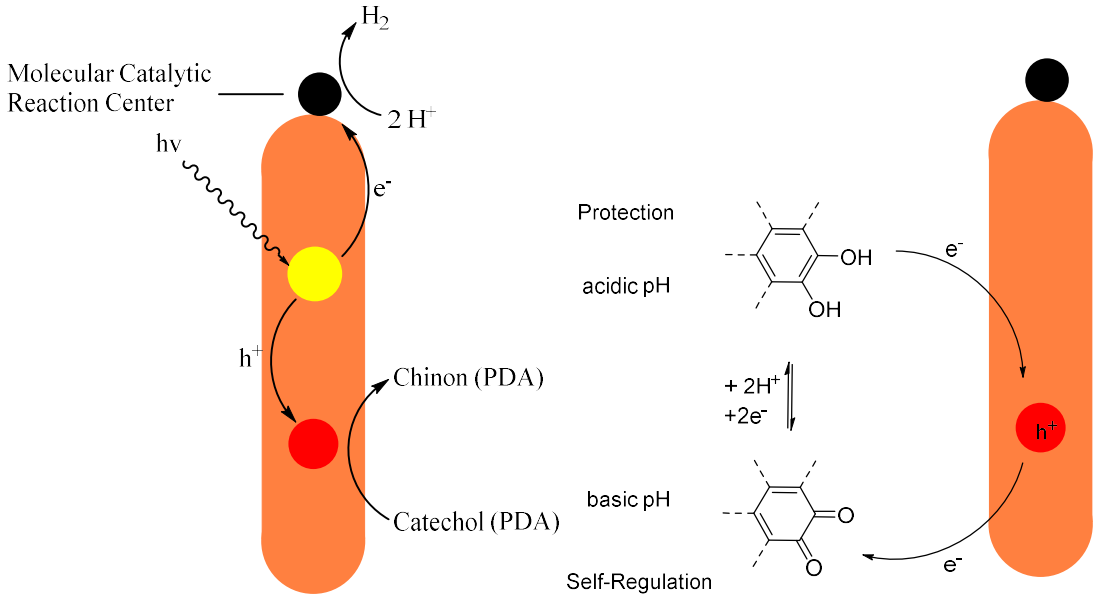

Figure 1: Scheme of the conceived model system for hydrogen production with postulated reaction scheme for hydrogen generation (left) and self-regulation or protection by PDA for the system (right).

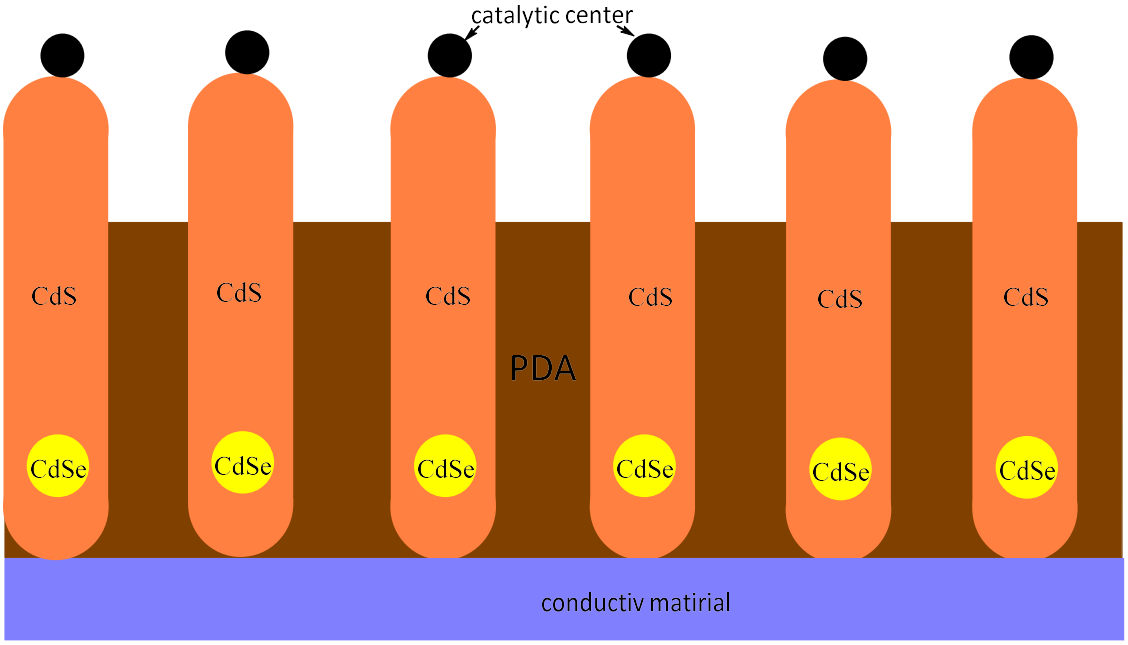

Figure 2: Scheme of the final system as film with vertically arranged nanorods embedded in a PDA film

The final system should consist of a film of vertical nanorods that are stabilized by a PDA film and a catalytically active center at the top. The PDA should not only enable better charge separation within the nanorods, but also prevent photo corrosion. For a precise control of the thickness of the PDA film the PDA is synthesized via electropolymerization. Due to the possibility to switch between the functional groups (catechol and quinone) in the PDA by adjusting the pH, self-regulation of the system or protection against photo corrosion is possible. Since there are more quinone groups at basic pH, the absorption of two photoelectrons can result in a reduction to catechol, which would lead to lower hydrogen production and thus corresponds to a self-regulation of the system. In the acidic environment, on the other hand, there are more catechol groups, these can oxidize to quinones and the electrons released can be transferred to the nanorods and quench the holes there, thus preventing photo corrosion. These expected electron and hole transfer mechanisms can be investigated using time-resolved spectroscopic methods (photoluminescence, transient absorption). For this, however, suitable samples are required, which allow by their optical density to be checked and adapted to the respective experiment and the pH value to be checked in a simple manner. A suitable approach for this is provided by corresponding CdSe@CdS nanorods with a thin polydopamine shell, which can be dispersed in buffer solutions with varying pH values. Therefore, the nanorods will be coated by the self-polymerization of dopamine in basic pH.

2. Introduction

This chapter first looks at the properties of polydopamine and its synthesis. The following explains the basics of cyclic voltammetry, which can be used on the one hand for the synthesis of polydopamine, and for the measurement of the photocurrent. Thereafter, catalysts for the final water splitting as well as catalysts for the reduction of nicotinamide adenine dinucleotide used in this work will be discussed. Then CdSe/CdS core shell nanorods are considered as a light harvesting system. Finally, the basics of the various analysis methods are explained.

2.1.Polydopamine

2.1.1. Structure and synthesis of polydopamine

Polydopamine (PDA) is obtained through the polymerization of dopamine and was inspired by the by adhesive properties of mussels[3]. It is believed that the adhesive properties of mussels come from the catechol and amino group of the side chain of the mussel foot protein.[3] Both functional groups are found in dopamine. Furthermore, PDA can be synthesized through self-polymerization of dopamine under marine conditions.[4] Therefore, alkaline conditions (pH > 7.5) with oxygen as oxidant are needed.[5] It is also possible to do the synthesis in acidic pH using ammonium persulfate ($(NH_4)_2S_2O_8$), Sodium periodate or potassium chlorate as oxidant.[6] Despite the simplicity of synthesis, the mechanism and structure of PDA is complicated.

During the polymerization, dopamine is first oxidized to dopamine quinone followed by the cyclization to leucodopaminechrome. A second oxidation leads to dopamine chrome, which rearranges to 5,6-dihydroxyindol (DHI). This is also used in literature as monomer for PDA synthesis.[7] For the structure of PDA different models were postulated. In 2007 Messersmith described PDA as Eumelanin like.[8] Also, aggregation mainly of DHI through charge-transfer, $\pi - \pi$ stacking and hydrogen bonds was suggested.[7] Five years later two different studies suggested that PDA is a supramolecular aggregate of monomers and non-bound trimers consisting of two dopamine and one DHI unit.[8] The trimer with its ratio of 2:1 dopamine to DHI was proved by ^{1}H-NMR.[9] Also, high-performance liquid chromatography-mass spectrometry (HPLC-MS) experiments support this.[10] Further investigations lead to the conclusion that PDA has three main structures. A non-cyclic amine component, a typical eumelanin indole (cyclized component) and pyrrolcarboxylic acid units, deriving from the oxidative breakdown of indole units.[7,8] ^{13}C and ^{15}N NMR measurements showed the presence of indole and non-cyclic components but the ratio of them depends on the synthesis conditions. With low dopamine concentration, a higher ratio of indole is obtained.[10,11] On the other hand a high dopamine concentration lead to higher amount of non-cyclic units.[10] If Tris-buffer (2-Amino-2-(hydroxymethyl)propan-1,3-diol) is used as a solvents, it is included in the PDA structure.[7,8] In summary, PDA is a mixture of oligomers of indole units with different saturation and dopamine, which generate charge transfer interactions between *O*-quinone and catechol.[8] But the main structure does not result from indole oligomers and calculations have shown that smaller oligomers are favored.[7] Following is the reaction scheme for the synthesis of polydopamine starting from dopamine via DHI and the subsequent proposed polymerization, as well as self-assembly shown.

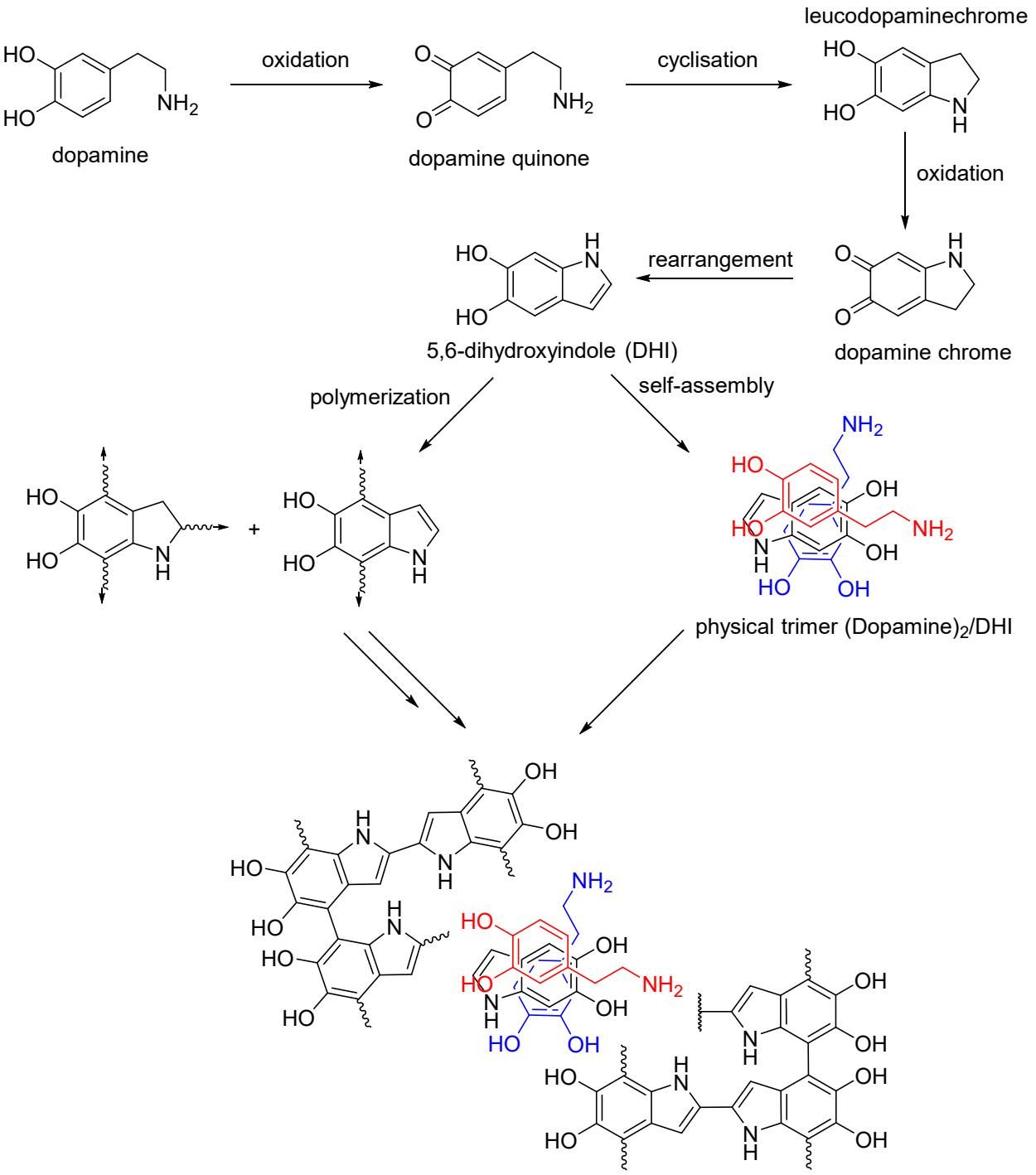

Figure 3: Self-polymerization of PDA. Adapted from [5,12].

2.1.2. Properties of polydopamine

First, the adhesive properties of PDA must be mentioned. Inspired by the mussel foot protein PDA can adhere to almost all surfaces, including noble metals (Au, Ag, Pt, Pd), metals (Cu, stainless steel), metal oxides (TiO_2, SiO_2 (crystal and amorphous), Al_2O_3), semiconductors (GaAs, Si_3N_4), ceramics (glass, hydroxyapatite) and polymers (PS, PE, PC, PET, PTFE, PDMS, PEEK).[4] However, the exact mechanism remains unclear and also depends on the surface properties of the respective substrate and can therefore be differentiated into two types: covalent binding and non-covalent binding.[5] The non-

covalent binding results from hydrogen bonding, $\pi - \pi$ stacking, charge transfer and chelating effects. Through Michael addition or Schiff base reaction PDA can covalently bind to amino or thiol groups.[5] Due to these coating properties and the biocompatibility, PDA is used as a coating for ceramics for implants and PE or PTFE, which has resulted in a reduction in cytotoxicity.[13] Although the adhesive properties are well known and used for coating various materials, there have been few studies regarding the stability of the resulting films. In one of those studies (Yang et al.)[14] it has been shown that PDA films on gold, which were synthesized by dip-coating and investigated by surface plasmon resonance imaging, are stable both in water in the pH range from 4 to 11 and in most organic solvents tested. The organic solvents that were tested are *n*-hexane, toluene, ethyl ether, tetrahydrofuran (THF), ethyl acetate, isopropanol, acetone, acetonitrile, dimethylformamide (DMF) and dimethyl sulfoxide (DMSO). The detachment ratio was below 15 % for all solvents except DMF (31 %) and DMSO (56 %).[14]

As mentioned before, PDA can chelate metals, which group (*o*-quinone, carboxy, amino, imine or phenol) chelates depends on the pH value.[5] Under basic conditions, PDA is not only able to chelate metals, but also to reduce noble metal salts (Au^{3+}, Ag^{+} and Pt^{3+}).[5] This property results from the redox character of the monomer.[5] It is also possible to functionalize PDA through chemical reactions such as Michael addition and Schiff base reaction with amino or thiol groups. This is possible due to the pH dependency of the catechol and quinone groups of PDA. The advantage over other coupling reagents is that the functionalization does not require harsh conditions. It can be carried out at room temperature and in water under basic pH, because under this condition the catechol group can be oxidized into the quinone group which is susceptible to nucleophilic attack. Functionalization via the amine or imine group is also possible. The amine can react with carbonyl chloride and the imine with carboxyl groups, which would, however, require organic solvents or high temperatures and vacuum.[5]

Not only does the structure of PDA resemble the structure of Eumelanin, the optical properties of PDA are also similar to those of Eumelanin. Eumelanin is a natural pigment that shows a broad absorption range from ultraviolet to the visible region. Those absorption properties can be interpreted as true absorption and more than 99 % of the absorbed energy is transformed in heat nonradiatively. Because of these properties eumelanin is the natural photoprotective agent which protect humans and animals from ultraviolet injuries.[5] The absorption increases exponentially towards the UV range. Because there is no distinct chromophoric band, like melanin (eumelanin) it is believed that PDA is a disordered organic semiconductor. Due to the absorption properties in the UV range, it is assumed that PDA can act as a photoprotective agent, but this has not yet been systematically investigated. What is also surprising is that PDA shows also fluorescence if it is excited by UV light with a fluorescence peak between 400 and 500 nm. The emission depends on the excitation wavelength used.[5]

Because of the similarity to natural melanin, biocompatibility is assumed for polydopamine, as already mentioned, but this has not yet been proven by studies. However, initial studies support this assumption, even if these tests were only carried out with isolated cells. The control group also showed no differences in in vivo experiments with animals. In addition, almost complete degradation was found after 8 weeks, even if the exact mechanism is unclear, it is assumed that the degradation takes place via an active oxygen species, such as H_2O_2. Degradation of the polydopamine by microorganisms was also observed. Another study suggests that polydopamine can reduce toxicity of coated materials, in the case of cadmium selenide quantum dots.[5] These quantum dots are well-known for their high quantum yields but can release the hazardous Cd^{+} and Se^{+} ions from the surface of the quantum dots and therefore show in vitro and in vivo toxicity. When coming in contact with blood plasma they can

trigger symptoms of pulmonary vascular thrombosis. In experiments with Balb/C mice the non-coated quantum dots showed after 4h of injection a serious distortion effect on the lymphocyte population which is not the case for the polydopamine-coated ones. Also, the neutrophil levels, which is an important immune response indicator, were nearly equal to the control group. These results are in contrast to those of the pure cadmium selenide quantum dots.[5]

2.2.Cyclic voltammetry

Cyclic voltammetry (CV), is an electrochemical method, that provides access to thermodynamic and kinetic information of redox and coupled chemical reactions.[15] Also, this method can be used for the controlled synthesis of polydopamine.[16] First of all, the difference between chemical and electrochemical redox processes should be mentioned, with only the reduction considered below for the sake of simplicity.

The chemical reduction is performed on the basis that the lowest occupied molecular orbital (LUMO) of the species to be reduced (acceptor) is lower than the highest occupied molecular orbital (HOMO) of the donor. For this reason, the electron transfer is thermodynamically favored, and the driving force of the reaction is the energy difference between the LUMO of the acceptor and the HOMO of the donor.[17] Electrochemical reduction by heterogeneous electron transfer involves the reaction between the electrochemically active species and an electrode. An electrode is an electrical conductor, typically made of platinum, gold or glassy carbon.[17] Through an external energy source (typically a potentiostat), a voltage can be applied to the electrode. Through the applied voltage the energy of the electrode electrons can be modulated. If the energy level of the electrons in the electrode is higher than the LUMO of the electrochemically active species, electron transfer from the electrode to the electrochemically active species occurs. Also, in this reaction, the energy difference is the driving force. However, the driving force in an electrochemical reaction is much easier to control, since this is done by applying the voltage.[17]

Since electrochemical reactions take place in CV, accordingly, an electrode on which the electrochemical reaction takes place is required. This electrode is called the working electrode (WE).[18] This stationary electrode rests in a quiescent electrolyte solution and is forced on a time-varying potential until the reversal potential is reached.[15] The change in the potential per unit time is called the scan rate or feed rate. This can also be used to set the time scale of the experiment. Since it is not possible to measure absolute single electrode potentials, a non-polarized reference electrode (RE) is needed, to which the WE potential is related.[15] As RE, a saturated calomel electrode or a silver/silver chloride electrode is typically used. For very small currents and high conductivity of the electrolyte solution, this two-electrode configuration would be sufficient.[15] Since the RE can be destroyed at high currents, however, the three-electrode arrangement is recommended. In this case, the current is passed through the WE and a counter electrode (CE). The RE remains de-energized due to its high impedance.[15] However, the RE should be placed as close to the WE as possible to minimize the ohmic voltage drop.[15,17,19]

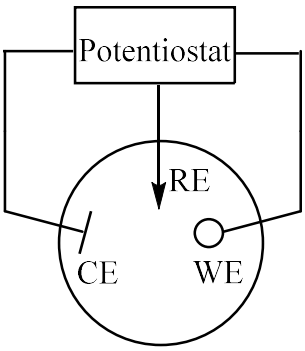

Figure 4: Schematic representation of the three-electrode arrangement adapted from [15].

The vessel in which the electrochemical reaction is carried out is called the electrochemical cell and is filled with the electrolyte solution and the electrochemically active species. The electrolytic solution serves to balance the charge generated by the electron transfer by ion movement.[17] The electrolyte solution is composed of a solvent and a dissolved salt (supporting electrolyte) which lowers the resistance of the solvent. The supporting electrolyte must be chemically and electrochemically inert under the experimental conditions.[17] In addition, depending on the solvent and the experimental conditions, the electrolyte solution should be cleaned of impurities. In aqueous systems, it is usually sufficient to remove the oxygen present in solution, since it can be reduced between -0.2 V and -0.8 V.[15]

In the following, heterogeneous electron transfer in cyclic voltammetry is discussed. It is the simplest Faraday electrode reaction that involves heterogeneous electron transfer from the electrochemically active species to the electrode or vice versa. For this purpose, a voltage is applied to the WE and this is changed at the specified feed rate v up to a specified limit, the so-called reversal potential. After reaching the reversal potential, the voltage is scanned in the opposite direction either to the start potential or to a second reversal potential.

The measured current is plotted as a function of the voltage.[19] It should be noted that there are two conventions for the representation of the cyclic voltammograms. According to the IUPAC convention, low to high potentials are applied, resulting in positive currents being measured on oxidation and negative currents on reduction.[17] The detected current is dependent on two steps, one of the electron transfer reaction and the other of mass transport, i.e. the movement of the electroactive species to the electrode surface.[19] Mass transport is determined by migration, diffusion and flow transport.[17] All theoretical approaches for cyclic voltammetry are only related to diffusion as mass transport. For this reason, a quiescent electrolyte solution (no flow transport) and a high concentration of electrolyte is used. The high electrolyte concentration decreases the probability that a molecule of the electrochemically active species will move to the CE for charge balancing, thus avoiding mass transport due to migration.[17]

Mass transport is given by equation (1).[20]

$$m = \sqrt{\frac{\pi n F D v}{RT}} \quad \textbf{(1)}$$

n – number of electrons

F – Faraday constant

D- Diffusions coefficient

v – scan rate

R – Gas constant

T – absolute temperature

If the mass transport is much smaller than the electron transfer rate, it is a reversible process. The electron transfer rate can be calculated by equation (2).[20]

$$k_{\mathrm{red}} = k_0 \cdot e^{\left(-\frac{\alpha \cdot n \cdot F\,(E-E^0)}{RT}\right)} \quad \textbf{(2)}$$

α – Transfer coefficient

E^0 - Standardpotential

It can be seen from the equation for the electron transfer rate that it is exponentially dependent on the applied potential E. Thus, one would expect that in a cyclic voltammogram the current also increases exponentially with the potential. However, this is not true for the reversible case. Due to the slower mass transport, the reaction is diffusion-controlled, which means that at the beginning of the reaction there is a high concentration of the electrochemically active species on the electrode surface. With increasing reaction time, this concentration continues to decrease and there is an ever-growing depletion zone. Thus, molecules of the electrochemically active species take longer and longer to reach the electrode surface, and this leads to a decrease in the measured current.[19] Due to the dependence on mass transport, the process is a dynamic equilibrium at the phase boundary (electrode / electrolyte solution).[15] For this reason, the calculation of the electrode potential can be calculated using the Nernst equation.[15]

$$E = E^{0\prime} - \frac{RT}{nF} \cdot \ln\left(\frac{[Red]}{[Ox]}\right) \quad \textbf{(3)}$$

$E^{0\prime}$ is the formal potential that is used instead of the standard potential if the activities of the species used are too complex or unknown.[18] It thus means that the effect of free energy of the reactants and products expressed by activities has been combined with the thermodynamic potential to obtain a measurable but solvent dependent term. For this reason, also in Equation (3), concentrations are used instead of activities of the products and starting materials.[19]

The standard potential E^0 characterizes the state of the thermodynamic equilibrium, where the concentration of the oxidized and the reduced form of the electrochemically active species is the same.[15] Thus, the standard potential can be calculated from the peak potentials using equation (4).[20]

$$E^0 = \frac{\left(E_{P,anodic} + E_{P,kathodic}\right)}{2} \quad \textbf{(4)}$$

There are three indications if cyclic voltammetry is reversible. First, the current of both peaks is the same.[20]

$$\frac{I_{P,Red}}{I_{P,Ox}} = 1 \quad \textbf{(5)}$$

Furthermore, the peak current according to the Randless-Sevcik equation (equation (6)) is proportional to the root of the scan rate.[20]

$$I_P = 0{,}4463nFAc\sqrt{\frac{FDv}{RT}} \quad \textbf{(6)}$$

A – electrode area in cm^2

c – concentration in $\frac{mol}{cm^3}$

D – diffusion coefficient

In addition, the potential difference in a reversible case is always constant regardless of the scan rate.[20]

$$\Delta E_P = E_{P,anodic} - E_{P,Kathodic} = \frac{0{,}059}{n} \quad \textbf{(7)}$$

Thus, for the reversible case, the number of electrons n involved can be calculated from the potential peak difference using equation (7).[20]

For the synthesis of polydopamine, the nonreversible electropolymerization can be initiated by cyclic voltammetry. A potential range of -0.5 V to +0.5 V is used for this electropolymerization. With each cyclic voltammetry scan the polymerization proceeds and the current which is observed decreases steadily. This decrease can be explained by the deposition of polydopamine on the surface of the WE. It was found that after 20 CV cycles the deposition of PDA lead to an almost complete insulation of the WE. It was also found that the PDA films almost growth linear with the number of CV cycles which opens the possibility to control the thickness of the film by the number of CV scans. This method also gives smooth films with a low roughness.[16]

2.3. Catalyst for hydrogen production and reduction of nicotinamide adenine dinucleotide (NAD^+)

As mentioned in the motivation hydrogen has a high fuel value $\left(H_2 + 0.5\ O_2 \rightarrow H_2O + 56.7\frac{kcal}{mol}\right)$ and with water an emission-free combustion product, which is also the raw material for the hydrogen production. Hydrogen is thus obtained from a cheap material that is available almost everywhere.[1] Therefore several system for hydrogen production existing. In the following only catalyst which are of interest for this work are considered.

Several Rh(II)-complex for water splitting driven by ceric ammonium nitrate are known.[21] A organometallic structural motive which combines high stability and capability of producing hydrogen photocatalytically and electrocatalytically is $[(1{,}2-\text{diimine})Rh(Cp^*)X]^{n+}$ with $X = Cl(n = 1)$ or

H_2O $(n = 2)$.[22] This chemical motive can be used for the reduction of hydrogen, ketone, flavine and NAD^+ with an hydride donor e.g. formate. But these complexes are not photocatalysts by themselves and must therefore be sensitized to sunlight with a photoelectron generating unit.[23]

In addition to water splitting and CO_2 reduction, photocatalysis can also be used for enzymatic transformation and thus bio catalysis, more precisely for nicotinamide cofactor production. The $[(1,2-\text{diimine})\text{Rh}(\text{Cp}^*)\text{X}]^{n+}$ complexes are also suitable for this, as they are highly active for the selective reduction of *meta*-functionalized pyridinium ions to the 1,4-dihydro form (see Figure 6). Formate or phosphite is usually used as reducing agent.[24]

The catalyst shown in Figure 5 is used in this work as a model catalyst to demonstrate the basic principle of PDA film´s functionalization and catalytic properties.

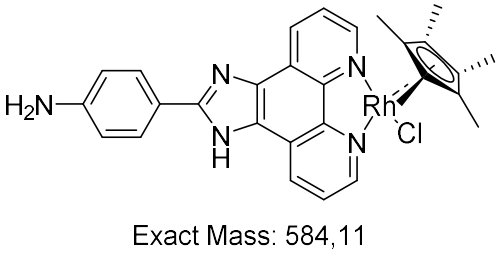

Exact Mass: 584,11

Figure 5: The used Rh catalyst in this work.

Due to the relatively simple detection of the reduction of NAD^+ using UV/VIS, the coupled reduction of NAD^+ to NADH is used as a model reaction. The reduction follows the scheme shown in Figure 6 where sodium formate is used as reduction agent and the production of NADH can be investigated through the strong absorption band at ~350 nm.[25]

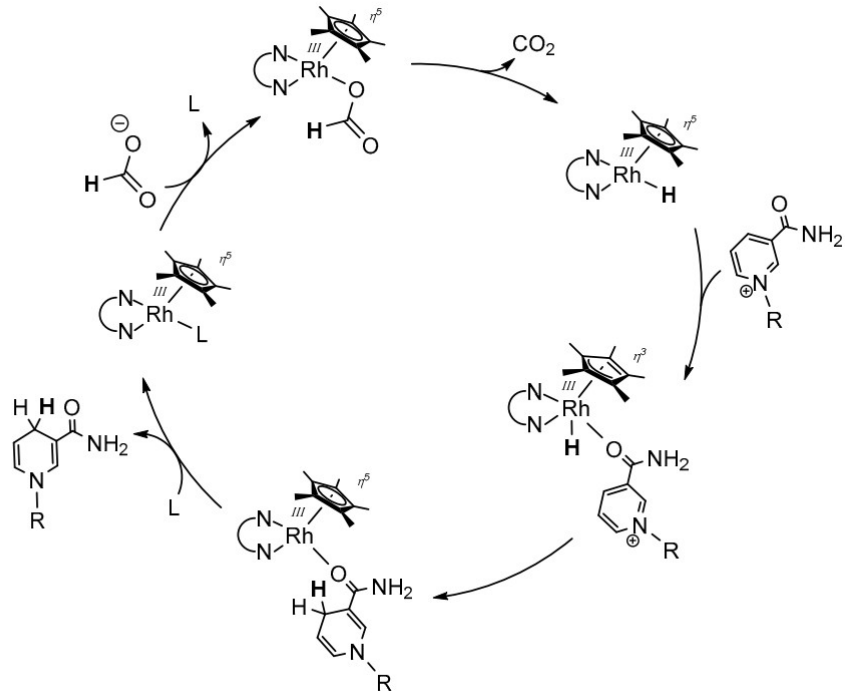

Figure 6: Scheme of the reduction of NADBr with an $RhCp^*$ catalyst.[25]

2.4.CdSe/CdS core shell nanorods

Due to the fact that the catalysts mentioned in the previous chapter are not photocatalytically active, a photon absorber is required to make photoelectrons available to the system. An ideal photo absorber for water splitting is an efficient light harvester, has a suitable bandwidth, fast interfacial charge transfer kinetics to the electrolyte and is corrosion-resistant under the conditions used. Today's systems do not fulfill all requirements and are limited by their photo-absorbing properties. For III-V semiconductors, good charge transport and a high photocurrent can be used. However, these systems have the disadvantage of undergoing photo corrosion if they are not protected by a protective layer.[26]

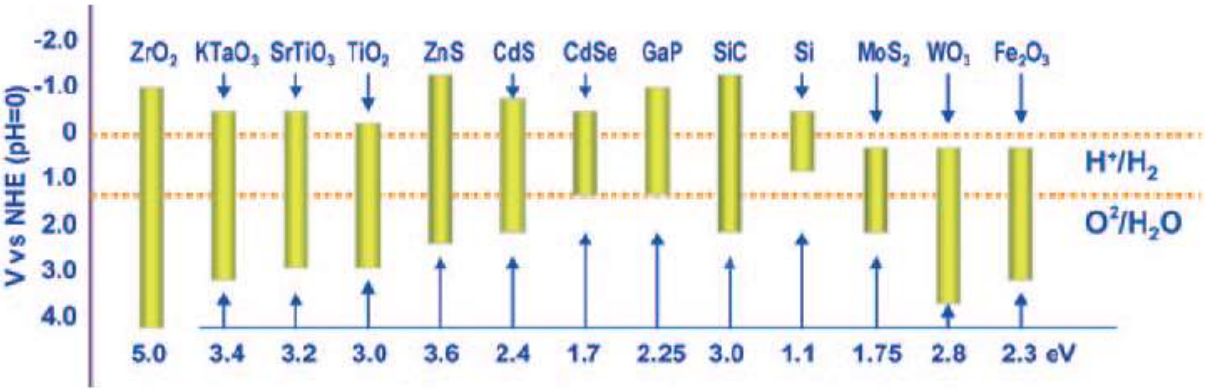

Figure 7: Band-gap energies and relative band positions of different semiconductors relative from [28]

Nevertheless, CdS has a suitable band gap for water splitting despite photo corrosion. Although the active centers for catalysis are transition metals, noble metals or their oxides (e.g. Rh, Pt, NiO).[27] A quantum dot cell device based on CdS has a high open circuit voltage but also a high bandgap of 2.25 eV, in bulk, thus only wavelengths smaller than 550 nm can be used to generate the electron-hole pair. CdSe help to extend the range of the absorbance to 720 nm[29] and thus the CdSe/CdS absorb more of the visible light than other semiconductors e.g. TiO_2.[30] The CdSe/CdS quantum dots thus show a strong photo response across the entire visual light spectrum.[29] For water splitting, the system needs a band gap energy matching the potential for water oxidation and reduction, which means that the bottom of the conductive band has to have a more negative potential than the proton reduction potential and the valence band edge must be higher than the oxidation potential of water. Therefore, a semiconductor needs a theoretical band gap with an energy of 1.23 eV. This corresponds to a photon with a wavelength of 1010nm, which means approximately 70 % of all solar photons have the required energy and can therefore be used for water splitting. These include the photons from the infrared range (920-1400, 29.4% of the total spectrum), near infrared (700-920nm, 23.5% of the total spectrum), the visible range (400-700nm, 44.4% of the total spectrum) and near ultraviolet (315-400nm, 2.9% of the total spectrum).[28] Therefore, the CdSe/CdS system can absorb photons from the near ultraviolet and visible range, which corresponds to 47.3% of the total photons of sunlight. In addition, CdS by itself has a band gap of 2.4 eV and thus fulfills the requirements to provide electrons for water splitting.[28]

If the system is in a rod shape, it also has compared to spheres a high fluorescent quantum yield (reaching 70 %)[31] and a linear polarization along the rod.[32] In the rod form, the system can be seen as a 1D electronic structure due to the narrow diameter. The shape of the material allows wave function tailoring and control of interfaces and thus control on the fate of injected energy and charges.[31] Also the elongation with CdS of the CdSe core leads to a two times larger quantum

efficiency at room-temperature compared to the core.[32] The system undergoes a charge separation after excitation with light due to the close conductive band alignment.[30] The previous mentioned linear polarization leads to a strong dipole moment along the *c*-axis which enables previously prohibited optical transitions of lowest excited states. This leads to confinement of the holes within the core which was confirmed by molecular dynamics and electronic structure simulation techniques these showed strong localization of the holes in the core and delocalization of the electrons over both conductions bands (CdS and CdSE).[30]

The semiconductor CdS normally shows an excellent response capability under visual light but also an unsatisfying photocatalytic efficiency due to the fact that charge carriers can easily recombine. In combination with PDA, the recombination of the charge carriers in the semiconductor CdS could be reduced. PDA resembles an amorphous organic semiconductor or an electronic-ionic hybrid conductor. Due to its π-system, PDA can be used as a further photosensitizer in this system and can therefore be seen as an electron donor that improves the separation of electrons and holes.[2] All of these characteristics make the CdSe/CdS dot/rod structure a well-fitting light harvesting system for water splitting.

2.5.Methods for analysis

2.5.1. MALDI-Imaging

With MALDI Imaging all types of tissue sections can be investigated. To extract molecules from the tissue these sections are covered with a Matrix to support desorption/ionization for analyzing the molecule further. Because ionization is necessary are Laser is used which irradiate only the matrix layer. Thus leave the underlying layer intact and unchanged and therefore the same tissue section used for the MADLI Imaging can be further investigated with other tissue examinations. Due to irradiation of the matrix the laser energy is absorbed by the matrix and is transfer by the matrix to the analyte which transfers the analyte into the gas phase.[33] The chemical properties of the analyte and the matrix as well as the absorption of the laser energy influences the ionization process.[34] The choice of the used matrix plays therefore an important role for the successful analysis. Depending on the class of the sample the best matrix has to be found by comparing the strengths and weaknesses of the different matrices. For MALDI Imaging the laser is scanned across the tissue.[34] Because this method is a “soft” ionization technique and therefore a wide range of molecular weights can be analyzed in a range from hundreds of Da to beyond 100 kDa. Also, it makes analyzation of complex mixtures easier because MALDI mass spectra consist of single charge molecules. The laser also allows to analyze the sample in very specific spatially distinct areas by turning the laser to these regions.[34]

2.5.2. ToF-SIMS

The Time-of-Flight Secondary Ion Mass Spectrometry (ToF-SIMS) is a characterization method for the chemical composition of surfaces. To analyzation a high power primary ion beam (e.q. Au^+ or Bi^+) is shot onto the surface. The energy of this beam is deposited through collisions between the primary ions and the atoms of the sample as well as among the atoms of the sample near the surface. A minor part of the contributed energy is transported back to the surface by this collision cascade and lead to emission of electrons, neutral particles and secondary ions. The secondary ions are then analyzed with a mass analyzer regarding the mass to charge ratio. For this technique a time of flight spectrometer (ToF) is used as mass analyzer. First this spectrometer accelerates the generated secondary ions to an equal energy. The mass of the secondary ions can be determined by the time the ions need for a subsequent drift distance. Through the precise time of flight determination, the chemical composition

of the generated ions and therefore of the sample surface can be determined. If the primary ion beam is scanned pixel wise the chemical distribution can be imaged. For every pixel the detected intensity of a secondary ion is revered to a color value and therefore images with mass resolution are obtained.[35,36]

If the chemical composition as a function of the sample depth is the target of interest the sample removal through the ion beam is used and high primary ion doses are used. Due to the resulting sample damages by the shelling only courses of elements and small inorganic molecules can be detected as a function of depth or erosion time.[35,36]

2.5.3. X-ray photoelectron spectroscopy (XPS)

The XPS measurement can divided into three stages, the energy transfer from X-ray photon to the core electron, the creation of the photoelectron and detection of the photoelectron. The energy transfer from the X-ray photon to the core electron is depends mainly on the energy of the core electron. This is called the initial stat energy which also includes all chemical shift due to the chemical characteristics of the material. The so-called final state effects affect this energy through the interaction between the photoelectron and the resulting core hole. The photoelectrons can also lose some of the kinetic energy by inelastic scattering processes on the way to the surface which lead to a contribution to a continuous photoemission intensity background.[37] For a typical XPS experiment the sample surface gets excited with mono-energetic X-rays causing the emittance of the photoelectrons. The detected kinetic energy of the photoelectron is characteristic for the element of the photoelectron. The chemical and bonding information derive from chemical shift which are the result of the chemical state of the atom because this state alters the binding energy of the photoelectron and therefore result in a change of the measured kinetic energy which is connected with the binding energy through the photon (x-ray) energy.[38]

2.5.4. Dynamic light scattering (DLS)

The basis of every light scattering experiment is the fact that when monochromatic light hits a solution with macromolecules, the light is scattered in all directions depending on the size and shape of the macromolecules. With dynamic light scattering, the intensity fluctuations, which are caused by Brownian molecular motion, of the scattered light are examined. In this way, the diffusion coefficient of the macromolecules can be obtained, since this is related to the hydrodynamic size of the macromolecules. This technique therefore primarily measures the brown molecular motion of the macromolecules in solution, which results from the bombardment of solvent molecules, and correlates them with the size of the particles. The movement of the macromolecules depends on their size, the temperature and the viscosity of the solvent. For this reason, the temperature and viscosity, which is also temperature-dependent, must be known for a DLS experiment. If this is the case and the movement is examined as a function of time, the fact that large particles move slowly compared to smaller ones allows conclusions about their size. As the molecules are in constant motion, the incident light experiences the phenomenon of so-called Doppler broadening. The scattered light results in mutually destructive phases that cancel each other out or mutually constructive phases, which leads to a detectable signal. A digital autocorrelator can then correlate the fluctuations in the intensity of the scattered light with time and thus determine how quickly the intensity fluctuates due to the diffusion behavior of the macromolecules. Although it is not possible to know the exact movement of each particle in solution in a typical light scattering experiment, the relative movement of the particles to one another can be represented and defined by means of a correlation function of the electrical

field. The correlation factor of the electric field decreases exponentially for monodisperse particles and is dependent on a decay constant for particles that are subject to Brownian motion. This decay constant is in direct connection with the translation diffusion coefficient as an expression of the diffusion behavior of the macromolecules. Other important hydrodynamic parameters can then be determined using the translation diffusion coefficient. The hydrodynamic radius for example, which is defined as the radius of a hypothetically spherical particle, can be obtained using the Stokes-Einstein equation.[39]

2.5.5. High resolution transmission electron microscopy (HRTEM)

In some cases, HRTEM images can provide structural information that is difficult or impossible to obtain with other methods. The HRTEM image shows an interference pattern of the electron wave function with itself after it has been deflected from the sample. The most important aspects of HRTEM can best be understood on the basis of the phase of the electron wave front and the change in this phase due to the sample and the objective lenses. The sample is interpreted as an object which gives the electron wave front a phase shift. The exact physical optics theory is omitted here and the interested reader is referred to the reference[40]. Basically, one can say that a lens aperture must be used for an HRTEM image that is large enough to accommodate both the transmitted and at least one deflected electron beam. The "forward scattered" beam provides the required reference phase of the electron wave front. High-resolution images are thus interference patterns which are formed from the phase relationship of the deflected rays. In order to correct the distortion of the objective lenses, the spherical aberration is corrected in the HRTEM, which is possible due to the progress in electron optics and in computer processing. This enables a spatial resolution of 0.8 Å to be achieved.[40]

3. Experimental Part

3.1.Ultra-Thin Polydopamine film

3.1.1. Synthesis of ultra-thin Polydopamine films

The ultra-thin Polydopamine films were synthesized through electro polymerization in a 3-electrode setup with a potentiostat (Metrohm Autolab B. V., Type: PGSTAT204, Software Nova 2.1.4). As working electrode, a gold slide (gold coated microscope slide) was used. The gold slide was cleaned by argon plasma for 10 min. The phosphate buffer (pH = 7) was bubbled with nitrogen for at least 15 min before the dopamine (0.1 mg/mL) was added. After the dopamine was dissolved, the solution was transferred into the electrochemical cell. It was taken care that the solution did not touch the electrode clamps. Ten cycles were performed by sweeping the potential from 0 V to 0.5 V to -0.5 V and back to 0 V for one cycle with a scan rate of 0.01 V/s. The resulting cyclic voltammogram is shown in Figure 8. The working electrode with the synthesized PDA film was removed from the electrochemical cell, rinsed with MilliQ water and dried under nitrogen flow.

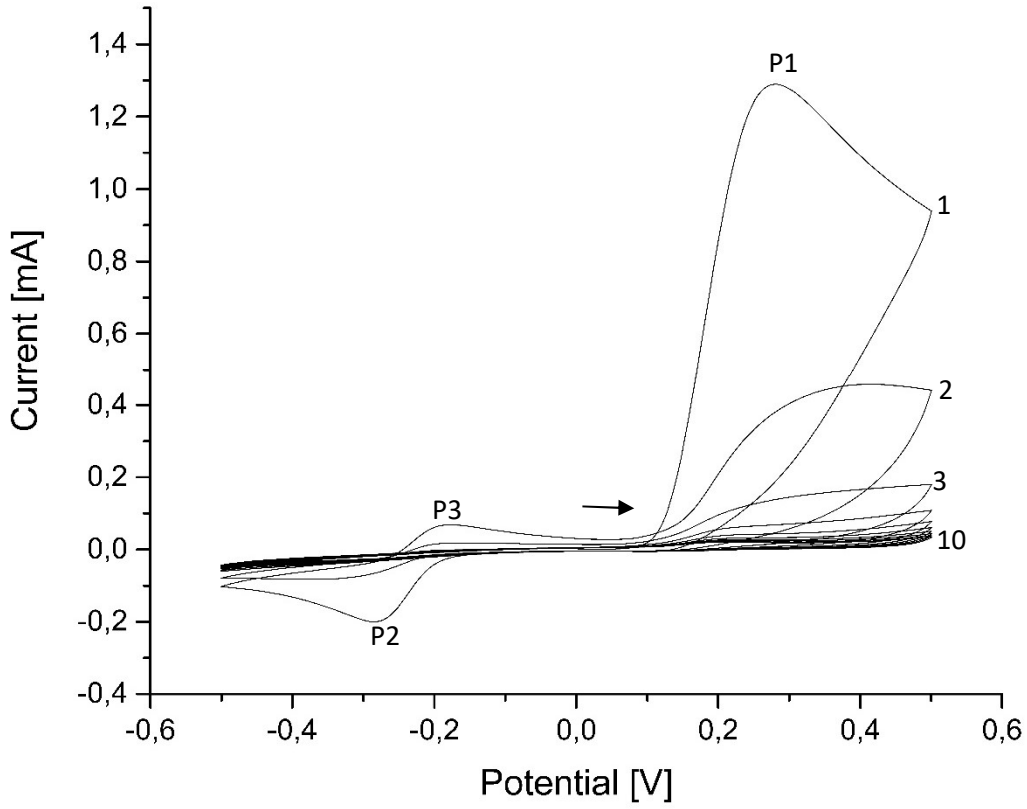

Figure 8: Cyclic voltammogram of the PDA synthesis.

Figure 8 shows the cyclic voltammogram of the electropolymerization of PDA. Following the first cycle, first an anodic peak (P1) at 0.27 V can be seen. A cathodic peak at -0.28 V (P2) can then be observed. Another anodic peak appears at -0.19 V (P3). The observed peaks can be assigned to the different redox couples. For the redox couple dopamine/dopaminequinone only the anodic peak (P1) can be seen, the associated cathodic peak is 0.12V according to literature[41], due to the low response this peak cannot be observed. The cathodic peak P2 and the anodic peak P3 can be assigned to the redox

couple leucodopaminechrome/dopaminechrome. It can also be seen that the measured current decreases as the number of cycles increases. This can be explained by the insulating properties of the resulting polydopamine film.

3.1.2. Functionalization of the PDA film with Rh catalyst

For the functionalization of the ultra-thin PDA film, a solution of the dissolved catalyst in acetonitrile (0.3 mg/mL) and phosphate buffer with ratios of 1:9 or 1:999 were used. The film was put into a petri dish and 200 µL of the reaction solution was topically applied on the film. To prevent drying, a waterlogged cotton ball was also put inside the petri dish before it was closed. After 18h, the remaining reaction solution was removed by rinsing the film with MilliQ water. For analyzing the behavior of the bounded catalyst on the film it was necessary to find a washing procedure which removes all the remaining free catalyst from the surface. Therefore, MALDI-Imaging was used to determine which washing procedure was effective to remove all the free catalyst from the film surface because if no catalyst can be detected by MALDI-Imaging only bounded catalyst if the functionalization worked should remain. Also, MALDI-ToF of the dissolved catalyst was performed. TCNQ (exact mass 204.0436) was used as matrix in all experiments. For the catalyst the exact mass was calculated to be 584.11 g/mol. With respect to the MALDI-Imaging results every film was thenceforth cleaned by ultra-sonication in acetonitrile for 5 min. This was done 12 times followed by rinsing the film with MilliQ water and drying under nitrogen flow.

To determine if still some covalently bound catalyst remained on the surface after the washing procedure ToF-SIMS measurements were performed using a liquid metal ion source employing 30 keV Bi_3 ions at a target current of 0.1 pA. The fields of view were adjusted to 100 x 100 µm² for the spectrometry and to 400 x 400 µm² for the stage raster (8 x 8 patches) imaging analyses. Depth profiles were acquired 100 x 100 µm² or 150 x 150 µm² field of view for the analysis gun and at 400 x 400 µm² for the sputter gun using Ar_{1000} clusters at 2.5 keV delivering a target current of 0.3 nA. The covalently bond of catalyst to PDA was proved by XPS measurements of a pure PDA film on gold as reference. A UHV multiprobe system (Scienta Omicron) with a monochromatic X-ray source (Al Kα) and an electron analyzer (Argus CU) with 0.6 eV spectral energy resolution was used. The spectra were fitted using Voigt functions (30:70) after background subtraction. For the quantitative elemental composition, the relative sensitivity factors (RSF) of 1.00 (C 1s), 2.93 (O 1s), 1.80 (N 1s), 14.21 (Rh 3d) and 2.29 (Cl 2p) are used, respectively.

3.1.3. Reduction of Nicotinamide adenine dinucleotide at the functionalized PDA films

Stock solutions of Nicotinamide adenine dinucleotide (NAD^+, 0.4 mM) and sodium formate (0.4 M) were prepared in a glovebox. As solvent deionized water which was bubbled for 1.5 min per mL with argon. The functionalized films were prepared using the method described in Chapter 3.1 with ratios of catalyst solution to phosphate buffer of 1 to 9 (high concentration) and 1 to 999 (low concentration). The films were each transferred to a UV/VIS cuvette and introduced into the glovebox. Under this protective gas atmosphere, a 1:1 mixture of NAD^+ and sodium formate stock solutions with a total volume of 3 ml was transferred to the respective cuvette. The cuvettes were sealed airtight and removed from the glovebox. Then an absorption and an emission spectrum of both solutions were measured. The solutions were then heated to 40 °C in a water bath for 10 minutes, then for 15 minutes and then four times for 25 minutes each. An absorption spectrum with pure sodium formate used as baseline and an emission spectrum were recorded after the respective time intervals. For the absorption spectrum a Jas.co V-670 spectrometer and for the emission spectrum a Jas.co FP-8500 spectrofluorometer were used.

3.2.CdSe@CdS nanorods in solution

The CdSe@CdS nanorods were obtained from a collaborator (Dr. Maria Wächtler, Leibniz Institute of Photonic Technology). The nanorods were dissolved in water (3 mg/mL) and were stabilized by mercapto propionic acid ligand.

The used Rh catalyst for the functionalization of the coated nanorods is shown below and was obtained from another collaborator (Alexander Mengele, Rau Group, University of Ulm). Because of the amine group it is possible to functionalize the PDA through Michael Addition/Schiff base reaction.

The functionalization of the nanorods follows the reaction scheme shown in Figure 9. In the first step the CdSe@CdS nanorods are coated with PDA through self-polymerization of dopamine followed by the functionalization with the Rh catalyst through Michael Addition/Schiff Base reaction between the PDA and the amine group of the catalyst. Moreover the PDA coated nanorods are also functionalized with PEG-SH (5k Da) to stabilize the nanorods in solution otherwise the functionalized nanorods would aggregate and precipitate (see chapter 4.3.1). The functionalization with PEG can be achieved by Michael Addition through the thiol group of the PEG.

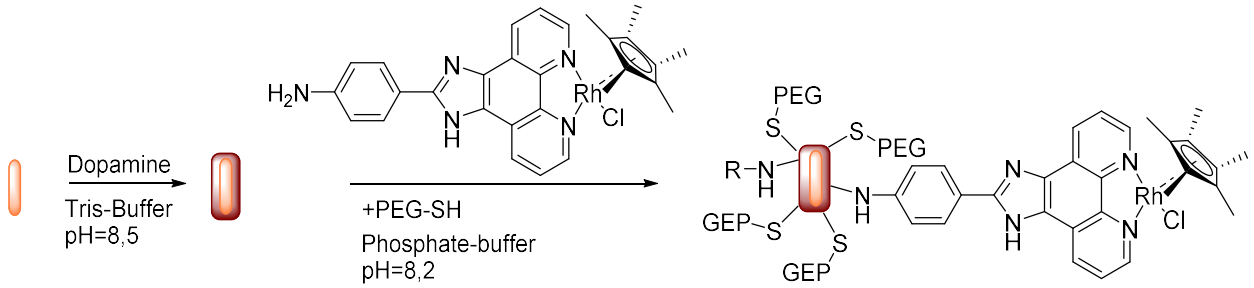

Figure 9: Reaction scheme of the functionalization of the nanorods.

3.2.1. Coating of CdSe@CdS nanorods with Polydopamine

For coating the nanorods with polydopamine a solution of 50 µL of the dissolved nanorods, 400 µL of Tris buffer (100mM, pH = 8.5) and 50 µL of dissolved dopamine in MilliQ water (1 mg/mL) were prepared. The solution was shaken for 24h, during this time the color of the solution changed from yellow to brown. For washing the solution was transferred to a centrifuge filter (Amicon® Ultra-0.5mL centrifuge filters, molecular weight cut-off 100kDa). It was centrifuged for 5 min at 4 g and the remaining particles were dissolved in 500 µL MilliQ water. This washing was repeated 3 times and the nanorods were dissolved in the solvent needed for the following experiment or in 450 µL MilliQ water for storing. The exact final concentration of coated nanorods in solution is unknown because of losses during the filtration and the fact that the solvent could not be removed completely by centrifugation. This is true for all following synthesis.

3.2.2. Coated CdSe@CdS nanorods functionalized with Rh catalyst

The catalyst was dissolved in acetonitrile with a concentration of 0.3 mg/mL whereby a yellow solution was obtained. From the dissolved catalyst solution 50 µL were mixed with 450 µL of phosphate buffer (pH = 8.2). In this mixture the PDA coated nanorods of one coating procedure were dissolved and the solution was shaken for 24h. For purification, the solution was transferred to a centrifuge filter

(Amicon® Ultra-0.5mL centrifuge filters, molecular weight cut-off 100kDa) and centrifuged for 5 min at 4 g. The remaining particles were dissolved in 500 µL MilliQ water. The washing was repeated 3 times and the functionalized nanorods were dissolved in 450 µL MilliQ water.

3.2.3. Coated CdSe@CdS nanorods functionalized with PEG

In 500 µL of phosphate buffer 0.3 mg of polyethylene glycol (PEG-SH, 5k Da) were dissolved to obtain the reaction solution. The PDA coated nanorods of one coating procedure were dissolved in the reaction solution. After shaking for 24h the solution was transferred into a centrifuge filter (Amicon® Ultra-0.5mL centrifuge filters, molecular weight cut-off 100k) and centrifuged for 5 min at 4 g. the remaining particles were dissolved again in 500 µL of MilliQ water. This washing was done 3 times and the nanoparticles were dissolved in 450 µL MilliQ water after the last washing.

3.2.4. Coated CdSe@CdS Nanorods functionalized with Rh catalyst and PEG

The PDA coated nanorods of one coating procedure are dissolved in a solution of 50 µL of the dissolved catalyst (0.3 mg/mL) in acetonitrile, 450 µL phosphate buffer (pH = 8.2) and 0.3 mg of PEG-SH (5k Da). After shaking the mixture for 24h it was transferred to a centrifuge filter (Amicon® Ultra-0.5mL centrifuge filters, molecular weight cut-off 100k) and centrifuged for 5 min at 4 g. The particles were dissolved again in 500 µL MilliQ water. The procedure was repeated 3 times and after the last washing the particles were dissolved in 450 µL of MilliQ water.

3.2.5. Absorption measurement settings

The influence of the PDA coating and the post functionalization for light harvesting absorption measurements were performed. The setup used for the absorption measurements consisted of a spectrometer (Avantes Starline AvaSpec-2048) which was controlled by the software Avasoft 8 and a lamp (Avantes AvaLight-DH-S-BAL) which covered the wavelength range from 200 nm to 1100 nm. All samples were dissolved in MilliQ water after the last purification step and using the amount described in Chapter 3.2 for the coated and functionalized nanorods. The pure nanorods were diluted to a concentration of 0.3 mg/mL. For the measurement always 100 µL of the samples were measured in a quartz cuvette (High Precision Cell from Hellma Analytics, light path: 10×2 mm).

3.2.6. Reduction of Nicotinamide adenine dinucleotide at the functionalized nanorods

To prove the hypothesis that the catalyst is covalently bound the reduction of the Nicotinamide adenine dinucleotide (NAD^+) was tested. Therefore, a solution of PDA coated nanorods functionalized with PEG and the catalyst, using the method described in chapter 3.2.4, in water with an optical density of 0.03048 at a wavelength of 465 nm was prepared. The solution was bubbled with argon for 1.5 min per milliliter and hereinafter referred to as the stock solution of the functionalized nanorods. Subsequently, a solution was prepared from the stock solutions of the functionalized nanorods, NAD^+ and sodium formate in a ratio of 2:4:4 under a protective gas atmosphere and transferred to a UV/VIS cuvette. The cuvette was sealed airtight and an absorption and an emission spectrum was recorded. The cuvette was then heated in a 40 ° C water bath. An absorption and emission spectrum were recorded five times after 10 minutes each using the same instruments as for the films.

3.2.7. Photocurrent measurements

Because the system is designed to produce hydrogen with solar energy, photocurrent measurements of the pure PDA films and of the coated nanorods on ITO were performed. An LED (ThorLabs M455L5) with a wavelength of 455 nm and a surface power density of $1163.74\,\frac{\mathrm{mW}}{\mathrm{cm}^2}$ was used controlled by the Thorlabs LED driver LEDD1B using the continuous wave mode. To pulse the light a shutter was used (Thorlabs SHB1T) which was synchronized with the potentiostat (Metrohm Autolab B. V., Type: PGSTAT204, Software Nova 2.1.4) to close or open the shutter every 10 seconds. Also, the resulting photocurrent was recorded with the potentiostat for the applied potential which was changed from -0.5 V to 0.5 V with a scan rate of $0.005\,\frac{\mathrm{V}}{\mathrm{s}}$. As electrochemical cell disposable cuvettes (Brand, UV-Cuvette macro) were used, always using 3 mL of buffer. The buffer that were used were 100 mM phosphate buffers at pH values of 2.6, 5.46, 7 and 7.98 and carbonate buffer at pH 10. As WE substrate ITO was used cut in slices 6 mm wide. The ITO slices were cleaned by ultra-sonication in acetone, ethanol and MilliQ water each for 15 minutes.

Figure 10: The used experimental setup for photocurrent measurements.

4. Results and discussion

4.1.Photocurrent

In this chapter the photocurrent is investigated because the final system should use light as energy source. Therefore, two PDA films with different thicknesses were measured. One film had a thickness which is comparable to the film thickness which would be used for the final system as a film. The other film had a thickness which is more comparable to the coated nanorods which were also measured.

4.1.1. Photocurrent of PDA films on ITO

Two PDA films were synthesized by the method described in 3.1.1 using ITO instead of gold as WE and instead of 10 cycles 5 or 15 cycles were used. Only the photocurrent measurements of the film with 15 cycles are shown. For the film with 5 cycles see appendix Figure 110 to Figure 114. The current of ITO resulting from the applied potential was removed by manual baseline correction with the software Origin 9. The manual baseline was used because of higher accuracy compared to the auto baseline correction or by abstracting the measured current of ITO in the dark.

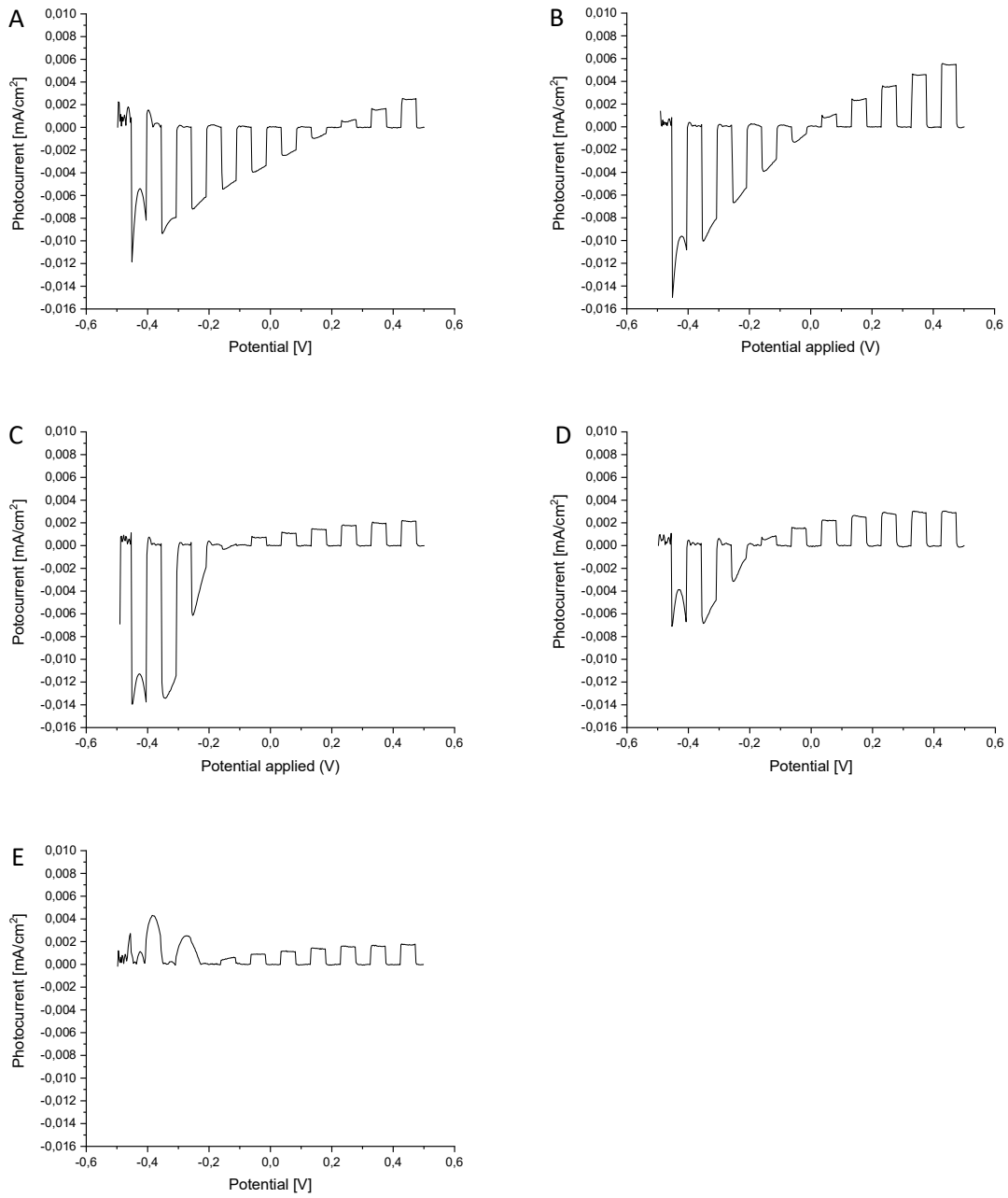

Figure 11: Photocurrent of the 15 cycle film at pH 2.6 (A), 5.46 (B), 7 (C), 7.98 (D), 10 (E) with pulsed light.

The photocurrent figures show that for all pH values a photocurrent can be observed. This was expected that photocurrent of pure PDA is known in literature.[42] Nevertheless, the observed photocurrent is really low but this is a hint with respect to the used wavelength of 455 nm that PDA can improve the photocurrent of the final system. Compering the different photocurrents it is possible to observe that the more acidic the solution, the higher the negative photocurrent. Also, the switching potential is shifted by the pH. The exact reason for this cannot be determined without further investigation. However, it is very likely that this is due to the pH dependency of the catechol to quinone ratio in the PDA film which influences the band structure of PDA. For basic pH the switching potential is reached quite early (-0.24 V for pH 10), where for pH 2.6 the switching potential is reached at 0.34 V. Therefore, the switching potential can be changed in a potential area of 0.58 V by simple pH changes. But the fact that pure PDA shows a photocurrent is in the case of the final system of high interest

because these photoelectrons can maybe also be used for the catalysis or provide additional electron for the quenching of the holes in the nanorods. The same is true for the PDA film with 5 cycles. The range of the switching potential is for the 5 cycle film of 0.44 V and therefore a little bit smaller than for the 15 cycle one.

The pH dependency of the potential is of great interest due to the fact that the system is intended to perform in different pH environments, depending on which interaction between PDA and nanorods is desired. To determine the potential dependence on the pH which is of high interest due to the fact that the system is the previous named values for the switching potential were determined by the intersection points of the dark and continuous light spectrum (see appendix Figure 115 to Figure 129). The intersection points were fitted using a linear regression in the software Origin.

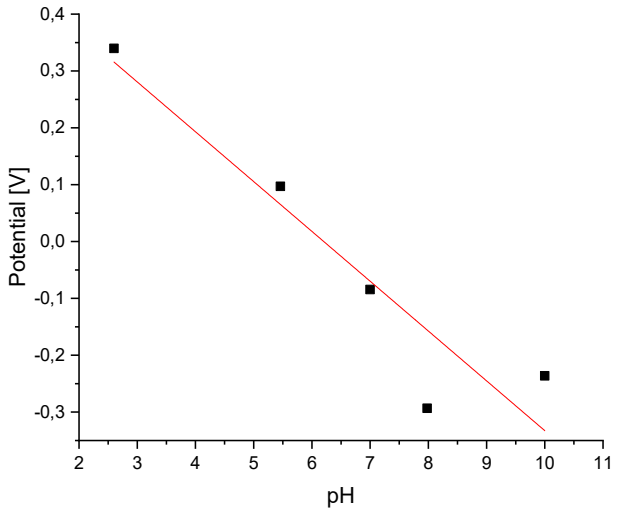

Figure 12: Linear fit of the intersection points of the dark and continuous light measurements of the 15 cycle film.

The slope of the linear regression gives the potential dependence on the pH. For the 15 cycle film the potential is changed by the pH with a value of -87.6 mV/pH and for the 5 cycle film -61.1 mV/pH With respect to the Nernst equation which connects the pH value to the potential a value of -59.2 mV/pH is expected.[43] That the determined pH dependence of the potential diverse from the theoretical value can maybe explained with the fact that the continuous light experiment was used and the system maybe reaches a permanent state. Therefore, the pH dependence was also determined mathematically from the pulsed data.

For the mathematical determination of the pH dependence, the average value of the illuminated parts of the pulsed spectra were plotted and fitted with a cubic polynomial regression. The intersection point was then determined by solving the obtained regression for a y value of zero.

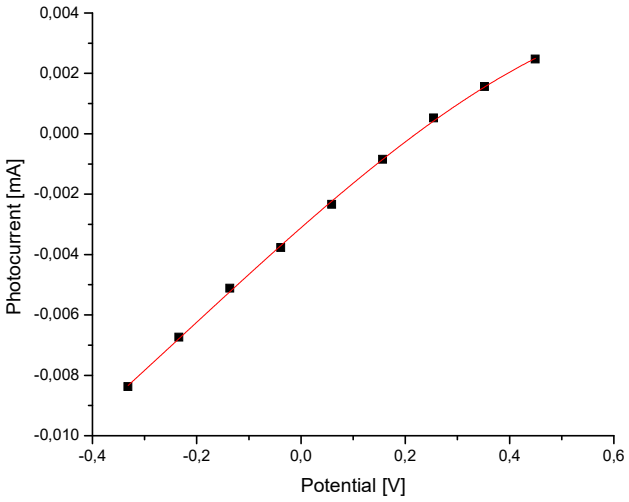

Figure 13: 3. polynomial regression of the average illuminated parts of the pulsed measurement of the 15 cycle film at pH 2.6.

The received intersection points were plotted against the pH and fitted by a linear regression.

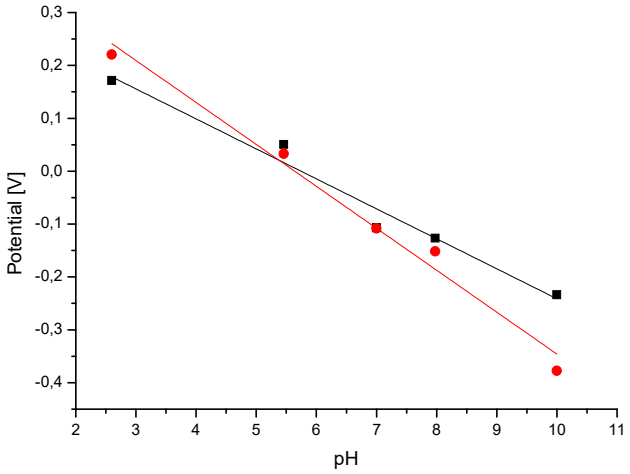

Figure 14: Plotted intersection points against the pH of the 5 cycle film (black) and the 15 cycle film (red) with the linear regression.

For the 5 cycle and 15 cycle film the following expressions were found for the linear regression.

5 cycle film	y=-0.0567*x+0.3257	**(8)**
15 cycle film	y=-0.0793*x+0.4474	**(9)**

Again, the slope of the linear regression gives the pH dependence of the potential. For the 15 cycle film the potential is changed by the pH with a value of -79.3 mV/pH and for the 5 cycle film -56.7 mV/pH. This time the value of the pH dependence of the potential of the 5 cycle film differs only slightly from the theoretical value. That the value of the 15 cycle film still differs significantly from the theoretical value can maybe be explained by the thickness of the film because the current which is

measured come from the lower layers and the interaction with the electrolyte only happened at the surface of the film. Thus, due to the thickness of the film the effect of the pH did not affect the lower layers of the film.

4.1.2. Photocurrent of the PDA coated nanorods

The nanorods were coated using the method described in chapter 3.2.1 and dissolved in MilliQ water. For four times 25 µL of the solution was spread in a circle with a diameter of 6 mm on an ITO slide and dried. The same was done for the pure nanorods but the pure nanorods were not stable on the ITO surface under these conditions. Therefore, no comprising of the photocurrent of the pure nanorods and the coated ones is possible and subsequently it is not possible to say if the measured photocurrent results from the nanorods or the combination of nanorods and PDA coating.

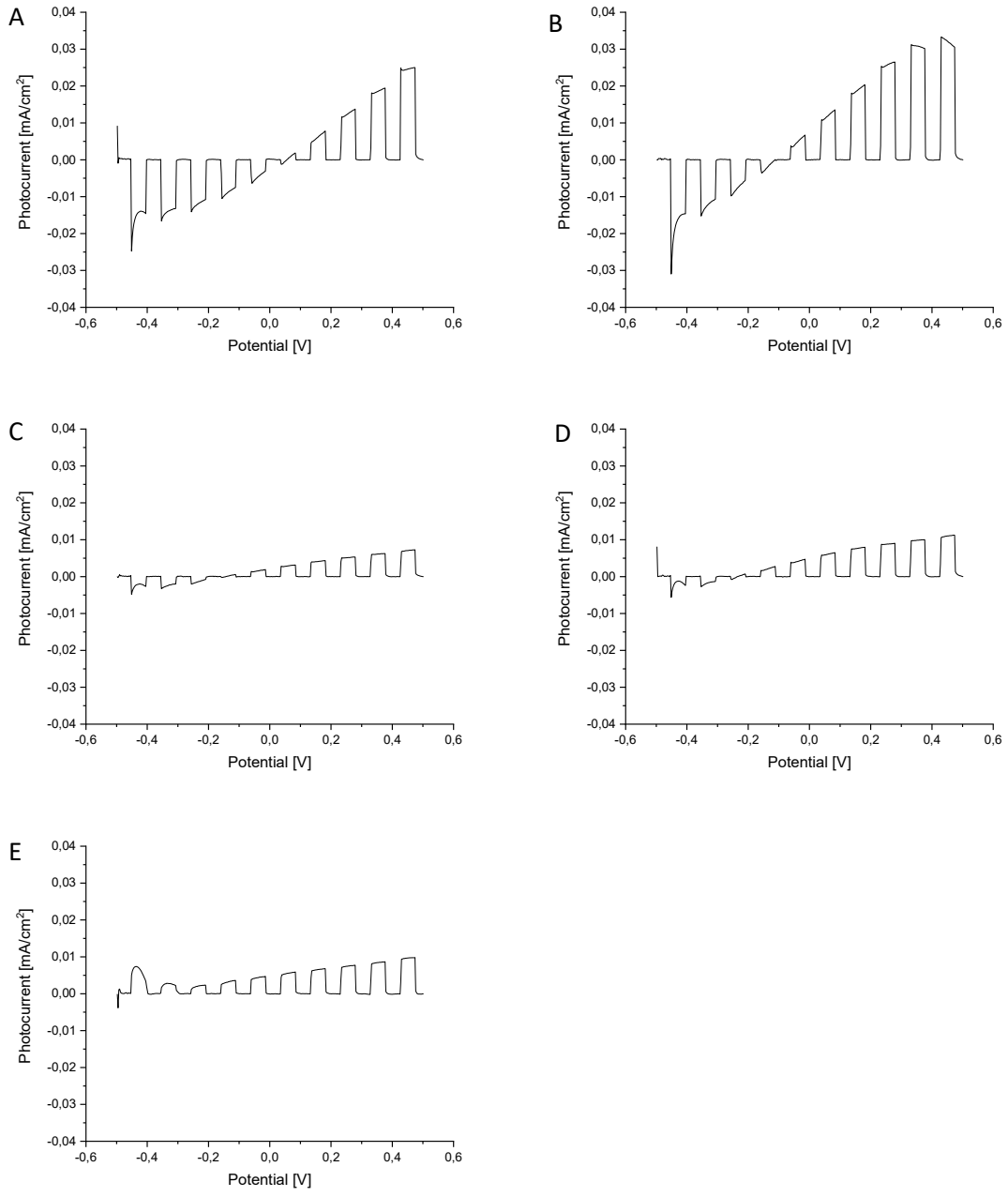

Figure 15: Photocurrent of the PDA coated nanorods at pH 2.6 (A), 5.46 (B), 7 (C), 7.98 (D), 10 (E).

In comparison to the photocurrent of the pure PDA films, it can be said that a higher current flow is measured (almost doubled), and the switching potential has also shifted for all pH values. But it is not clear if the current which is measured is a result only from the coated nanorods attached to the ITO surface or not. If the current comes only from the first layer of coated nanorods the measured current should then be lower because the upper coated nanorods are blocking light for the lower ones and cannot contribute their photoelectrons. Nevertheless, the greatest current flow is measured in an acidic environment (pH = 2.6). Under these conditions there are predominantly catechol groups in the polydopamine. These groups can oxidize to quinone groups with electron donation. The holes in the nanorods created by the photocurrent can be quenched by the electrons released during the oxidation of the catechol group. Since the comparison with the pure nanorods is missing, no statement can be made as to whether the current of the coated nanorods is really higher and thus the expected quenching of the holes takes place. In addition, the measured current in the basic pH is lower, which can be explained by the reduction of the quinone groups, which are mainly present in basic pH. This can be seen as proof that in basic environment the system is self-regulating. Basically, it should be said that the nanorods as a light-harvesting system, as expected, lead to a higher current flow. Furthermore, polydopamine does not appear to block the flow of current, although it is not considered to be conductive. The detected photoelectrons can thus be used by further functionalization, as already shown by the photocatalytic reduction of the NAD^+ (see chapter 4.3.2.4). By using different catalysts, these photoelectrons could be used for versatile reductions in the future.

In order to determine the pH dependence of the potential, the different switching potentials of the different pH values were again determined and plotted using the intersection points of the dark and continuous light spectrum (see appendix) using Origin. As with the films, a linear regression was carried out again. This time only three intersection points could be used because for pH 10 no intersection point occurred and for pH 5.46 the intersection point had a higher potential than for pH 2.6 therefore it is believed that the light did not match exactly with the covered area of the PDA coated nanorods.

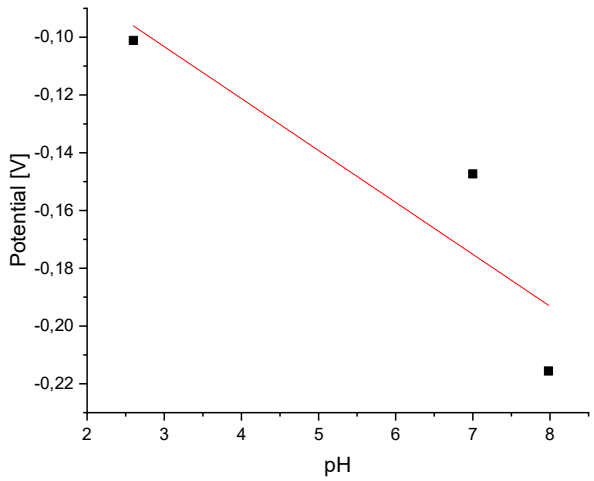

Figure 16: Linear regression of the intersection points of the dark and continuous light measurements of the PDA coated nanorods.

Again, the slope of the linear regression is the potential dependence on the pH. The potential for the PDA coated nanorods is changed by the pH with a value of -18.0 mV/pH. This is far from the theoretical value -59.2 mV/pH from the Nernst equation.[43] This can be explained with the same argument as for

the films that for the continuous light experiment a steady state is reached at some point. Therefore, the pH dependence was again determined mathematically. This was done with the same procedure as the films.

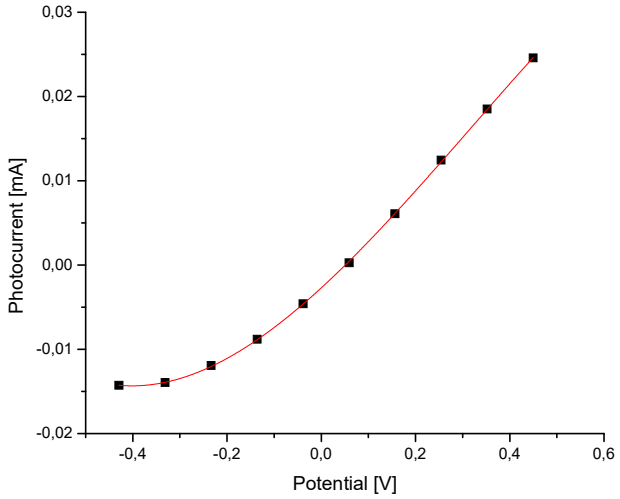

Figure 17: 3. polynomial regression of the average illuminated parts of the pulsed measurement of the coated nanorods at pH 2.6.

Analogous to the films the received intersection points were plotted against the pH and fitted by a linear regression.

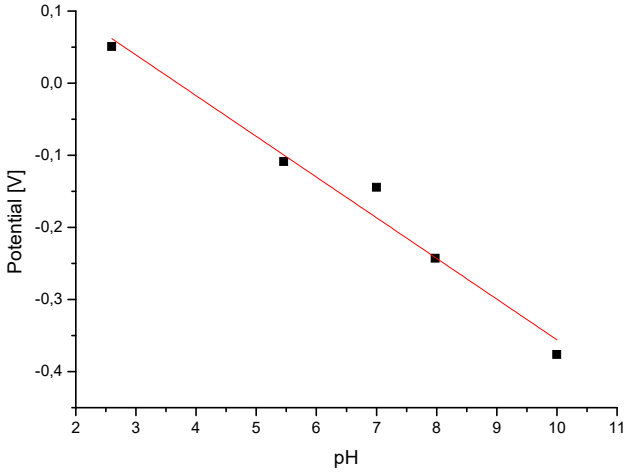

Figure 18: Linear regression of the plotted intersection points against the pH of the coated nanorods.

The following expression was found for the linear regression.

$$y=-0.0564*x+0.2084 \quad \textbf{(10)}$$

Again, the slope of the linear regression is the potential dependence on the pH. Therefore, the potential for the PDA coated nanorods is changed by the pH with a value of -56.4 mV/pH. Like for the 5 cycle film this matches with the theoretical value of -59.2 mV/pH from the Nernst equation.[43]

4.2.Functionalized PDA films

The films were functionalized using the protocol. To find a washing procedure which removes all of the free catalyst from the surface MALDI-Imaging was performed. ToF-SIMS was afterwards measured to prove that after the washing procedure still some catalyst is attached to the surface which is believed to be covalently bound. For proving the covalently bond between catalyst and PDA XPS measurements were performed. In the end, the catalytic activity was investigated by the thermochemical reduction of NAD^+.

4.2.1. MALDI-Imaging

For the pure catalyst the spectrum shows three peaks one at 584.0776 m/z, belonging to the catalyst, a second peak by 548.1043m/z, which match the catalyst without the chlorine and a third peak by 576.0937 m/z. The third peak would fit to the catalyst if the chlorine was substituted by CN and a proton, but this could not be proven.

Table 1: The theoretical and measured masses of the three different catalyst species.

specie	theoretical mass [m/z]	Measured mass [m/z]
Catalyst	584.11	584.0776
Catalyst without Cl	549.14	548.1043
Catalyst with exchanged Cl	576.15	576.0937

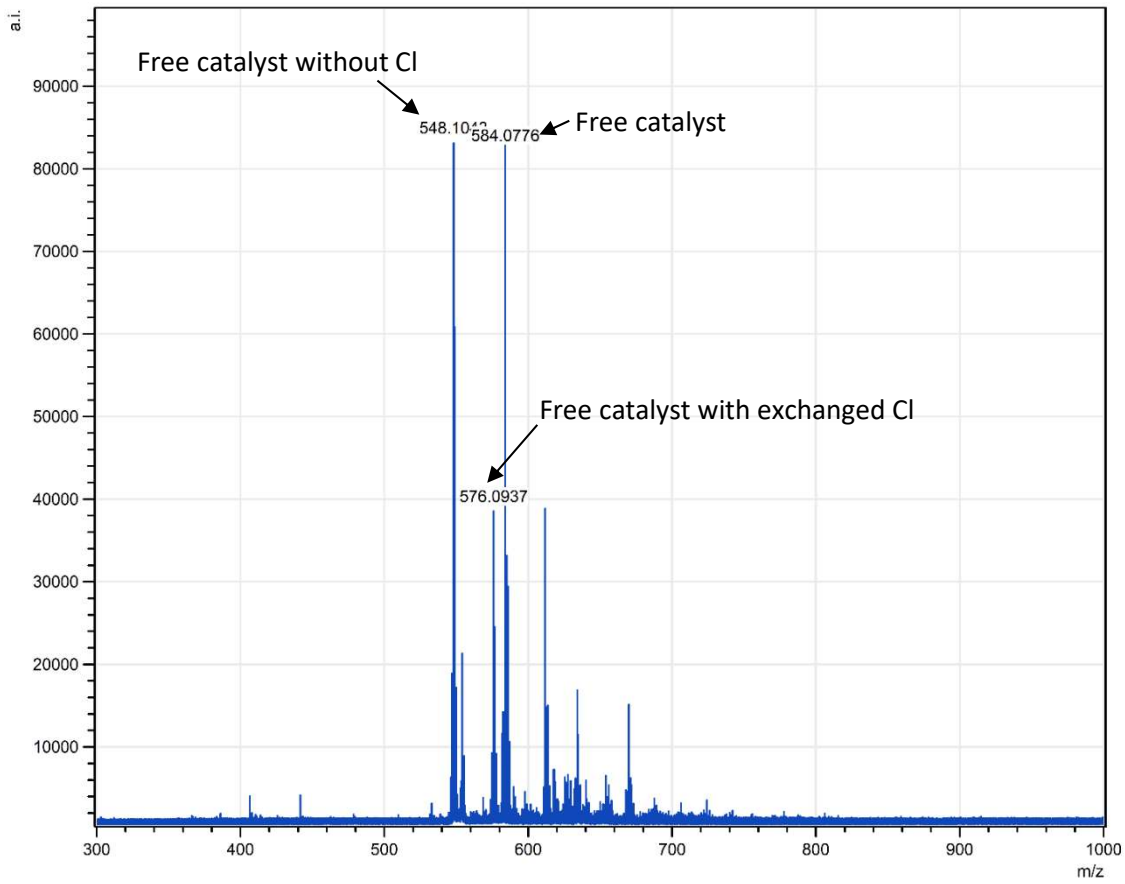

Figure 19: Mass spectra of the catalyst with TCNQ as matrix.

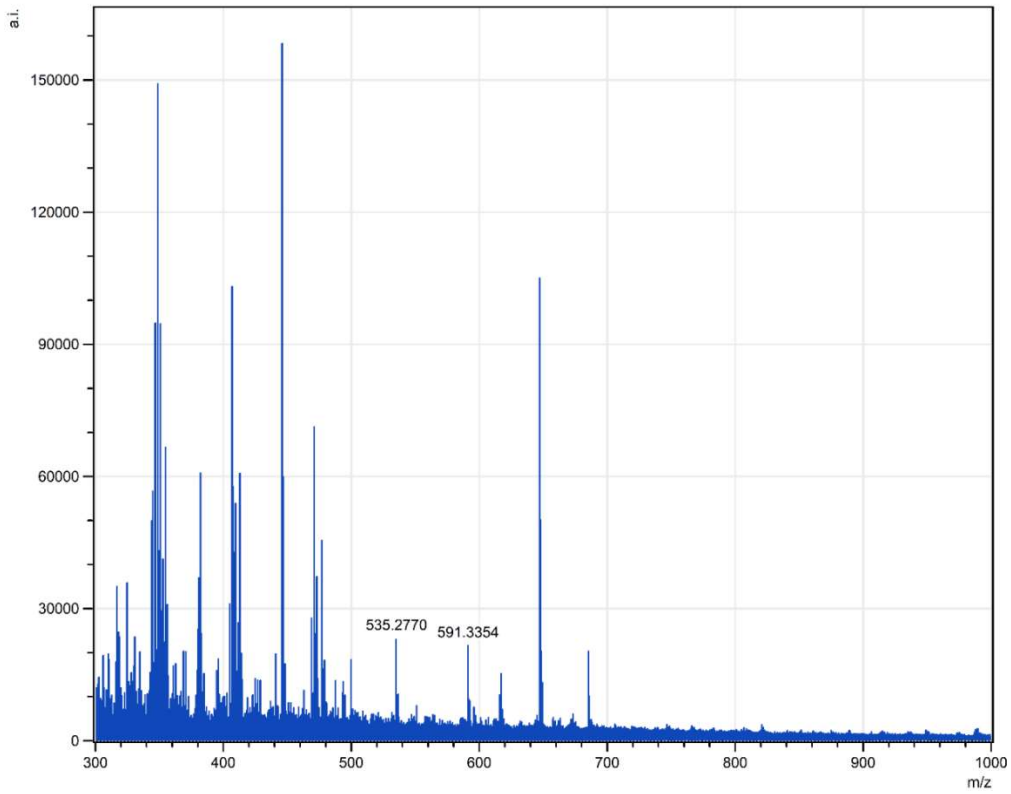

Figure 20: Mass spectra of the pure PDA film with TCNQ as matrix.

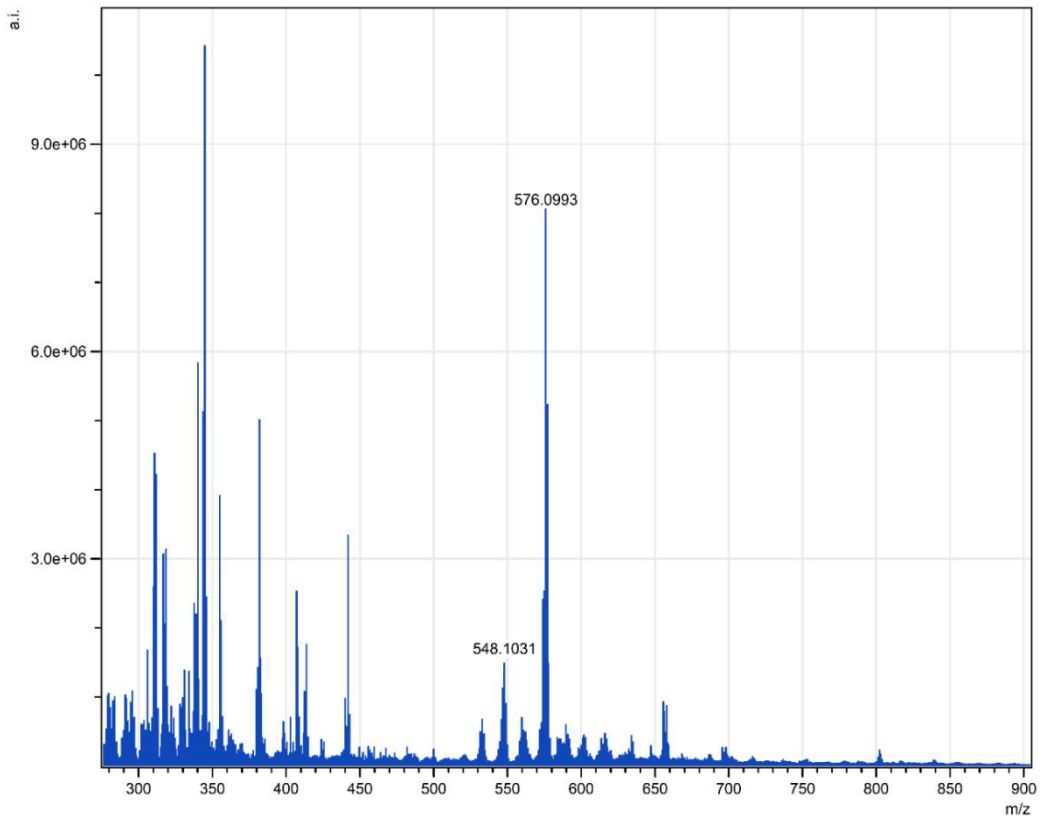

Figure 21: Mass spectra of the functionalized film, using dissolved catalyst to phosphate buffer (1:9), without washing and TCNQ as matrix.

Figure 20 shows the spectrum of the pure PDA film. Only two peaks are near the area of interest. One lower than the peaks of the catalyst with 535.2770 m/z and one higher mass with 591.3354 m/z. Therefore, the peaks of PDA film have a mass difference that is big enough to not interfere the measurements of the free catalyst. Also, a functionalized film without washing was measured. The spectrum is shown in Figure 21. The mass spectra of the functionalized film without any washing steps shows clearly two peaks of the catalyst. The highest intensity is found for the peak of the catalyst where chlorine was substituted with CN and a proton (576.0993 m/z) and the peak of the catalyst without the chlorine (548.1031 m/z) appears with lower intensity. This indicates that not all the catalyst during the functionalization (chapter 3.1.2) covalently bound to the PDA film. With respect to the final system were the catalyst is covalently bound only the covalently bound catalyst is of interest for further investigation. Because of this several washing procedures were tested to remove the remaining free catalyst. All washing procedure were done after rinsing the films with MilliQ water, drying under nitrogen flow and with acetonitrile as solvent. The tested washing procedure are listed in the table below.

Table 2: Washing procedures for the functionalized films with the reaction time, the ration of the solution used for the functionalization, the washing time and if ultra-sonication was used.

Reaction time	$V_{\text{catalyst in MeCN}}$: V_{PB}	Washing time	Ultra sonication
18 h	1:9	Rinsed shortly	No
18 h	1:9	1 min	No
18 h	1:9	1 min	Yes
18 h	1:9	5 min	No
18 h	1:9	5 min	Yes
18 h	1:9	30 min	No
18 h	1:9	30 min	Yes
18 h	1:9	2 h	No
18 h	1:9	24 h	No
18 h	1:9	60 min every 5 min exchanging the solvent	Yes
3 h	1:9	60 min every 5 min exchanging the solvent	Yes
18 h	1:99	60 min every 5 min exchanging the solvent	Yes
18 h	1:999	60 min every 5 min exchanging the solvent	Yes

All films showed a clearly detectable amount of free catalyst on the surface. Only the films which were washed for 60 min with ultra-sonication and exchanging the acetonitrile every five minutes showed that the removing of the free catalyst from the surface was efficient because only peaks of low intensities could be found for the free catalyst. Because this method do not show the covalently bound catalyst further analyzation is needed to prove that the covalently bound catalyst is still there. Also, only the film with the lowest concentration of catalyst for the functionalization showed two peaks of non-bound catalyst with higher intensity than the background (see Figure 22). All MALDI-Imaging spectra are shown in the appendix (Figure 42 to Figure 53).

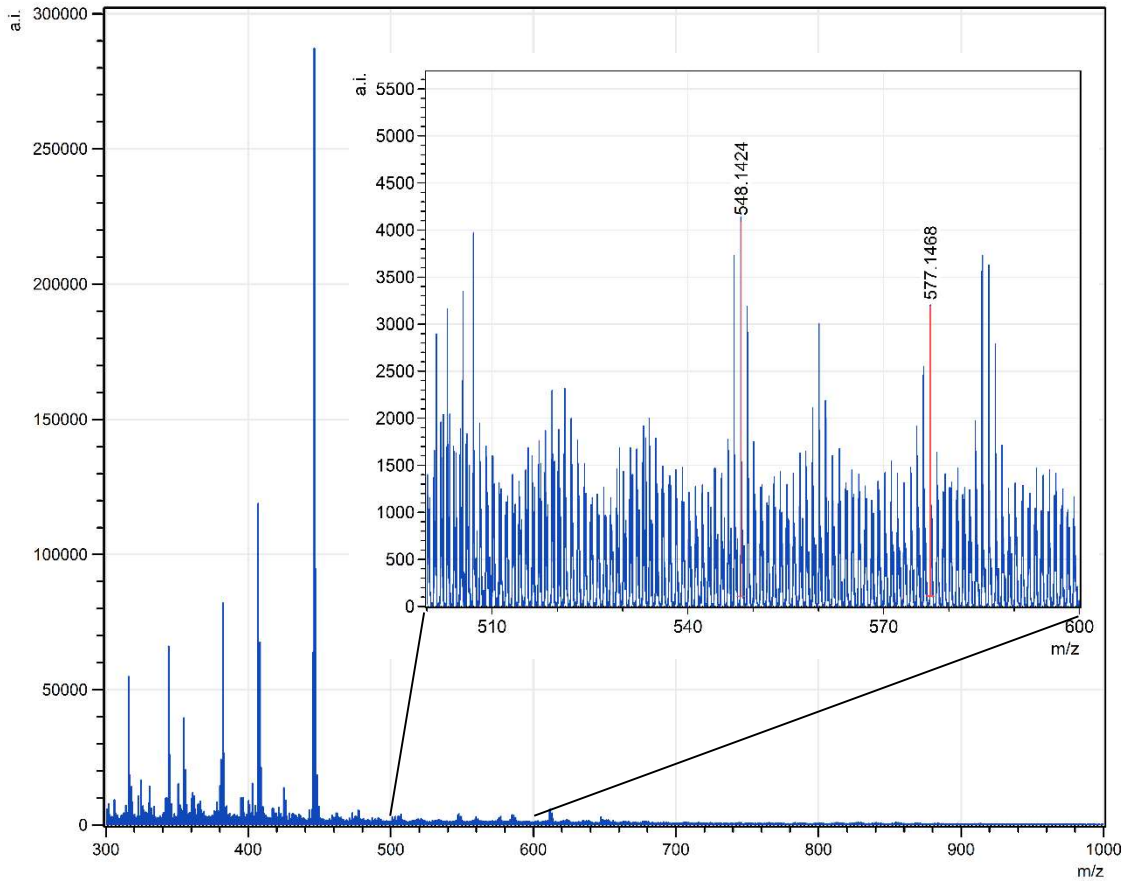

Figure 22: Mass spectra of the film functionalized with a ratio of 1:999 catalyst in MeCN (0.3mg/mL) to phosphate buffer (pH = 7) and after ultra-sonication for 60 min with exchanging the acetonitrile every 5 minutes.

As shown in Figure 22 the two peaks of the free catalyst are slightly higher than the background. This means, with respect to the very high sensitivity of these measurements, that all the non-bound catalyst was removed during the washing procedure and only the covalently bound catalyst remained on the surface of the film. For this reason, 60 min ultra-sonication in acetonitrile with exchanging the solvent every five minutes was set as the washing procedure performed for all functionalized films that follow and from this point referred as the functionalized film.

4.2.2. ToF-SIMS measurement of the film after removing the free catalyst

After proving that all the non-bounded catalyst was removed the question whether some catalyst remained on the surface (expected through covalent bounds) was still unanswered. In order to address this problem ToF-SIMS[44] measurements were performed, to get information on the presence of the catalyst on the surface and the homogeneity of its distribution. Via ToF-SIMS depth profiling the influence of the washing procedure on the film was assessed. The same film from the MALDI-Imaging, which showed almost no signal of free catalyst, was used for ToF-SIMS measurements. To perform the measurements the matrix of the MALDI-Imaging measurement had to be removed. This was done by rinsing the film with acetone and drying afterwards under nitrogen flow. As a reference a pure PDA film was also synthesized according to the protocol.

First ToF-SIMS surface spectrometry was recorded for the catalyst, the PDA film and the functionalized film. Only the positive ion polarity spectrum is shown because the negative ion polarity spectra did not

show any signals of Rh, $RhCl_2$ or any other species related to the catalyst. This can be explained by a lower secondary ion yield for the electropositive Rh species and consequently worse detection limits in the negative polarity for such species. Also, only medium to low signal intensities related to PDA could be detected in the negative ion polarity spectra.

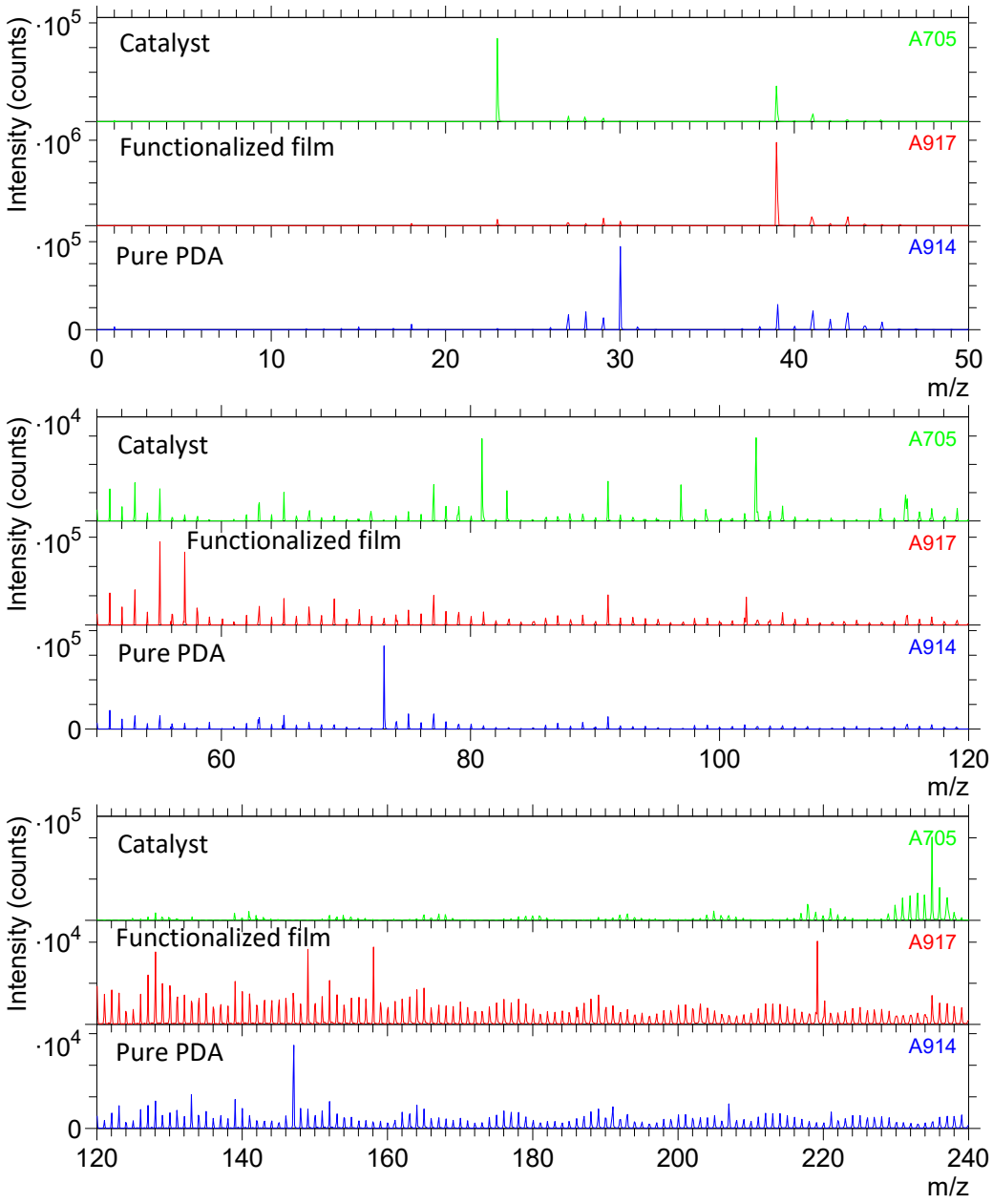

Figure 23: ToF-SIMS surface spectra (positive ion polarity spectra) from 0 m/z to 240 m/z of the catalyst (green), the functionalized film (red) and the pure PDA film (blue).

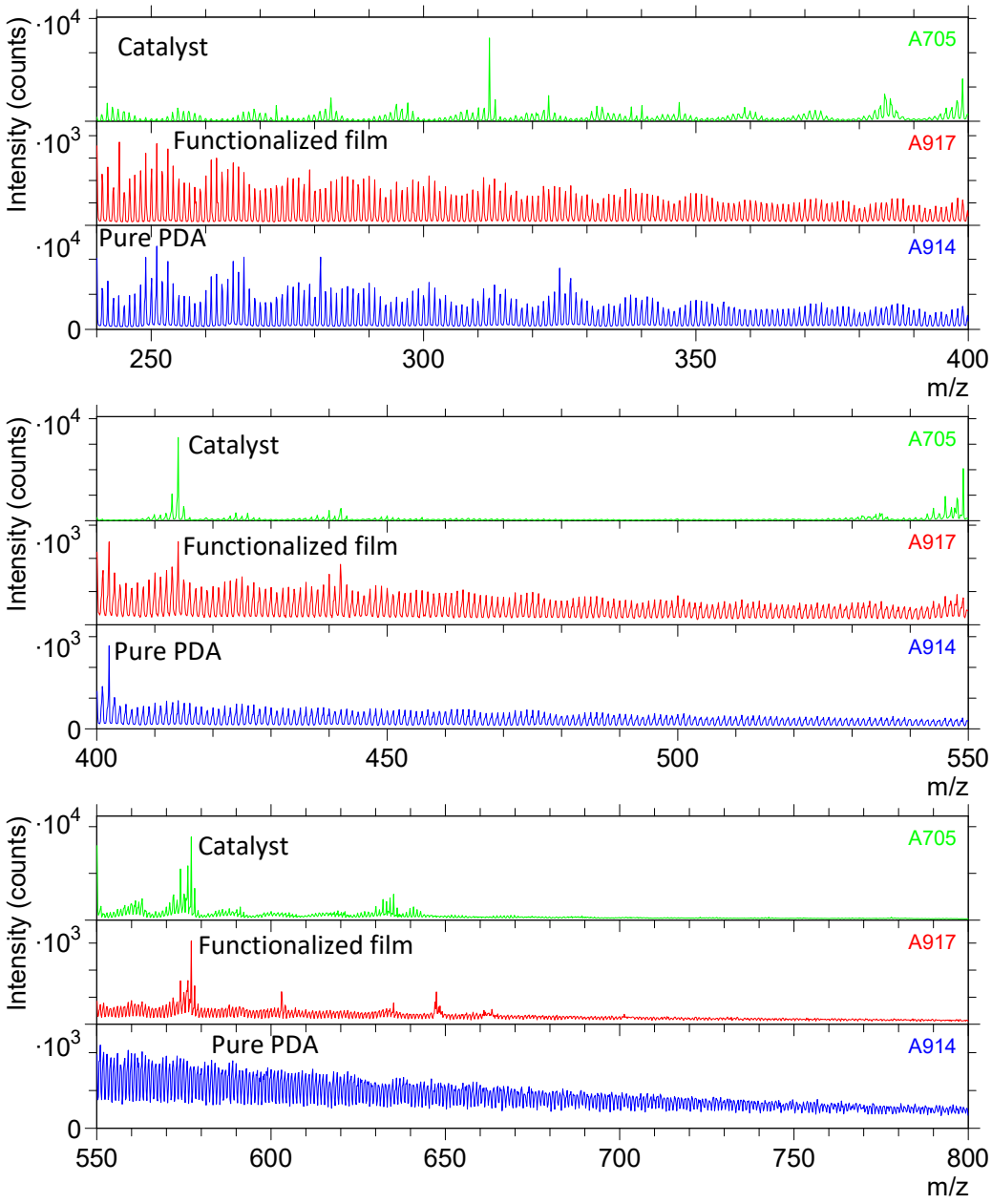

Figure 24: ToF-SIMS surface spectra (positive ion polarity spectra) from 240 m/z to 800 m/z of the catalyst (green), the functionalized film (red) and the pure PDA film (blue).

The spectra of the positive ion polarity reveal similarities between the catalyst (green) and the functionalized film (red). The signals of the reference at m/z 234.95, 235.00, 414.01, 442.01, 549.14, 577.13 and 635.18 are also found in the spectra of the functionalized film. Additionally, at m/z 102.90 a small signal of the metal ion Rh was detected. Intense siloxane signals ($Si_wC_xH_yO_z$, i.e. PDMS) could be found on the PDA film. These siloxane signals are most likely arising from the fact that the film was stored in gel boxes, which revealed intense PDMS signals in earlier analyses. Nevertheless, at m/z 402.14 a typical fragment of PDA films was detected, which is believed to originate from a stable trimer building block.[45] Most likely secondary ion suppression caused by a thin PDMS film prevented the detection of further PDA signals. In summary, the ToF-SIMS spectra still show signals of the catalyst on the film surface after washing, leading to the assumption that these catalysts are covalently bound to the PDA film.

After proving that catalyst remained on the surface of the film even after washing the question arises how homogenous the distribution of the catalyst is. To answer this question surface images (chemical maps) were acquired. Since only in the positive ion polarity spectra significant catalyst related signals were detected, only the positive ion polarity was used to obtain surface images. The chemical maps of the surface ("images") reveal a few different contrasts found for the modified film. The distributions of Si (Figure 25 B), C_2H_5O (Figure 25 E) and nitrogen containing hydrocarbon ($C_xH_yN_z$) (Figure 25 C, D, G, H) reveal several spots with diameters ranging from 10-100 µm on the surface. The potassium (K) distribution (appendix Figure 55) reveals a nearly complementary distribution to the spots. A large area of Ca (appendix Figure 56) is found in the lower right of the images. This area also shows up as a shadow in the distributions of Na (appendix Figure 54) and K. The relatively high intensities of the Na, K and Ca signal are common in ToF-SIMS measurements. The Rh distribution (Figure 25 A) is used to follow the distribution of the catalyst on the surface. It appears to show some intensity across the complete surface but with a higher concentration in the center-left area. SiC_3H_9 (Figure 25 F) indicates the distribution of the common surface contaminant PDMS, which is found most intense towards the border of the sample. This hint indicates a migration of the PDMS onto the surface of the sample originating from storing the film in a gel box.

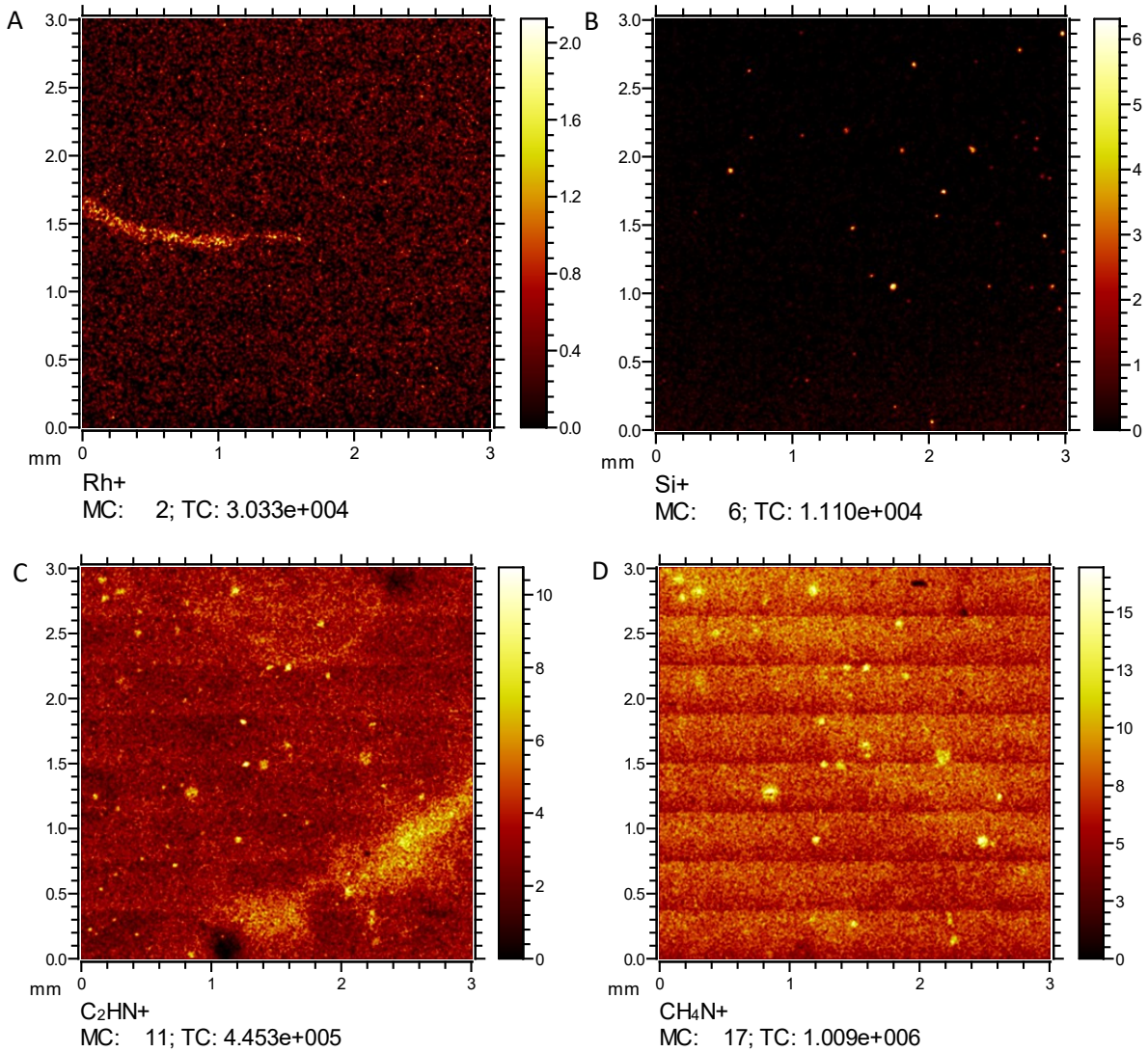

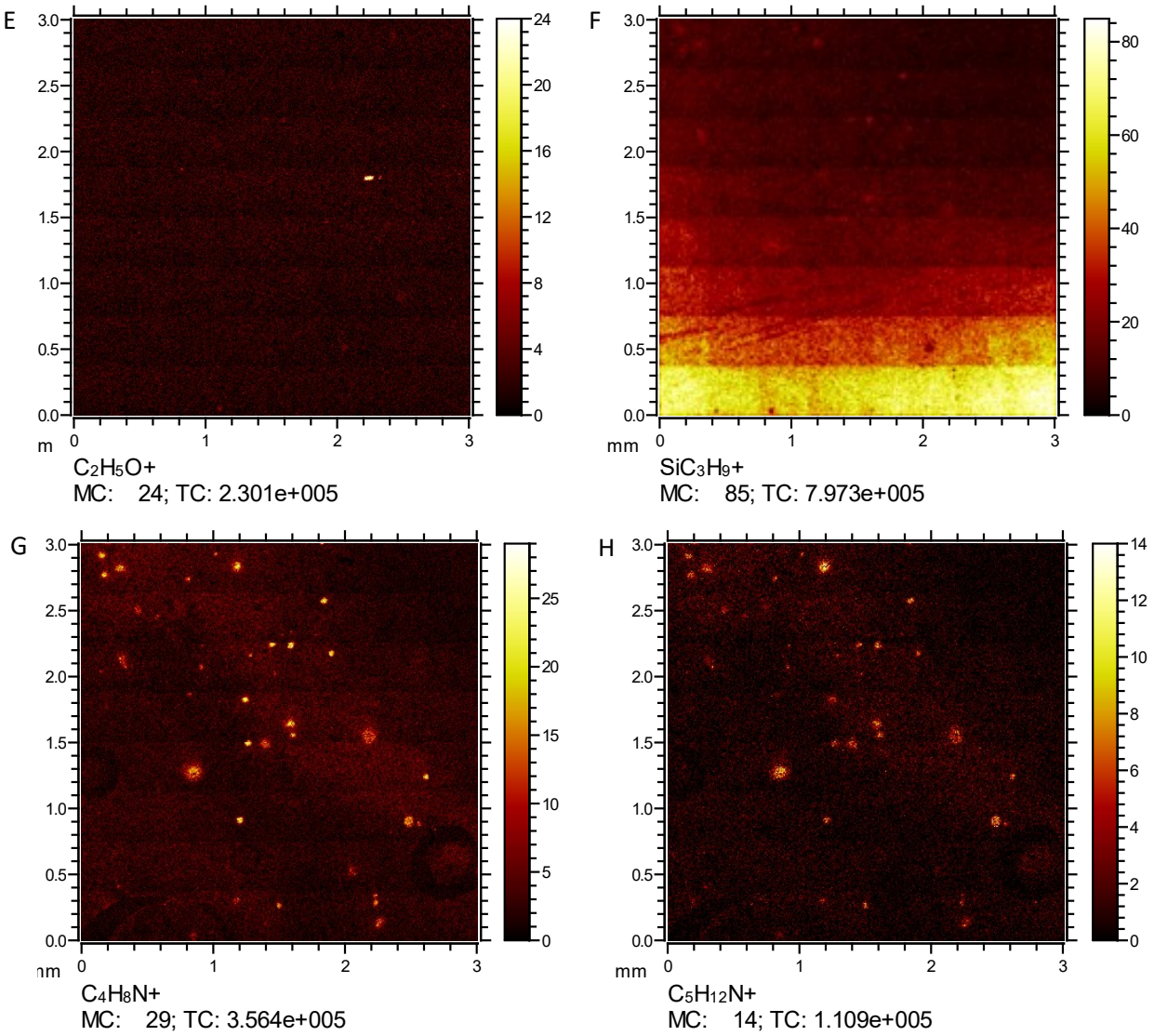

Figure 25: Chemical maps of the surface of the functionalized film for selected ions. The respective signal intensities (displayed in counts) for individual pixels are color-coded according to the key on the right of each image. MC: maximum counts per pixel. TC: total counts per image.

In the end, depth profile measurements were performed to answer the question if the film is affected by the washing procedure in the sense of removing the top layer of the film and therefore losing most of the catalyst on the surface. The positive polarity was used for these measurements because of the same reasons mentioned for the surface images and the surface spectra. The measured area was $150 \times 150\ \mu m^2$ for the analysis gun with extremely soft sputtering conditions of $2.5\ keV$ for the Ar_{1000} clusters. These conditions lead to a slow, gradual removal of the film but at the same time provided a reasonable number of data points within 1000 seconds of sputtering.

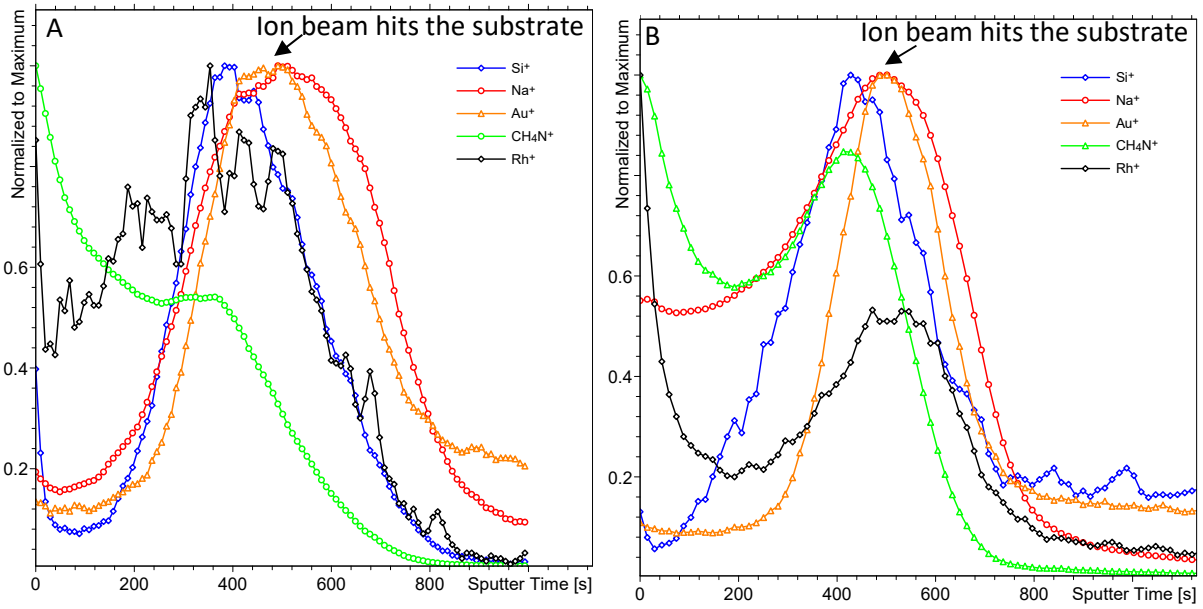

Figure 26: Depth profiles of the pure PDA film (A) and the functionalized film after washing (B). Signal intensities were normalized to its maximum values to enable comparison between the profiles. The arrows indicate the point when the substrate is exposed, i.e. the film is removed.

When comparing the depth profile of the PDA film and of the functionalized film one can see that the profiles of Na, Si and Au are similar to each other. The representative species CH_4N for the film starts its decline of about 400 sputter seconds and being completely gone after 800 sputter seconds. When the signal of CH_4N is decreasing the Au signal is increasing in both cases this leads to the assumption that the pure film and the functionalized one are about of the same height. Therefor the washing procedure is not expected to affect the film and only removes the free catalyst which is adhering to the sticky surface of PDA. The Rh signal for the pure PDA film is only in the range of 20 cts (compare Figure 57 in the appendix) which is in the range of the background noise. For the functionalized film the signal is about 200 cts, suggesting the presence of Rh in the analyzed volume (compare Figure 58 in the appendix). Furthermore, the Rh signal decreases quite fast after a few sputter seconds leading to the conclusion that the Rh and therefore the catalyst is mostly bound to the surface. ToF-SIMS measurements for the unwashed film was not performed because of the high sensitivity of the measurement and the relatively high amount of catalyst used for the functionalization.

4.2.3. X-ray photoelectron spectroscopy (XPS) measurements of the functionalized film

Another method to characterize the catalyst on the surface is XPS. This method also provides the opportunity to determine if the catalyst on the surface is covalently bound to the PDA by changes in the distribution of the different bonding types of the carbon and nitrogen signal.

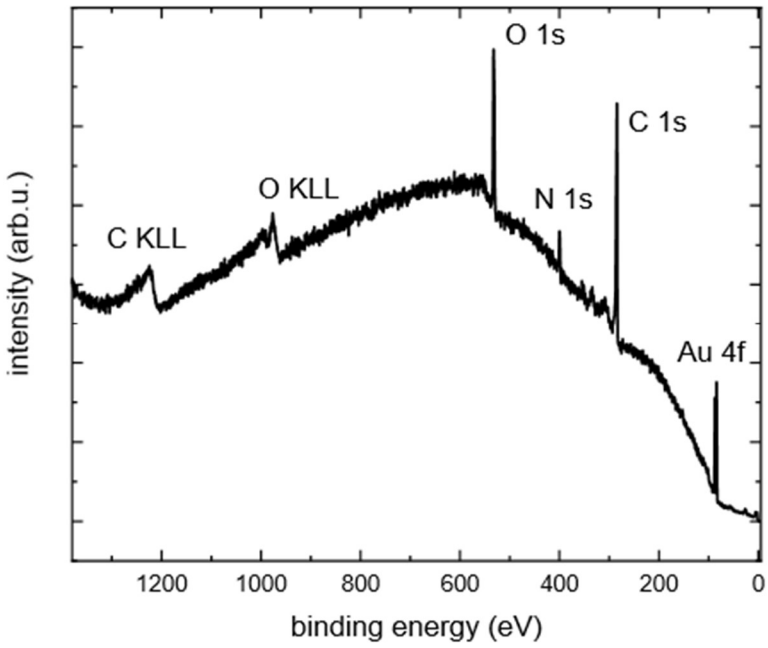

Figure 27: XPS spectra of the pure PDA film on gold.

The sample is composed of the elements C, O, N and Au with the atomic ratio of C 73.6 at%, O 20.1 at% and N 6.3 at%. Gold was not included in the calculations for all samples. The signals of the C 1s, O 1s and N 1s match qualitatively with the literature.[46] The different species are tagged in the respective spectra (for C and N see Figure 28 and **Error! Reference source not found.**, for O see appendix Figure 61). Also, the reference signals of Rh and Cl are not visible as expected (see appendix Figure 62 and Figure 63).

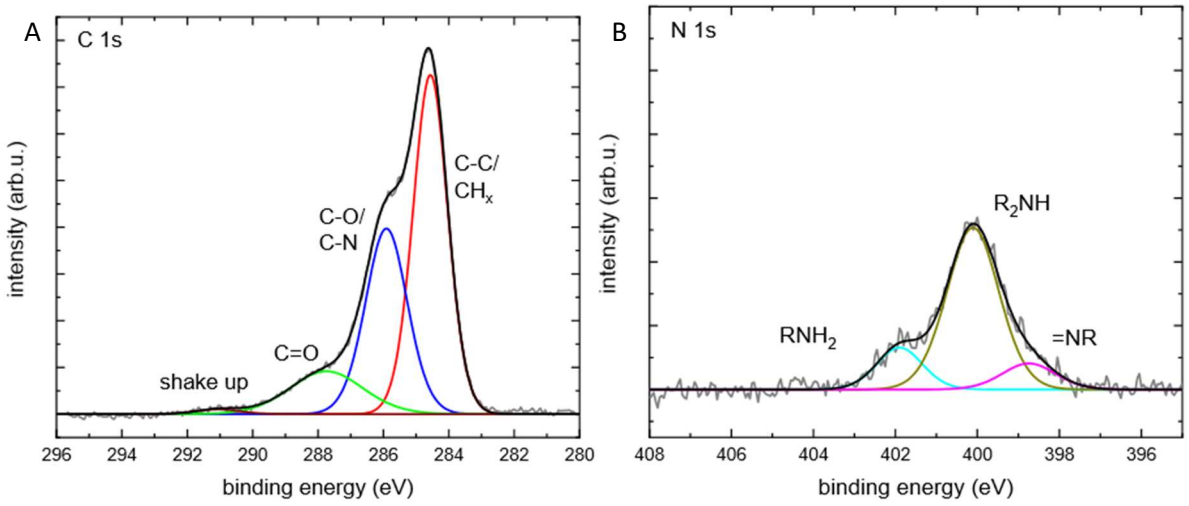

Figure 28: XPS spectra of the C 1s (A) signal (black) with the different species C-C and CH_x (red), C-O and C-N (blue) and C=O (green), and of the N 1s signal (B) arising from the R_2NH (yellow), RNH_2 (cyan) and =NR (magenta).

For the C 1s spectra the different contributions to the signal are subject to the structure of PDA. The most bounds in PDA are carbon-carbon single and carbon-hydrogen bounds. Therefore, the signal of these have the highest contribution to the C 1s signal followed by the signal of carbon-oxygen single and carbon-nitrogen single bounds. The lowest amount of bondages is from carbon-oxygen double bounds. The same is true for the N 1s spectra. Most of the nitrogen bounds in PDA are secondary amines bounds resulting in a high contribution of this bounds to the N 1s signal. Notably, the low

contribution of the imine bounds to the signal which should increase if the catalyst is covalently bound after the functionalization. These signals should increase if the catalyst is covalently bound to the PDA through Schiff base reaction. Also, the low signal of the primary amine should increase with respect to the Michael addition of the catalyst and PDA.

Therefore, a functionalized film after the washing procedure was measured. Which is also composed of carbon, oxygen and nitrogen but it also shows a very small rhodium signal. For the different elemental spectra see appendix. Gold was again not included in the calculation of the atomic ratio which are for carbon 70.9 at%, oxygen 21.1 at %, nitrogen 7.9 at% and rhodium 0.1 at%. Also, the C 1s, O 1s and N 1s signals are qualitatively from PDA and the additional C and N groups (C-C, C-N) of the catalyst are not distinguishable from PDA. The rhodium signal with 0.1 at% is at the detection limit of the instrument but because of the fitting binding energy and the difference of the Rh $3d_{5/2}$ and Rh $3d_{3/2}$ signal of 4.7 eV (see appendix Figure 68) it is sure that this signal belongs to rhodium. A chlorine signal was not detected but because of the cross section which is seven times lower for chlorine than for rhodium it is believed that the chlorine signal is too small to be detected. With respect to the rhodium signal the presence of the catalyst on the surface is proven. To prove a covalently bounding a more intense signal was needed. Therefore, an unwashed film was measured (see appendix Figure 69) but still the signal was not intense enough.

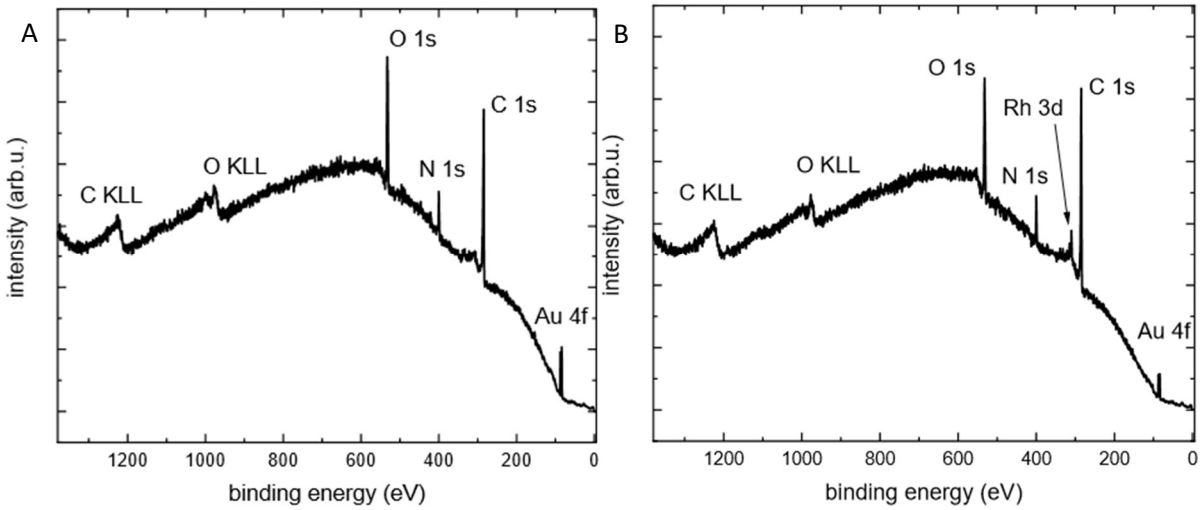

Figure 29: XPS spectra of the functionalized film after the washing procedure with a ratio of 1:999 catalyst to phosphate buffer for functionalization (A) and of the unwashed film functionalized with a ratio of dissolved catalyst to phosphate buffer of 1:9 (B).

But to prove the covalently bound between the catalyst and PDA a higher signal was needed. Therefore, a films which was functionalized with a ratio of dissolved catalyst to phosphate buffer of 1:9 was measured before washing. This sample was composed of carbon, oxygen, nitrogen, rhodium, chlorine and gold with atomic ratio as follows (gold not included), carbon 74.1 at%, oxygen 16.1 at%, nitrogen 8.3 at%, rhodium 0.7 at% and chlorine 0.5 at%. As the previous samples the structure of PDA is good to see and the related C, N and O spectra are related to the PDA spectra of these elements. The only difference in the spectra are the contribution of the carbon-nitrogen single bound in the C 1s signal which is higher compared to the pure PDA.

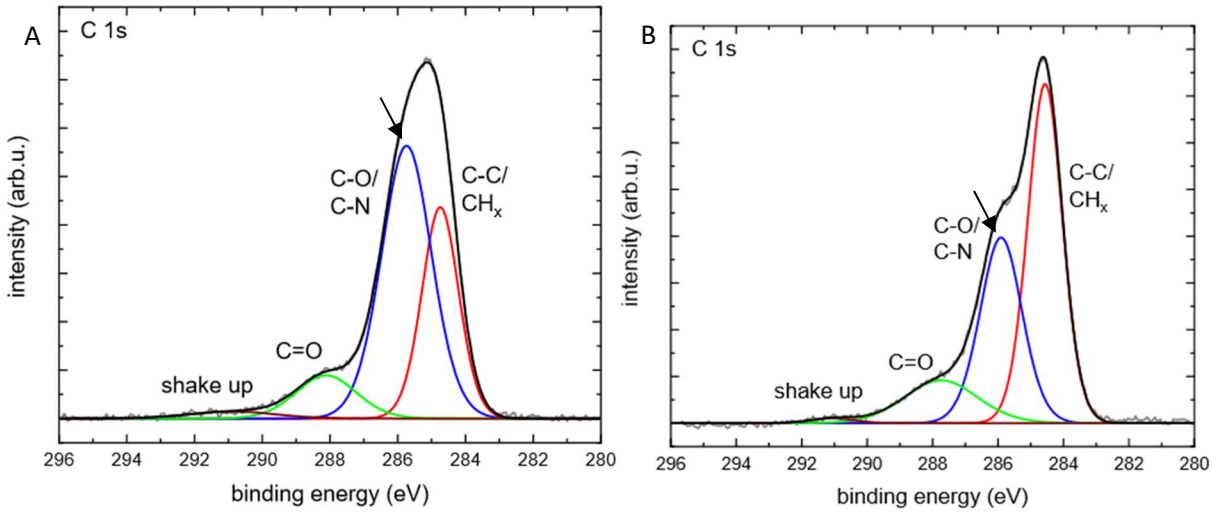

Figure 30: XPS spectra of the C 1s signal of the unwashed film functionalized with a ration of dissolved catalyst to phosphate buffer of 1:9 (left) and of the pure PDA film (right).

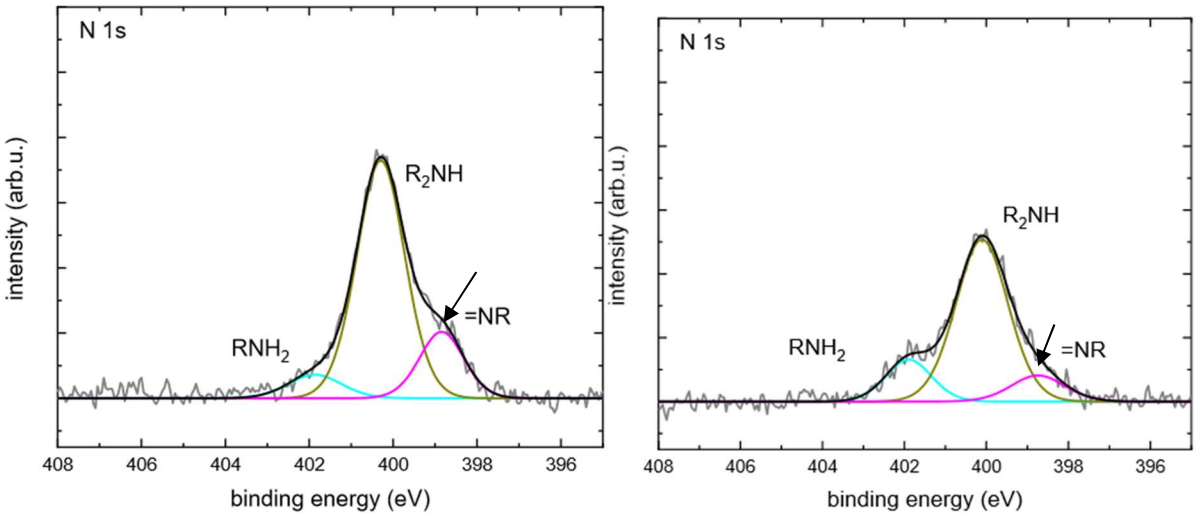

Figure 31: XPS spectra of the N 1s signal of the unwashed film functionalized with a ration of dissolved catalyst to phosphate buffer of 1:9 (left) and of the pure PDA film (right).

Also, the contribution of the imine to the N 1s signal is higher compared to PDA. The higher contribution of these two bounds to the related signal are most likely because of the covalently bounding of the catalyst through Michael addition and Schiff base reaction as mentioned above. Additionally for this sample a signal for chlorine was detected because of the signal to noise ratio of chlorine the theoretically ratio of chlorine to rhodium (1:1) is in accordance with the spectra.

After proving the covalently attachment of the catalyst to the surface also the washed film was measured to check that the washing does not affect the attachment of the catalyst.

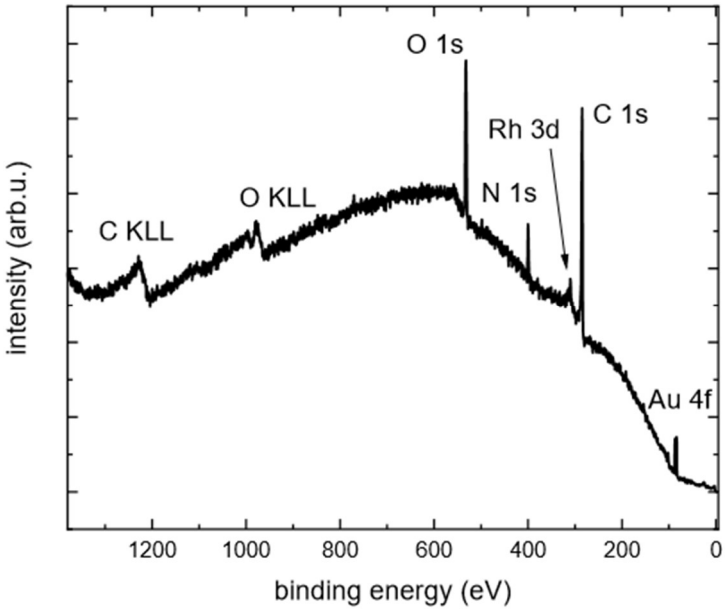

Figure 32: XPS spectra of the washed film functionalized with a ratio of dissolved catalyst to phosphate buffer of 1:9.

Like the last sample this one contains the elements carbon, oxygen, nitrogen, rhodium, chlorine and gold with the following atomic ratio of carbon 71.5 at%, oxygen 19.7 at%, nitrogen 8.0 at%, rhodium 0.4 at% and chlorine 0.4 at%. All spectra are qualitatively equal to the last sample and the theoretically ratio of rhodium to chlorine (1:1) is shown by the spectra. The only differences are for the carbon-nitrogen bounds (C 1s, blue), the imine bounds (N 1s, magenta), the rhodium and chlorine. All these boundary signatures are reduced after washing which is also shown by the atomic ratio. With respect to the accuracy of the measurement only the half of the catalyst (Rh and Cl signal) is remaining after the washing. But because the binding energies of these species and also no new species are detected it led to the conclusion that the catalyst is still on the surface and identically bound as before the washing.

4.2.4. Reduction of nicotinamide adenine dinucleotide (NAD^+) catalyzed by the functionalized film

To prove that the catalyst is still active after binding to the PDA film the thermochemical reduction of nicotinamide adenine dinucleotide (NAD^+) was performed. Two films were used with a high concentration of catalyst by using the ratio of 1:9 of dissolved catalyst to phosphate buffer and with a low concentration using a ratio of 1:999. The functionalization was done by using the protocol.

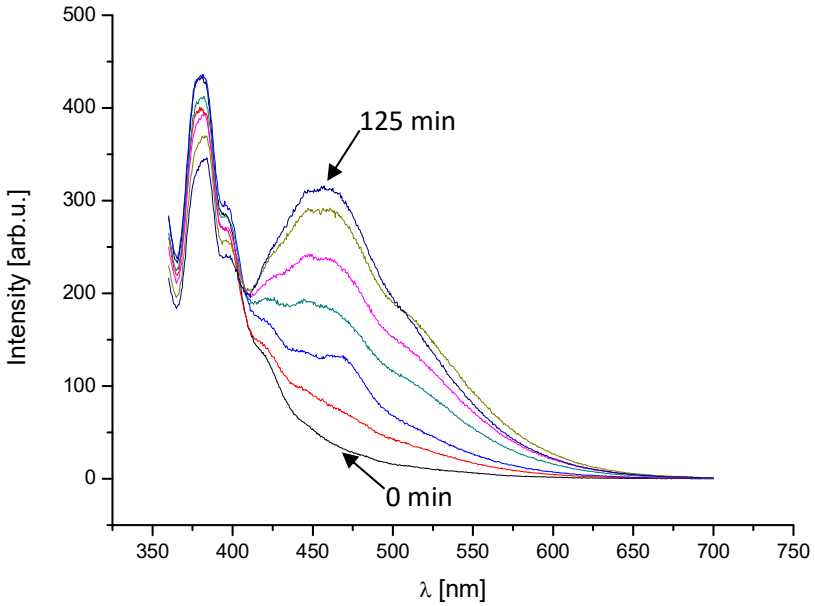

Figure 33: Emission spectrum of the thermochemical reduction of NAD^+ catalyzed by the functionalized film (high concentration) after 0 min (black), 10 min (red), 25 min (blue), 50 min (cyan), 75 min (magenta), 100 min (dark yellow) and 125 min (navy blue) of heating.

Only in the emission spectrum of the thermochemical reduction of NAD^+ catalyzed by the functionalized film with high catalyst concentration a product peak at 460 nm could be observed. It is believed that due to the low amount of product the absorption spectrum is not sensitive enough to show a peak. Nevertheless, this suggests that the catalyst which is covalently bound is available for catalysis. To be sure that this peak is a result of the reduction control experiments were performed with the film and sodium formate and a homogenous catalysis with the same catalyst were performed under the same conditions. For the film with only sodium formate no emission peak at 460 nm appeared and for the absorption spectrum only noise could be observed. The homogenous catalysis was stopped after 25 min because the detection limit was almost reached for the absorption and emission spectra. It is believed that the homogenous catalysis has a higher turnover number compared to the heterogenous at the films because of thermodynamic reasons.

4.3.CdSe@CdS nanorods in solution

4.3.1. Stabilization of the coated nanorods

To characterize the final system in which nanorods are embedded the nanorods and the functionalization of them are studied in solution. Therefore, the nanorods were coated with PDA using the coating procedure described in Chapter 3.2.1. After the coating it was found that the coated nanorods were only stable in MilliQ water and Tris-buffer (pH = 8.5, the same used for the coating). In other solvents and pH values aggregation followed by precipitation of the coated nanorods occurred (see Figure 34).

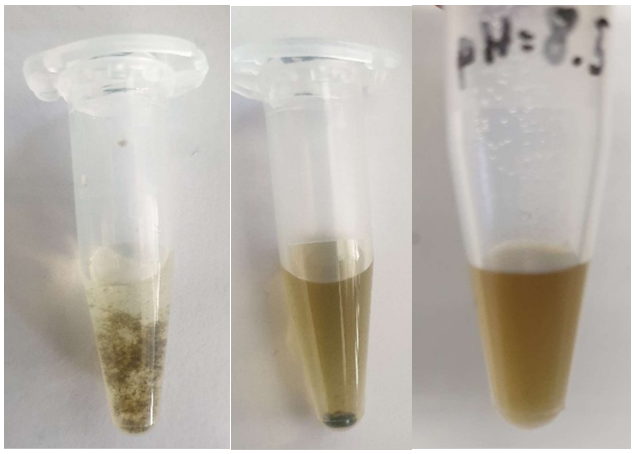

Figure 34: coated nanorods in 100 mM KCl (pH = 2.87)(left), in phosphate buffer (pH = 8.2) (middle) and Tris-buffer (pH = 8.5)(right).

The aggregation of the particles depends less on the pH than on the salt concentration in solution. This was shown by zeta potential measurements by Maria Wächtler from Leibniz Institute of photonic technologies. As Figure 35 (A) shows the zeta potential slightly increased from pH 5 to 9. A sharp decline was observed for pH 11. Figure 35 (B) shows the dependency of the zeta potential to the concentration of KCl in a pH buffer solution of coated nanorods. For low concentrations it leads to a decrease but for high concentrations to an increase of the zeta potential. The temporal evolution of the zeta potential at pH 5 and [KCl] = 50 mM (Figure 35 C) shows that the zeta potential decreases for ~3 minutes and stabilize afterwards. But there is still no answer why and how the coated nanorods aggregate in buffer solution and pH and why they are only stable in pure water and Tris buffer with pH 8.5.

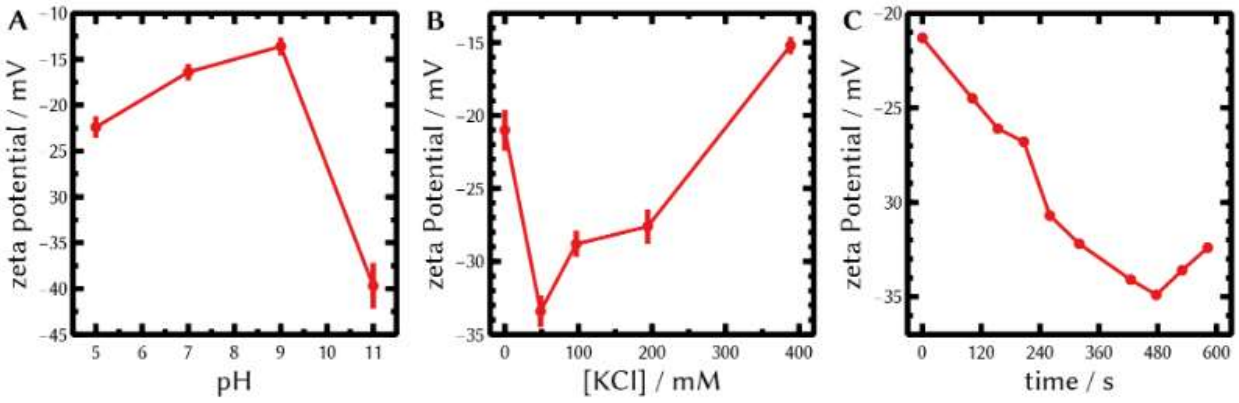

Figure 35: (A) zeta potential of coated nanorods in different PBS buffer (c = 50 mM) solutions. (B)Zeta potential of coated nanorods in PBS buffer (c = 50 mM, pH = 5) with different concentrations of KCl. (C) Temporal evolution of zeta potential at pH 5 (c = 50 mM).

To stabilize the coated nanorods in solution they were functionalized with PEG-SH using the procedure described in Chapter 3.2.3. It was found that the PEG stabilizes the coated nanorods in phosphate buffer (pH = 8.2) and KCl buffer (pH = 2.87) (see Figure 36). Therefore it was possible to get dispersions which are stable for several days.

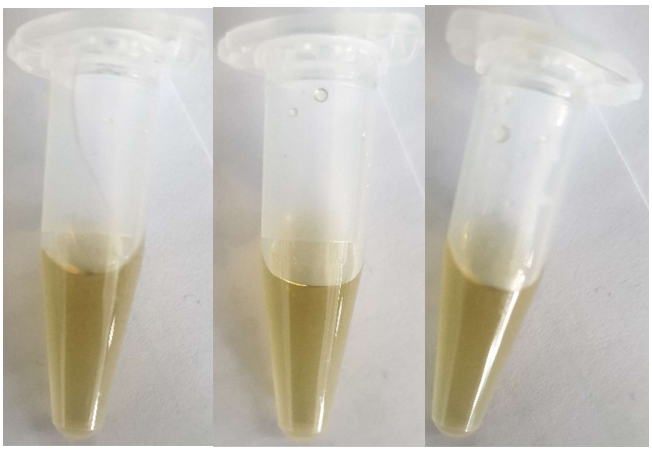

Figure 36: coated nanorods functionalized with PEG in 100 mM KCl (pH = 2.87) (left), phosphate buffer (pH = 8.2) (middle) and Tris-buffer (pH = 8.5) (right).

4.3.2. Characterization of the coated nanorods

After stabilizing the coated nanorods it was possible to characterize them also with the catalyst attached after proving for the films that the functionalization worked. The different samples were synthesized with the methods described in Chapter 3.2.

4.3.2.1. Absorption

After coating and functionalizing the nanorods which are supposed to act as light harvesting system absorption measurements were performed to check the range of the spectra which can be used for absorption.

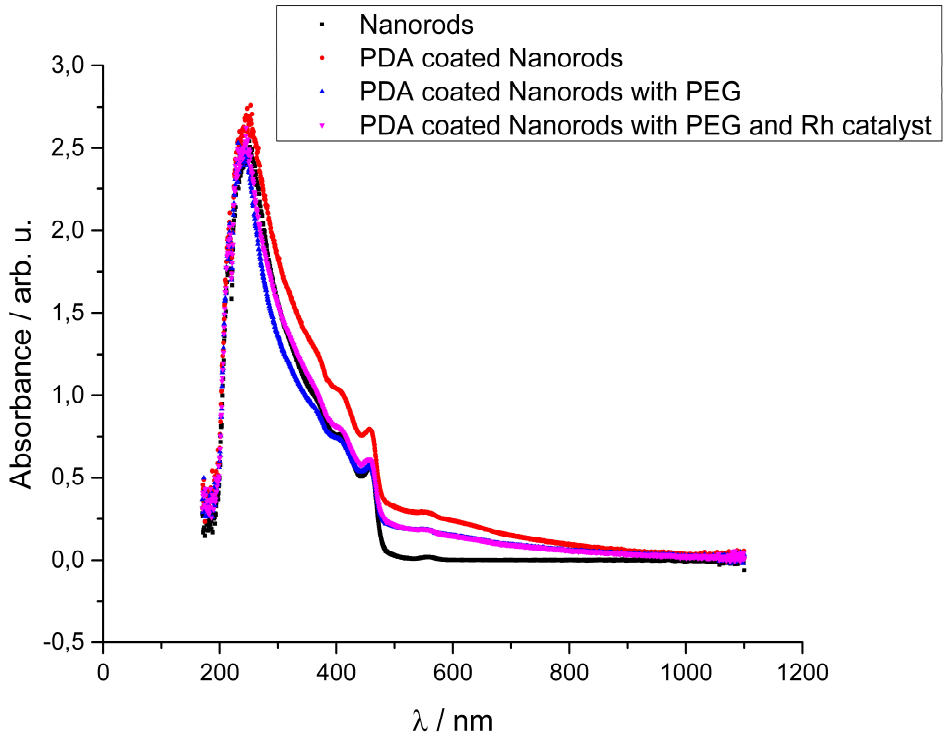

Figure 37: Absorption spectra of the pure nanorods (black), the PDA coated nanorods (red), the PDA coated nanorods with PEG (blue) and the complete functionalized nanorods (magenta).

The black spectrum shows the typically spectrum of CdSe@CdS dot/rod structure. Referring to the literature[31] the low energy peak (560 nm) belong to the first electronic transition in the CdSe dot. The peak at 460 nm is associated to the lower transition to the CdS shell. The remaining peaks/shoulders are a result to the contribution of the rod shape.

The three sample of the coated nanorods with different functionalization show the same shape as the pure nanorods with just higher absorbance. It is believed that the absorbance is lower for the functionalized nanorods with PEG and PEG + catalyst because of the losses during the purification. Also it is clear to see that the PDA increases the absorption over the complete spectra especially from 500 nm to 900 nm due to the optical properties of PDA.

4.3.2.2. Dynamic light scattering (DLS) and high-resolution transmission electron microscopy (HRTEM)

DLS measurements were performed for the pure nanorods (NR), the PDA coated (cNR), coated and functionalized with PEG (cNR+PEG) and for the coated ones functionalized with PEG and catalyst (cNR+PEG+cat) (see appendix Figure 92 to Figure 95). For all samples, even for the pure nanorods, aggregation could be observed in DLS experiments, such that the hydrodynamic radius of a single rod could not be measured which seems to be impossible. However, for the pure nanorods two dynamic radii were found $R_{\mathrm{h1,\,NR}}=10.3\ \mathrm{nm}$ and $R_{\mathrm{h2,NR}}=240\ \mathrm{nm}$. The main part of the scattering intensity resulting from the slower processes. A hydrodynamic radius of $R_{\mathrm{h,cNR}}=231\ \mathrm{nm}$ was found for the PDA coated nanorods. Whereas for the PDA coated and PEG functionalized one again two hydrodynamic radii could be observed $R_{\mathrm{h1,cNR+PEG}}=15.2\ \mathrm{nm}$ and $R_{\mathrm{h2,cNR+PEG}}=360\ \mathrm{nm}$. Also, for this sample the main part of the scattering intensity comes from the slower processes. For the PDA coated and functionalized nanorods with PEG and catalyst a hydrodynamic radius of $R_{\mathrm{h,cNR+PEG+cat}}=47\ \mathrm{nm}$ was found. But the peaks of this sample were mostly bi-, tri- or multi-modal and not baseline separated. Therefore, this hydrodynamic radius is not reliable and will not be furthered considered. With respect to the fact that all samples showed aggregation the hydrodynamic radii of the pure nanorods and the PDA coated ones are quite the same. The PDA coated and PEG functionalized ones show a much bigger hydrodynamic radius which is believed due to the good water absorbing ability of PEG.

In addition, HRTEM measurements were performed to determine the thickness of the PDA coating and the functionalization. The same samples used for the DLS measurements were analyzed.

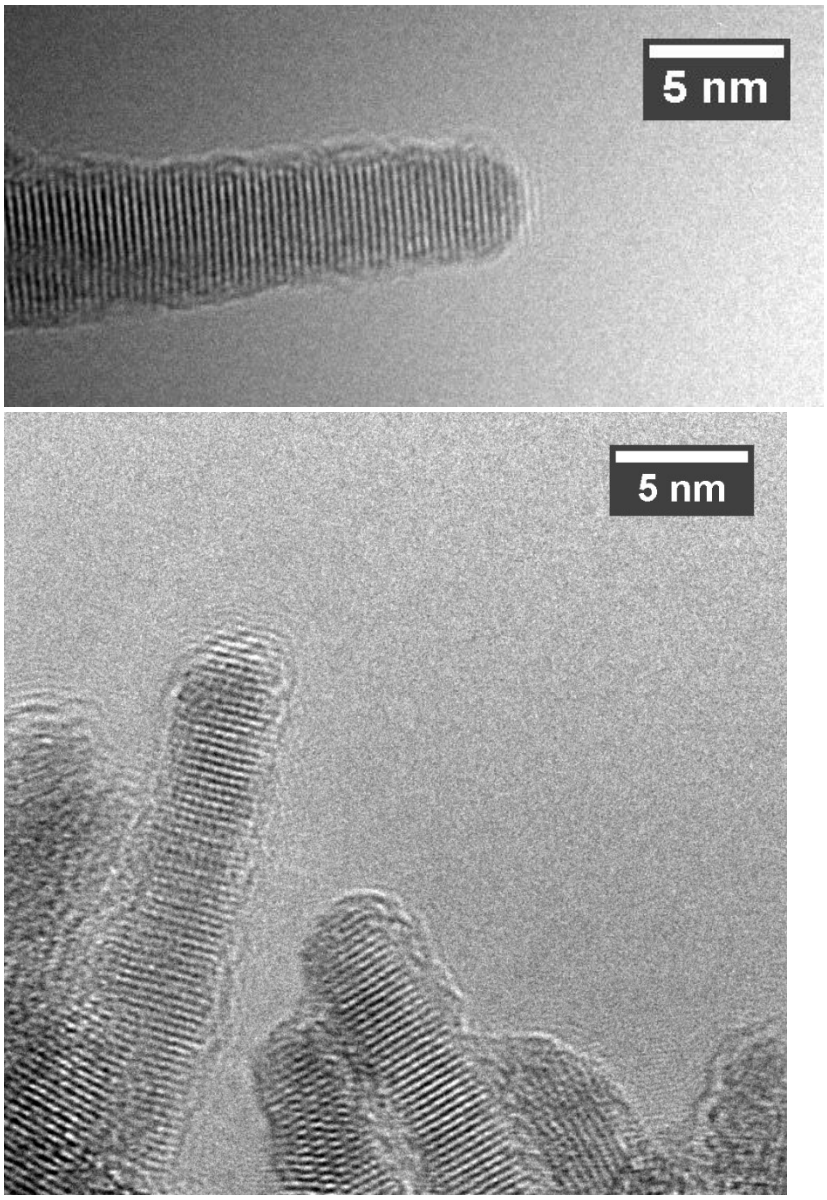

Figure 38: TEM picture of the pure nanorod with ligand (top) and of the PDA coated nanorods (bottom).

For the pure nanorods there is clear a layer of the ligand with a thickness of 1.1 nm to see. Also, the TEM picture of the PDA coated nanorods shows a layer around the nanorods of 1.2 nm. This leads to the assumption that the ligand is properly exchanged during the coating with respect to the intense color change. Furthermore, the PDA formed during the drying of the sample for the HRTEM measurement a film like structure. It is believed that this is caused by aggregation during the drying. For the functionalized nanorods no difference in the shell size was observed (compare Figure 96 and Figure 97 in the appendix). The functionalization with PEG made it difficult to get a good picture because during the drying the PEG formed also a layer like PDA. In addition, EDX was measured for the PDA coated nanorods functionalized with PEG and catalyst to verify the presence of the catalyst. But no catalyst related signal could be detected. It is believed that this is because of the low catalyst concentration.

4.3.2.3. Diffusion Ordered Spectroscopy (DOSY)

In order to be able to determine whether the functionalization of the system is covalent, DOSY measurements of the pure nanorods, the PDA-coated nanorods, the PEGylated and the PEG and

catalyst-functionalized PDA-coated nanorods were measured in D_2O. The respective diffusion coefficient could be obtained from the measured spectra with the topspin software. To compare the different synthesis stages of the system, the DOSY spectra of the pure nanorods, the PDA coated, the coated and PEGylated, and the coated and functionalized with PEG and catalyst nanorods were overlaid (individual spectra see Appendix). The DOSY spectrum of the pure catalyst could not be measured due to the low solubility of the catalyst in the solvent used.

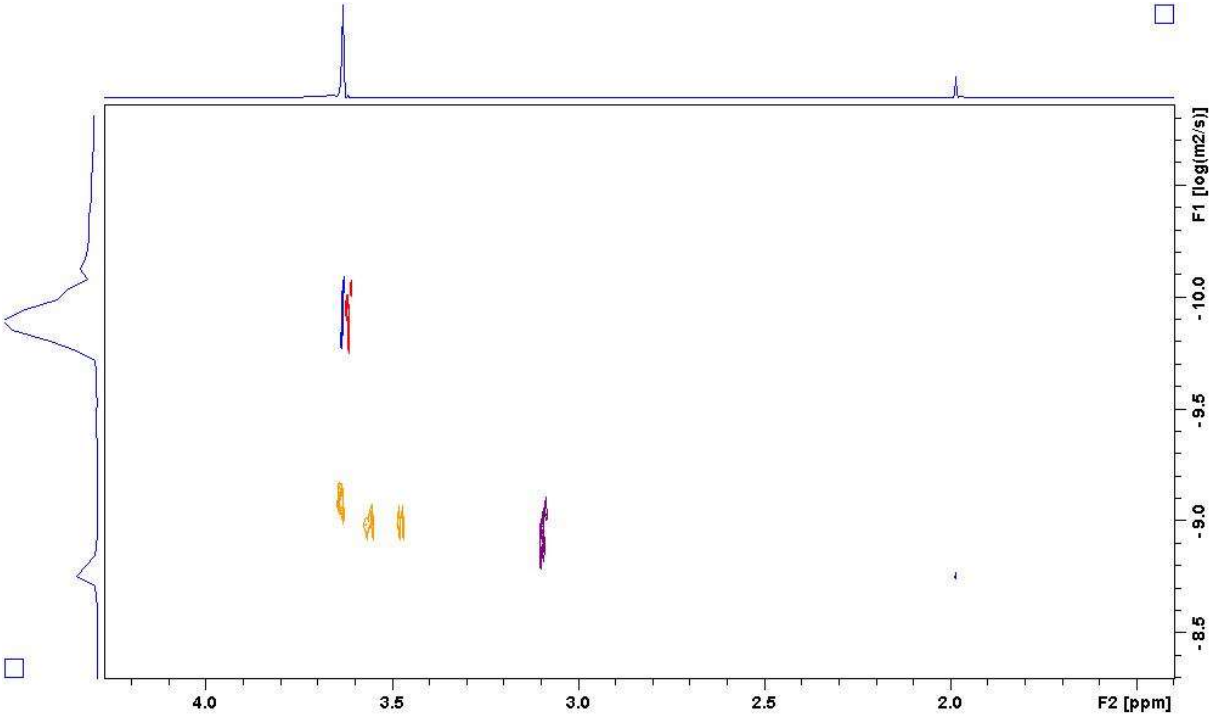

Figure 39: The stacked DOSY spectra of the pure nanorods (purple), the PDA coated (yellow), the coated and PEGylated (red) and the coated and functionalized with PEG and catalyst (blue).

The stacked DOSY spectra show that after coating the nanorods with PDA lead to new peaks in the spectrum which suggests that the coating of the nanorods with was successful. The same is true for the PEGylation of the coated nanorods. Again, the peaks of the coated nanorods disappear and a new peak is visible. All peaks show different diffusion coefficients listed in the table below.

Table 3: Diffusions coefficients D of the different synthesis stages.

Sample	$D\left[\frac{\mathrm{m}^2}{\mathrm{s}}\right]$
Pure nanorods	$1.055 \cdot 10^{-9}$
PDA coated nanorods	$9.097 \cdot 10^{-10}$
PDA coated and PEGylated nanorods	$1.595 \cdot 10^{-10}$
PDA coated and functionalized with PEG and catalyst (shift (3.731-3.428)	$1.568 \cdot 10^{-10}$
PDA coated and functionalized with PEG and catalyst (shift 2.028-1.942)	$1.599 \cdot 10^{-9}$

With respect to the different diffusion coefficients one can say that with each synthesis step of the system a new species is formed. If the functionalization is due covalent bonds all peaks should have the same diffusion coefficient which is true for all samples except the coated nanorods functionalized

with PEG and the catalyst. The peak from 2.028 ppm to 1.942 ppm (the methylene groups of the Cp^* of the catalyst) has a different diffusion coefficient than the peak of the PDA coated and PEGylated nanorods. Because the functionalization with the catalyst does not change the size of the particle only minimally and thus have not change the diffusion coefficient. Also the fact that no DOSY spectrum of the pure catalyst could be measured which is why no statement can be made as to whether the diffusion coefficient for the methylene groups of the Cp^* changes as a result of the functionalization and would thus confirm the covalent attachment. Also, it is questionable if the attached catalyst can give a signal because PDA has free radicals and therefore is in some spots paramagnetic, which makes NMR measurements challenging. Because of this, it is more likely that the signal from 2.028 ppm to 1.942 ppm belongs to impurities or unbound catalyst. However, since the comparison with the pure catalyst is missing, as previously mentioned, no final statement can be made regarding the covalent functionalization.

4.3.2.4. Reduction of Nicotinamide adenine dinucleotide (NAD^+)

To prove the hypothesis that the catalyst is covalently bound the reduction of the Nicotinamide adenine dinucleotide (NAD^+) was tested because it is believed if the catalyst is not attached the reduction would not work because no electron could be transferred. This was not tested with free catalyst because pure catalyst in solution is also able to reduce the NAD^+ thermochemical by using sodium formate as reduction agent. In addition, photocatalytic reduction was tested because the system is supposed to use light as energy source.

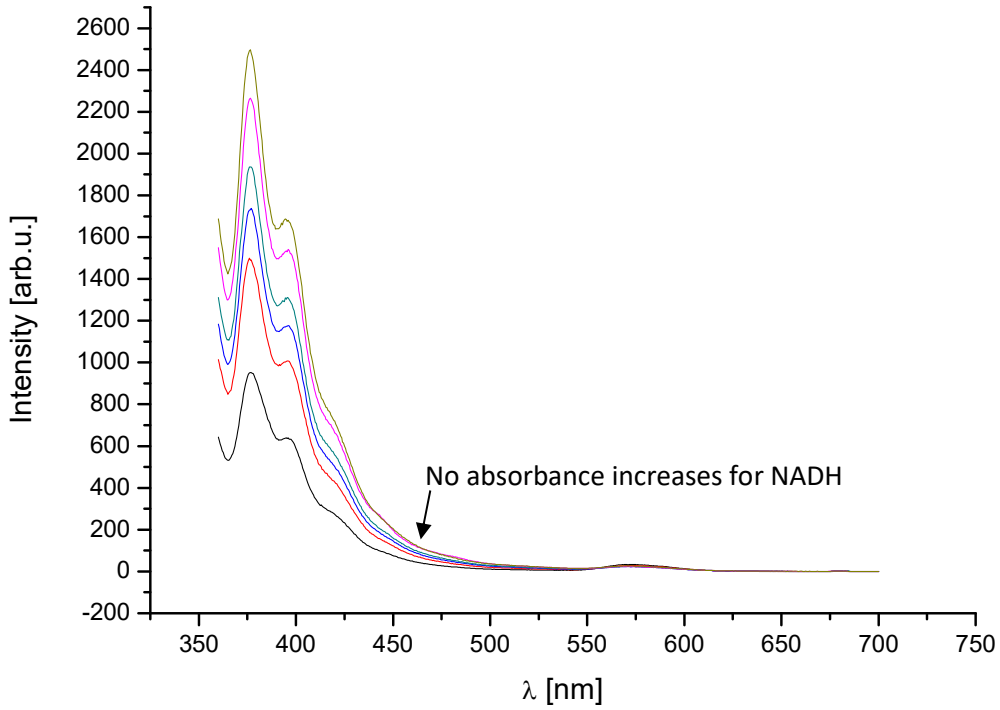

Figure 40: Emission spectrum of the thermochemical reduction of NAD^+ with the functionalized nanorods after 0 min (black), 10 min (red), 20 min (blue), 30 min (cyan), 40 min (magenta) and 50 min (dark yellow) of heating at 40 °C.

For the thermochemical reduction of NAD^+ no product peak at 460 nm can be observed. It is believed with respect to the fact that the thermochemical reduction worked for the film with a high catalyst

concentration that no product peak is observed because of the low concentration of catalyst. The Absorption spectrum also did not show any product peak (see appendix Figure 102).

In addition, a solution was prepared from the stock solutions of the functionalized nanorods, NAD^+ and water in a protective gas atmosphere in a ratio of 2:5:3. The solution was transferred to a UV/VIS cuvette and the cuvette was sealed airtight. An absorption and an emission spectrum were then recorded. The solution was then irradiated for 60 minutes with light of the wavelength 465 nm, an absorption and emission spectrum being recorded every 10 minutes.

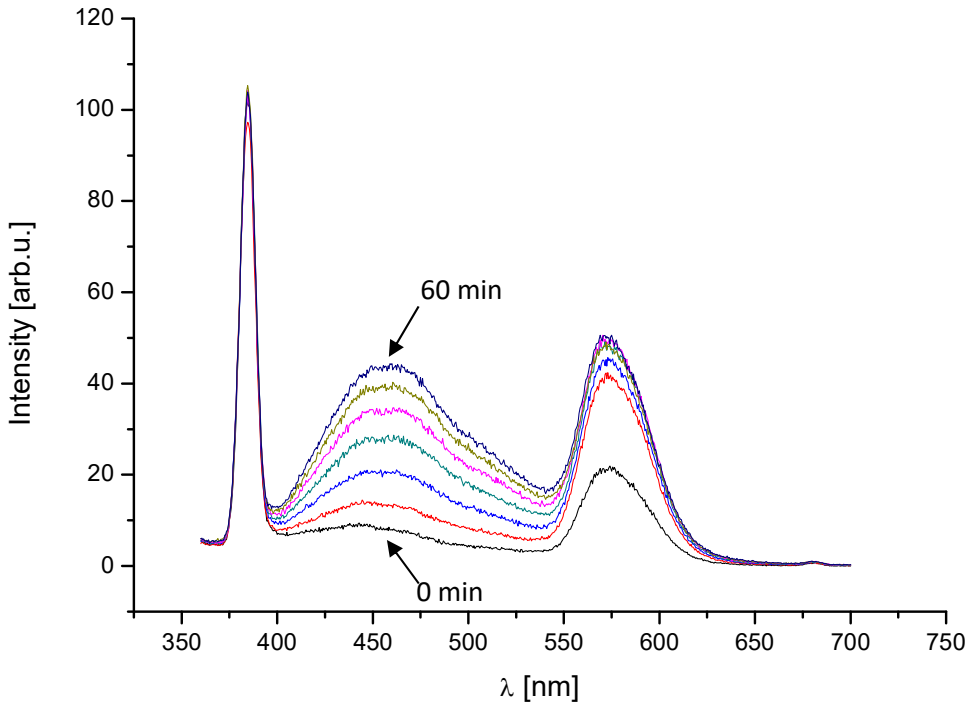

Figure 41: Emission spectrum of the photocatalytic reduction of NAD with the functionalized nanorods after 0 min (black), 10 min (red), 20 min (blue), 30 min (cyan), 40 min (magenta), 50 min (dark yellow) and 60 min (navy blue) of irradiation at wavelenght 465 nm.

A clear product peak of the reduction can be observed at 460 nm. This peak is also increasing with irradiation time which leads to the assumption that the electrons excited by light can travel through the PDA layer to the catalyst and there reduce the NAD^+. It is also surprising that even after 60 min of irradiation the reduction continues without a molecule present which can provide electrons. It is believed that this reduction can only take place because of the ability of PDA to quench the holes in the nanorods. In comparison with the thermochemical reduction catalyzed by the functionalized film only low amounts of product can be observed. Certainly, this is the case because only a low amount of functionalized nanorods were used. Also, there is method to determine the amount of the catalyst attached to the nanorods or to the film, but it is believed with respect to the used amount of catalyst for the different functionalization that on the film more catalyst is available. The absorption spectrum again did not show a product peak, but it is believed that is the fact because of the low amount of product.

To be sure that the peak at 460 nm in the emission spectrum is evoked by the reduction product control experiments were performed. Therefore three control experiments were performed, a solution of NAD^+, the pure nanorods and without the protective gas atmosphere were measured under the same conditions. All three control experiments did not show a product peak at 460 nm (see appendix Figure 103-Figure 109). Because of the spectra of the photocatalytic reduction without a protective gas atmosphere it seems that oxygen is somehow reacting with the system under these conditions. In conclusion this experiment proved that the system of nanorods, PDA and a catalyst can do photocatalysis as expected.

5. Conclusion and Outlook

In summary, the photocurrent of pure PDA films and for the coated nanorods were measured. Due to the fact that the photocurrent of the pure nanorods could not be measured it is not clear if the PDA coating reduces, increase or do not influence the photocurrent. With respect to the photocurrent of the pure PDA films it is believed that the coating should increase the resulting current. However, it could be shown that by coating the nanorods with PDA, the photoelectrons generated are not blocked and are available for the desired catalysis. It was also possible to bind a model catalyst to polydopamine without losing its catalytic activity (successful reduction of NAD^+ on the functionalized PDA film). However, it was not possible to quantify the amount of catalyst on the film surface. Due to the reduction of NAD^+ it was possible to prove that the covalently bounding of the catalyst to the PDA is not interfering the catalytic activity. For the nanorods in solution it was possible to coat them with PDA and post functionalize them with the catalyst and PEG. Even though the attachment of the catalyst on the coated nanorods was not possible to be proven by different methods (EDX and DOSY) the reduction of NAD^+ can be taken as a proof because it is believed that the reduction takes place only if the catalyst is attached to the light harvesting system. Surprisingly, the reduction could only observed for the photo catalysis by using the functionalized nanorods. Nevertheless, the amount of catalyst bound to the surface of the coated nanorods or the films is low. A higher concentration through better bounding can maybe achieved by using a different catalyst with a more reactive amine group. This could be achieved by using a catalyst which has the amine group at an alkyl side and a smaller π-system.

For the future it might be good to use a different catalyst which has a more reactive amine group. The results shown in this work show that the system used is fundamentally suitable for the target application of water splitting. However, using the system in solution instead of a film is more promising at the current time because of the big difficulties in arranging the nanorods vertically by the collaborator. Also, the protection of the nanorods should be better in solution due to the fact that the nanorods are completely covered by PDA instead for the film. If this is done for the vertically nanorods the PDA film would block a high amount of the light because of the film thickness and absorption properties of PDA. Additionally, the surface area of the system in solution is higher which allows a higher amount of functionalization. Furthermore, the reduction of NAD^+ has shown that the system does not only have to be limited to future hydrogen production (which still has to be proven). By using different catalysts, different photo catalysis may be possible in the future. For various catalysis and for the generation of hydrogen, it may also be possible to dispense the catalysts using the PDA's reducing properties and using noble metal nanoparticles (Pt and Au) instead of a catalyst. To determine the electron and hole transfer processes the interactions between CdSe@CdS nanorods will be characterized spectroscopically after the successful stabilization with PEG depending on the pH value. In order to identify the electron transfer mechanisms and to obtain possible changes in the mechanism with the pH value, results from the determination of the emission quantum yields, emission lifetimes and time-resolved transient absorption measurements as a function of the pH value of the dispersions will be combined. These measurements will be performed by Maria Wächtler from the Leibniz Institute of photonic technologies. Nevertheless, the first photoluminescence measurements of nanorods dispersed in water have shown that the photoluminescence has been quenched, which indicates a strong interaction between the matrix and the nanorods. The reason for the significantly lower photoluminescence can be both electron transfer processes from the matrix to the light-excited nanorods and from the excited nanorods to the matrix. In addition, transient absorption measurements, with which the occupation of the conduction band of the CdSe @ CdS nanorods with

electrons can be tracked, show that after excitation of the nanorods with light, a rapid electron transfer from the conduction band to the matrix takes place.

In conclusion, it can be said that the development of a film for hydrogen production has not yet succeeded in this work, but the results suggest that this will be possible in the future. In addition, the results suggest that the system with corresponding modifications has not to be limited to the production of hydrogen.

6. References

[1] G. Ajayakumar, M. Kobayashi, S. Masaoka, K. Sakai, *Dalton transactions (Cambridge, England : 2003)* **2011**, *40*, 3955.

[2] M. Wang, Z. Cui, M. Yang, L. Lin, X. Chen, M. Wang, J. Han, *Journal of colloid and interface science* **2019**, *544*, 1.

[3] J. Liebscher, R. Mrówczyński, H. A. Scheidt, C. Filip, N. D. Hădade, R. Turcu, A. Bende, S. Beck, *Langmuir : the ACS journal of surfaces and colloids* **2013**, *29*, 10539.

[4] H. Lee, S. M. Dellatore, W. M. Miller, P. B. Messersmith, *Science (New York, N.Y.)* **2007**, *318*, 426.

[5] Y. Liu, K. Ai, L. Lu, *Chemical reviews* **2014**, *114*, 5057.

[6] Q. Wei, F. Zhang, J. Li, B. Li, C. Zhao, *Polym. Chem.* **2010**, *1*, 1430.

[7] M. L. Alfieri, R. Micillo, L. Panzella, O. Crescenzi, S. L. Oscurato, P. Maddalena, A. Napolitano, V. Ball, M. d'Ischia, *ACS applied materials & interfaces* **2018**, *10*, 7670.

[8] M. d'Ischia, A. Napolitano, V. Ball, C.-T. Chen, M. J. Buehler, *Accounts of chemical research* **2014**, *47*, 3541.

[9] S. Hong, Y. S. Na, S. Choi, I. T. Song, W. Y. Kim, H. Lee, *Adv. Funct. Mater.* **2012**, *22*, 4711.

[10] C.-T. Chen, F. J. Martin-Martinez, G. S. Jung, M. J. Buehler, *Chemical science* **2017**, *8*, 1631.

[11] N. F. Della Vecchia, R. Avolio, M. Alfè, M. E. Errico, A. Napolitano, M. d'Ischia, *Adv. Funct. Mater.* **2013**, *23*, 1331.

[12] F. Bernsmann, V. Ball, F. Addiego, A. Ponche, M. Michel, J. J. d. A. Gracio, V. Toniazzo, D. Ruch, *Langmuir : the ACS journal of surfaces and colloids* **2011**, *27*, 2819.

[13] D. R. Dreyer, D. J. Miller, B. D. Freeman, D. R. Paul, C. W. Bielawski, *Chem. Sci.* **2013**, *4*, 3796.

[14] W. Yang, C. Liu, Y. Chen, *Langmuir : the ACS journal of surfaces and colloids* **2018**, *34*, 3565.

[15] Jürgen Heinze, *Angewandte Chemie* **1984**, *96*, 823.

[16] B. Stöckle, D. Y. W. Ng, C. Meier, T. Paust, F. Bischoff, T. Diemant, R. J. Behm, K.-E. Gottschalk, U. Ziener, T. Weil, *Macromol. Symp.* **2014**, *346*, 73.

[17] N. Elgrishi, K. J. Rountree, B. D. McCarthy, E. S. Rountree, T. T. Eisenhart, J. L. Dempsey, *J. Chem. Educ.* **2017**, *95*, 197.

[18] F. Harnisch, S. Freguia, *Chemistry, an Asian journal* **2012**, *7*, 466.

[19] G. A. Mabbott, *Journal of Chemical education* **1983**, 697.

[20] A. H. N. Aristov, *World Journal of Chemical Education* **2015**, 115.

[21] F. L. Huber, D. Nauroozi, A. K. Mengele, S. Rau, *Eur. J. Inorg. Chem.* **2017**, *2017*, 4020.

[22] A. K. Mengele, S. Kaufhold, C. Streb, S. Rau, *Dalton transactions (Cambridge, England : 2003)* **2016**, *45*, 6612.

[23] T. K. Todorova, T. N. Huan, X. Wang, H. Agarwala, M. Fontecave, *Inorganic chemistry* **2019**, *58*, 6893.

[24] A. K. Mengele, G. M. Seibold, B. J. Eikmanns, S. Rau, *ChemCatChem* **2017**, *9*, 4369.

[25] Alexander K. Mengele and Sven Rau, *Inorganics* **2017**, *5*, 35.

[26] T. Sick, A. G. Hufnagel, J. Kampmann, I. Kondofersky, M. Calik, J. M. Rotter, A. Evans, M. Döblinger, S. Herbert, K. Peters et al., *Journal of the American Chemical Society* **2018**, *140*, 2085.

[27] C. Haeßner, K. Köhler, K. Wussow, *Chemie in unserer Zeit* **2014**, *48*, 246.

[28] R. M. Navarro Yerga, M. C. Alvarez Galván, F. del Valle, J. A. La Villoria de Mano, J. L. G. Fierro, *ChemSusChem* **2009**, *2*, 471.

[29] Z. Pan, H. Zhang, K. Cheng, Y. Hou, J. Hua, X. Zhong, *ACS nano* **2012**, *6*, 3982.

[30] V. L. Bridewell, R. Alam, C. J. Karwacki, P. V. Kamat, *Chem. Mater.* **2015**, *27*, 5064.

[31] M. G. Lupo, F. Della Sala, L. Carbone, M. Zavelani-Rossi, A. Fiore, L. Lüer, D. Polli, R. Cingolani, L. Manna, G. Lanzani, *Nano letters* **2008**, *8*, 4582.
[32] D. V. Talapin, E. V. Shevchenko, C. B. Murray, A. Kornowski, S. Förster, H. Weller, *Journal of the American Chemical Society* **2004**, *126*, 12984.
[33] M. Aichler, A. Walch, *Laboratory investigation; a journal of technical methods and pathology* **2015**, *95*, 422.
[34] J. L. Norris, R. M. Caprioli, *Chemical reviews* **2013**, *113*, 2309.
[35] "ToF-SIMS", can be found under https://www.tascon.eu/media/de/Praxis/Analysetechniken/ToF-SIMS_de.pdf.
[36] A. Benninghoven, *Angew. Chem. Int. Ed. Engl.* **1994**, *33*, 1023.
[37] Toma Susi, Thomas Pichler, Paola Ayala, *Beilstein J. Nanotechnol.* **2015**, 177.
[38] a) "X-ray Photoelectron Spectroscopy (XPS)", can be found under https://www.kratos.com/applications/techniques/x-ray-photoelectron-spectroscopy; b) M. P. Seah, W. A. Dench, *Surf. Interface Anal.* **1979**, *1*, 2.
[39] J. Stetefeld, S. A. McKenna, T. R. Patel, *Biophysical reviews* **2016**, *8*, 409.
[40] B. Fultz, J. M. Howe, *Transmission electron microscopy and diffractometry of materials*, Springer, Berlin, Heidelberg, **2008**.
[41] J.-l. Wang, B.-c. Li, Z.-j. Li, K.-f. Ren, L.-j. Jin, S.-m. Zhang, H. Chang, Y.-x. Sun, J. Ji, *Biomaterials* **2014**, *35*, 7679.
[42] G. Loget, J. E. Yoo, A. Mazare, L. Wang, P. Schmuki, *Electrochemistry Communications* **2015**, *52*, 41.
[43] M. M. Walczak, D. A. Dryer, D. D. Jacobson, M. G. Foss, N. T. Flynn, *J. Chem. Educ.* **1997**, *74*, 1195.
[44] "TOF-SIMS", can be found under https://www.vom-muenster.de/analyseverfahren/tof-sims/.
[45] Y. Ding, L.-T. Weng, M. Yang, Z. Yang, X. Lu, N. Huang, Y. Leng, *Langmuir : the ACS journal of surfaces and colloids* **2014**, *30*, 12258.
[46] R. A. Zangmeister, T. A. Morris, M. J. Tarlov, *Langmuir : the ACS journal of surfaces and colloids* **2013**, *29*, 8619.

7. Appendix

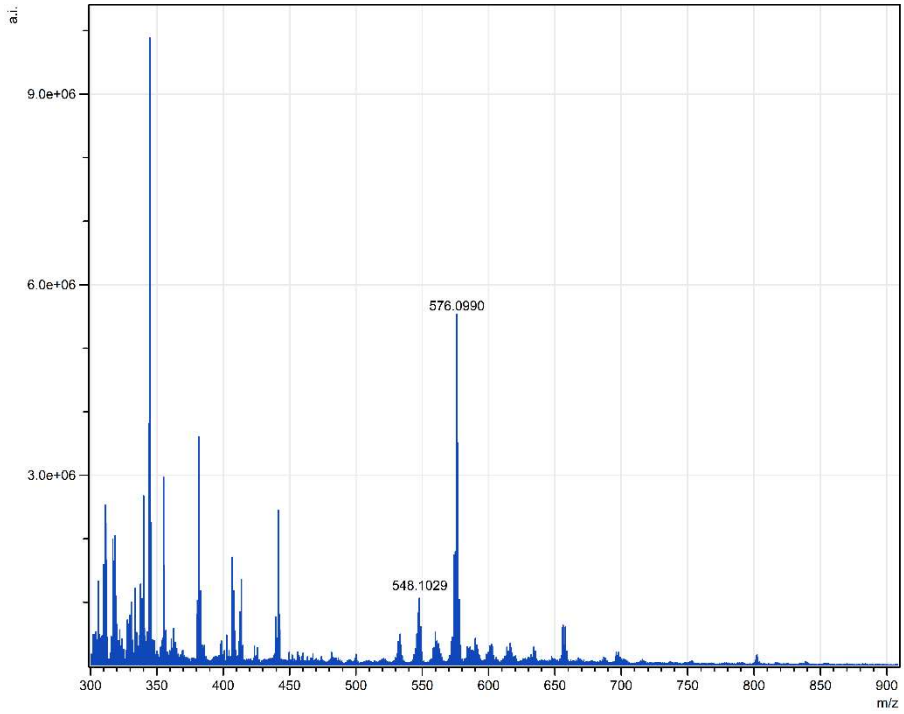

Figure 42: Mass spectra of the functionalized film, using dissolved catalyst to phosphate buffer (1:9), after rinsing with Acetonitrile and TCNQ as matrix.

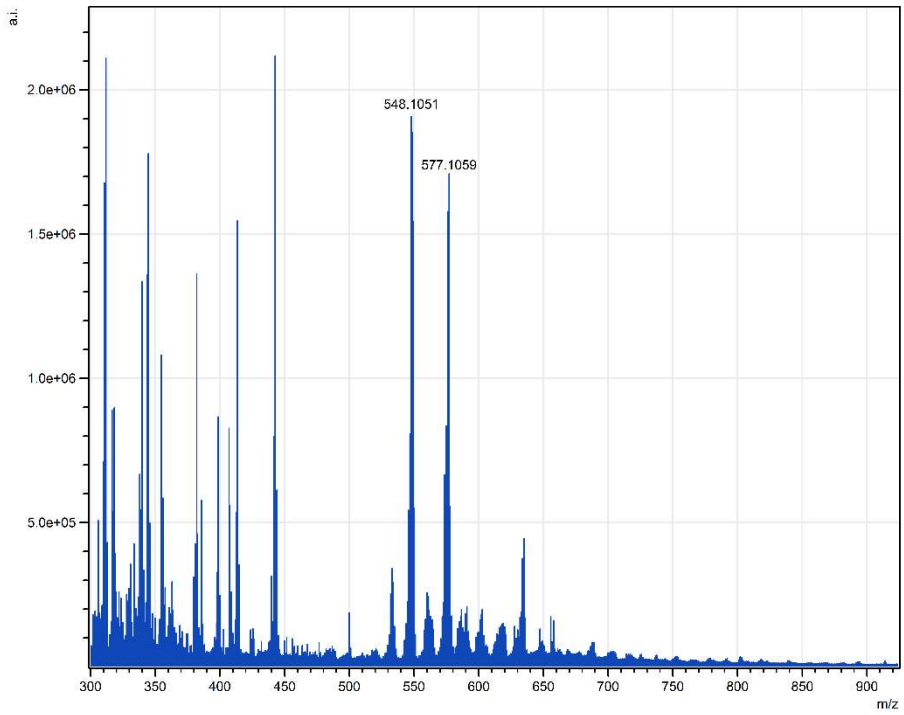

Figure 43: Mass spectra of the functionalized film, using dissolved catalyst to phosphate buffer (1:9), after incubating in Acetonitrile for 5 minutes and TCNQ as matrix.

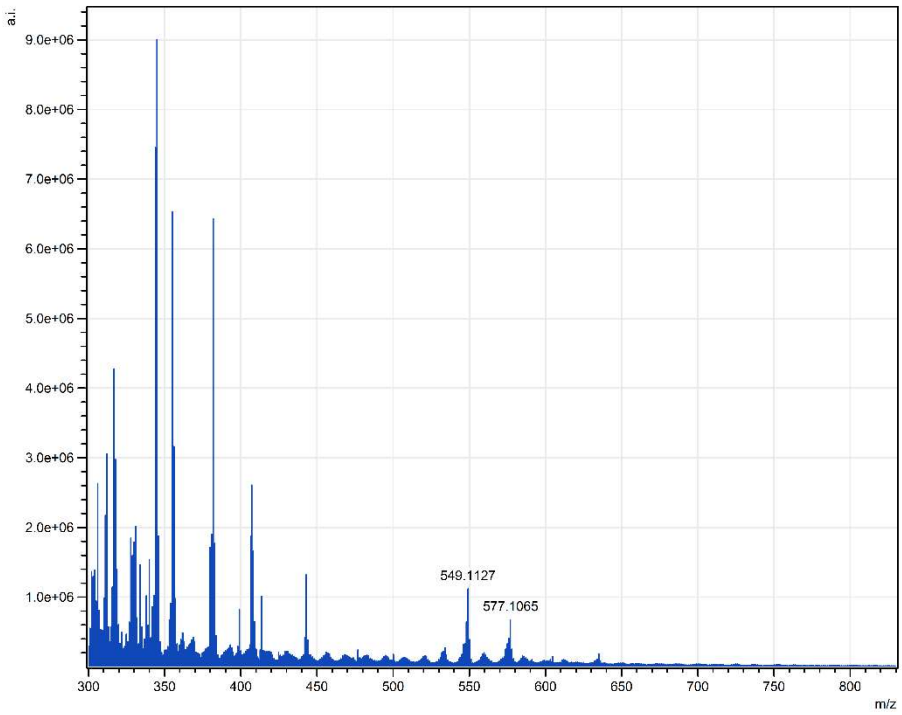

Figure 44: Mass spectra of the functionalized film, using dissolved catalyst to phosphate buffer (1:9), after incubating in Acetonitrile for 30 minutes and TCNQ as matrix.

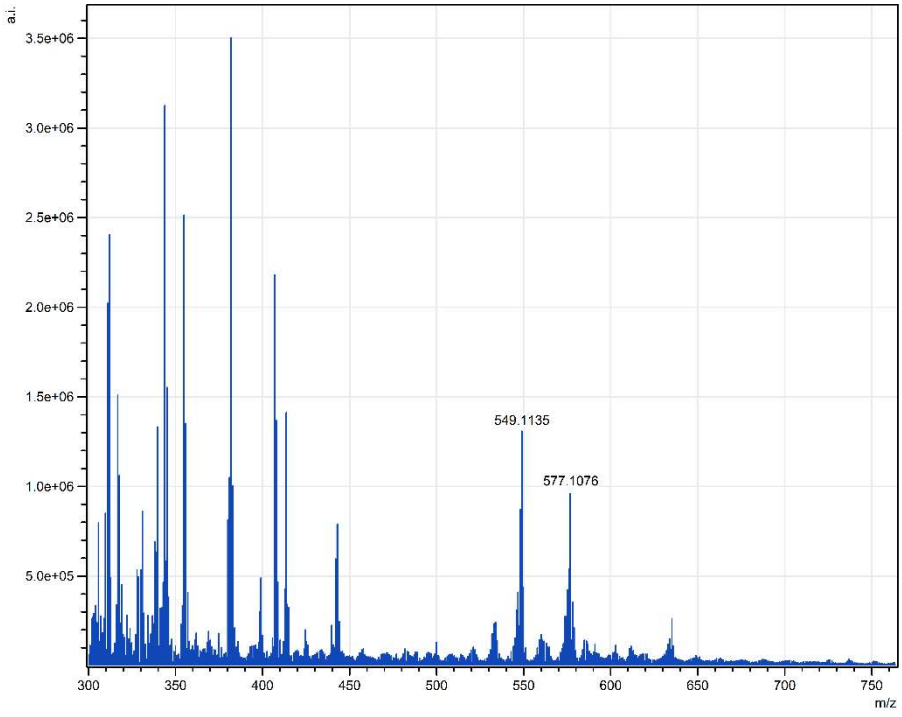

Figure 45: Mass spectra of the functionalized film, using dissolved catalyst to phosphate buffer (1:9), after incubating in Acetonitrile for 1 h and TCNQ as matrix.

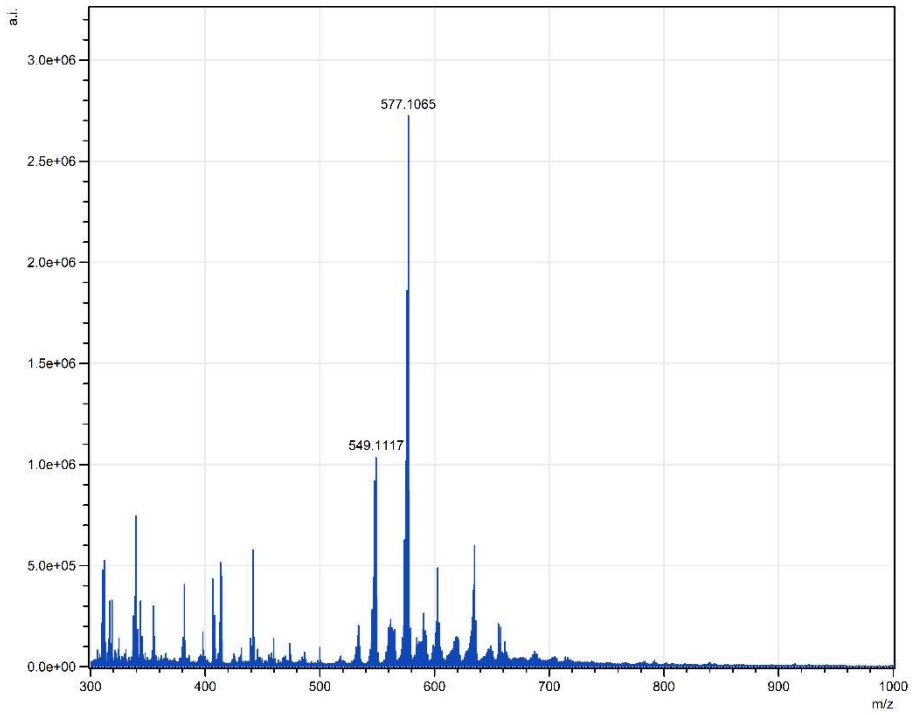

Figure 46: Mass spectra of the functionalized film, using dissolved catalyst to phosphate buffer (1:9), after incubating in Acetonitrile for 2 h and TCNQ as matrix.

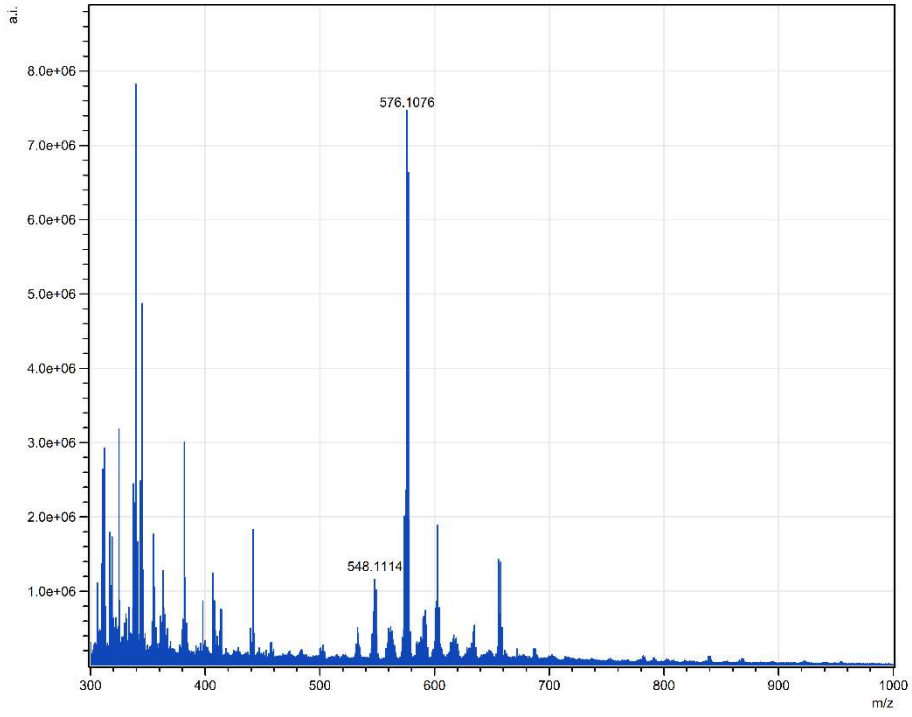

Figure 47: Mass spectra of the functionalized film, using dissolved catalyst to phosphate buffer (1:9), after incubating in Acetonitrile for 24 h and TCNQ as matrix.

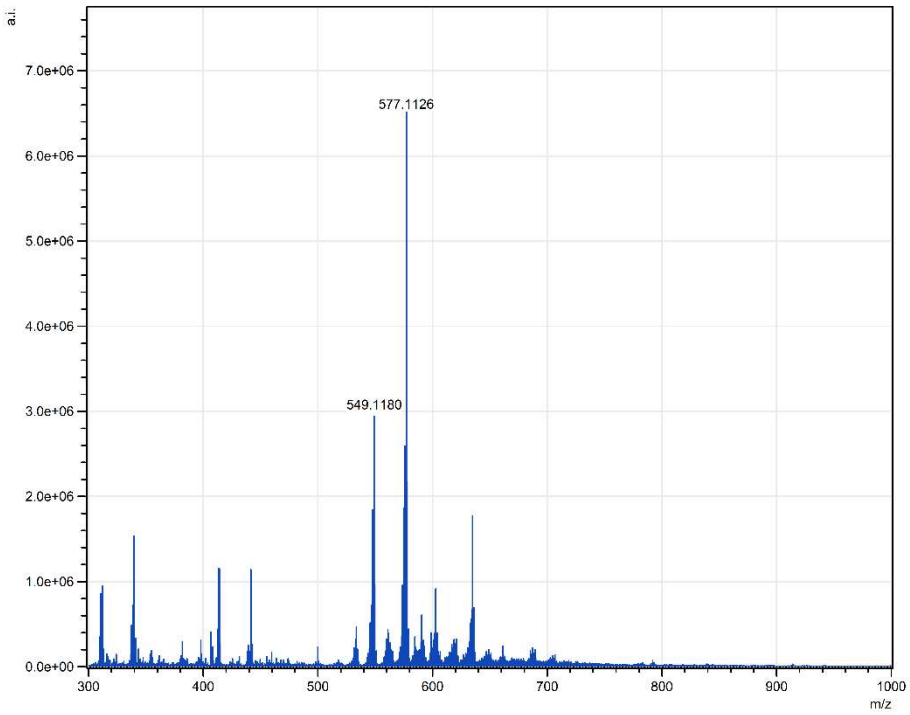

Figure 48: Mass spectra of the functionalized film, using dissolved catalyst to phosphate buffer (1:9), after ultra-sonication in Acetonitrile for 1 min and TCNQ as matrix.

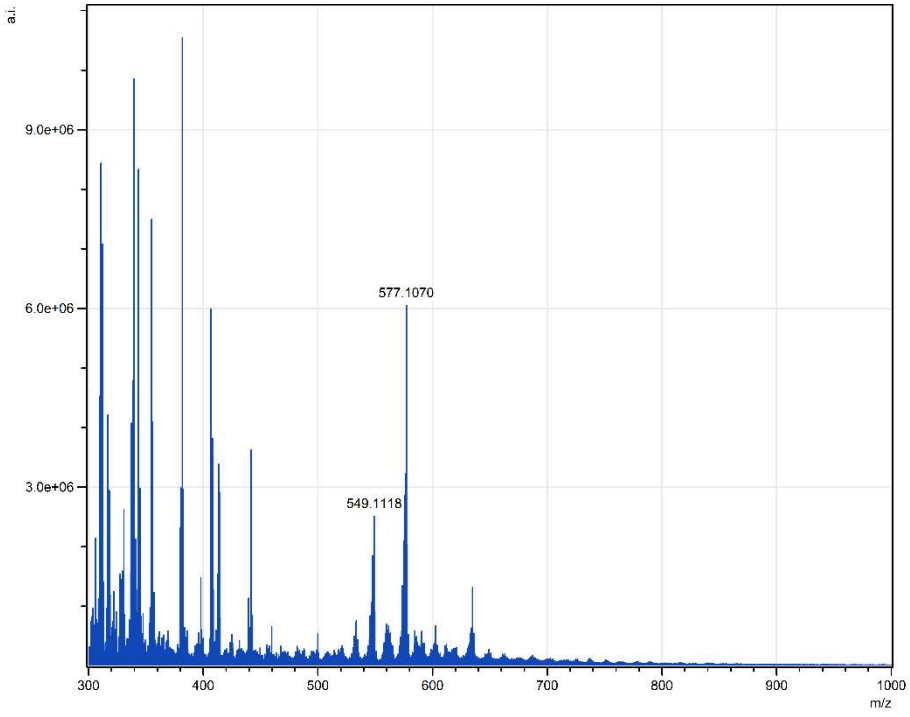

Figure 49: Mass spectra of the functionalized film, using dissolved catalyst to phosphate buffer (1:9), after ultra-sonication in Acetonitrile for 5 minutes and TCNQ as matrix.

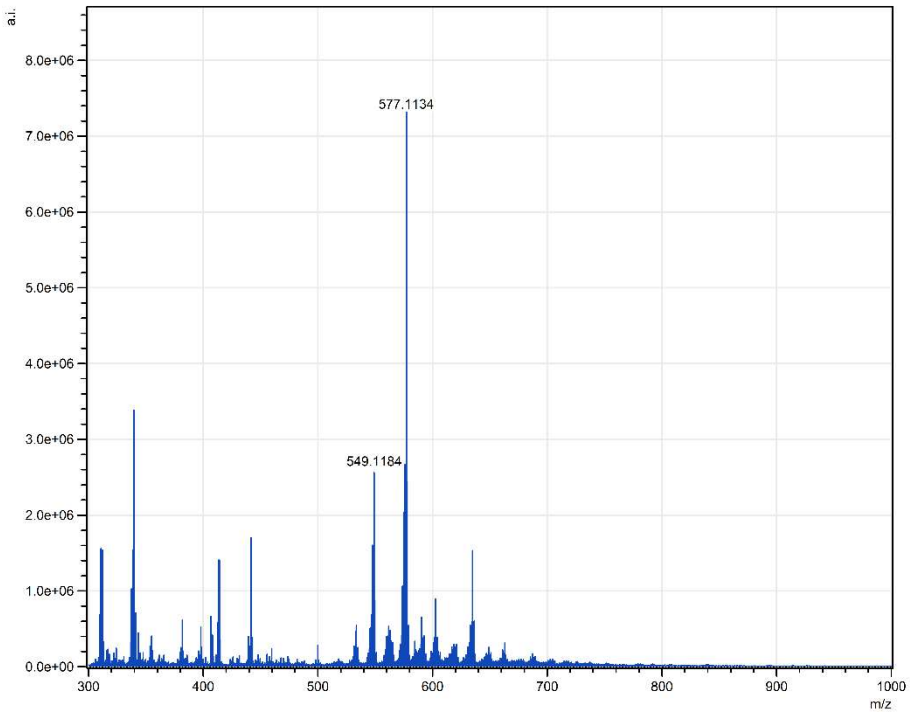

Figure 50: Mass spectra of the functionalized film, using dissolved catalyst to phosphate buffer (1:9), after ultra-sonication in Acetonitrile for 30 minutes and TCNQ as matrix.

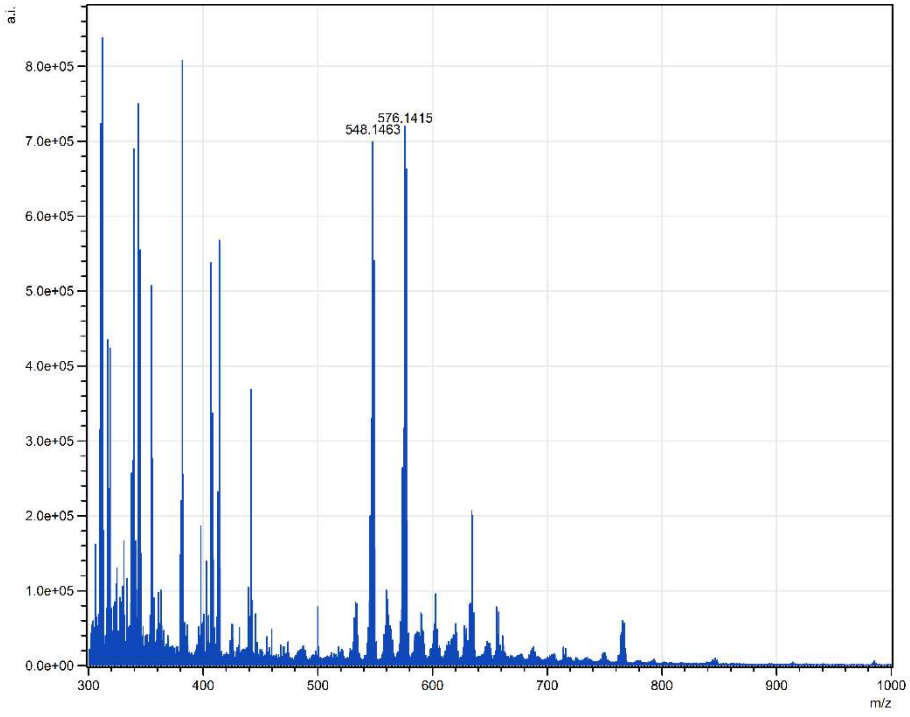

Figure 51: Mass spectra of the functionalized film, using dissolved catalyst to phosphate buffer (1:9), after ultra-sonication in Acetonitrile for 60 minutes with exchanging the solvent every 5 min and TCNQ as matrix.

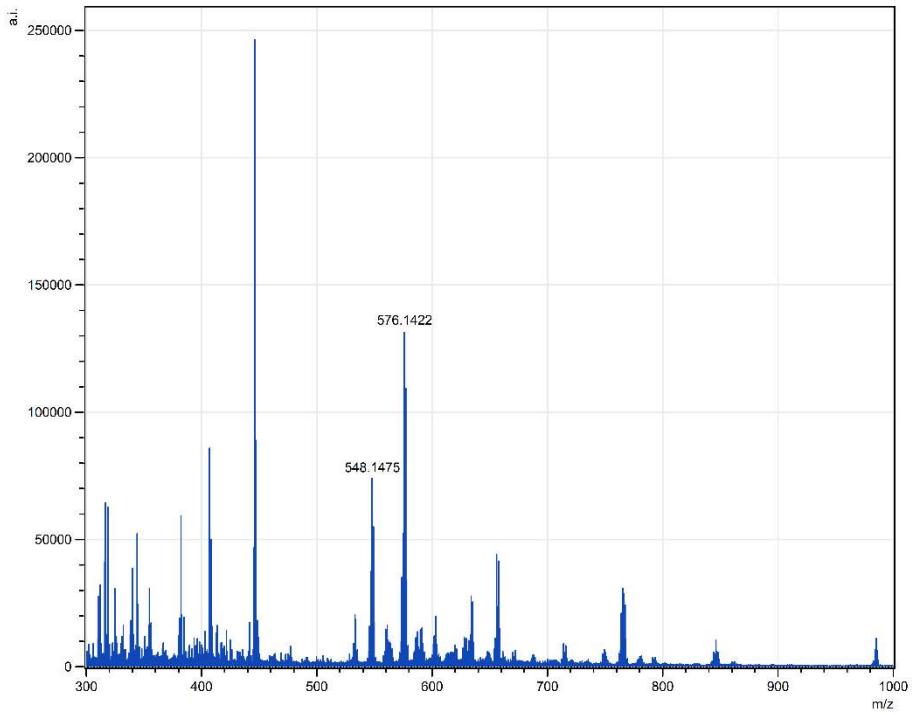

Figure 52: Mass spectra of the functionalized film, using dissolved catalyst to phosphate buffer (1:99) for the functionalization, after ultra-sonication in Acetonitrile for 60 minutes with exchanging the solvent every 5 min and TCNQ as matrix.

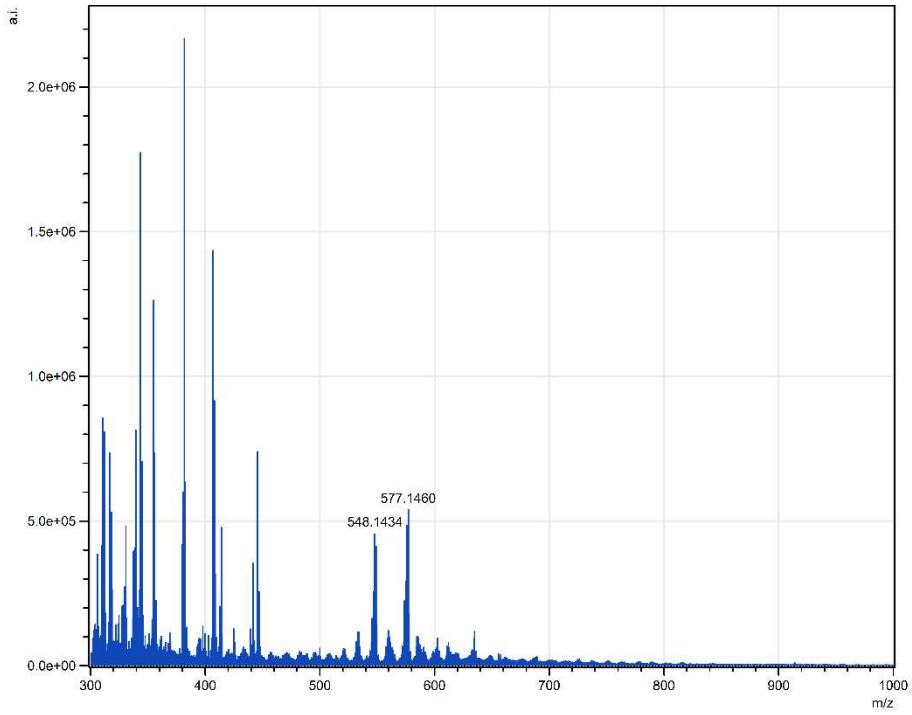

Figure 53: Mass spectra of the functionalized film, using dissolved catalyst to phosphate buffer (1:9) and 3 h reaction time for the functionalization, after ultra-sonication in Acetonitrile for 60 minutes with exchanging the solvent every 5 min and TCNQ as matrix.

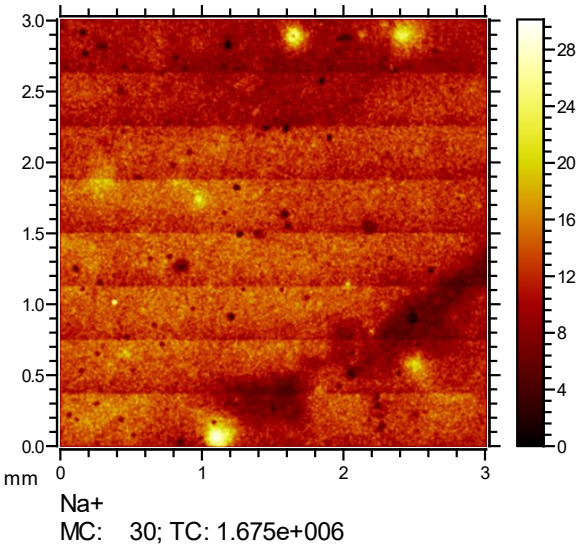

Figure 54: Chemical map of the surface of the functionalized film for sodium ions. The respective signal intensities (displayed in counts) for individual pixels are color-coded according to the key on the right of each image. MC: maximum counts per pixel. TC: total counts per image.

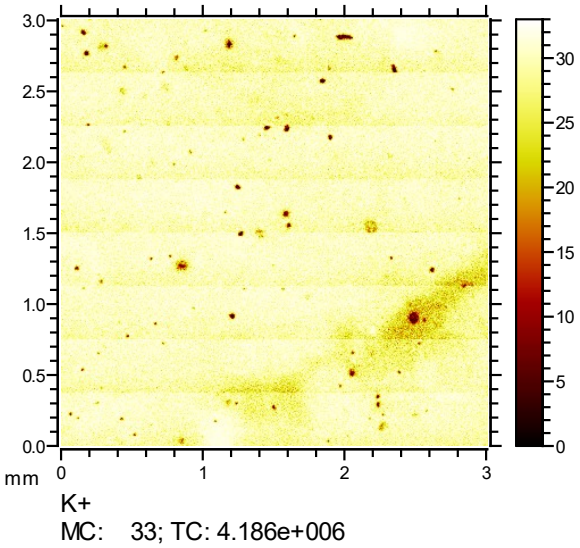

Figure 55: Chemical map of the surface of the functionalized film for potassium ions. The respective signal intensities (displayed in counts) for individual pixels are color-coded according to the key on the right of each image. MC: maximum counts per pixel. TC: total counts per image.

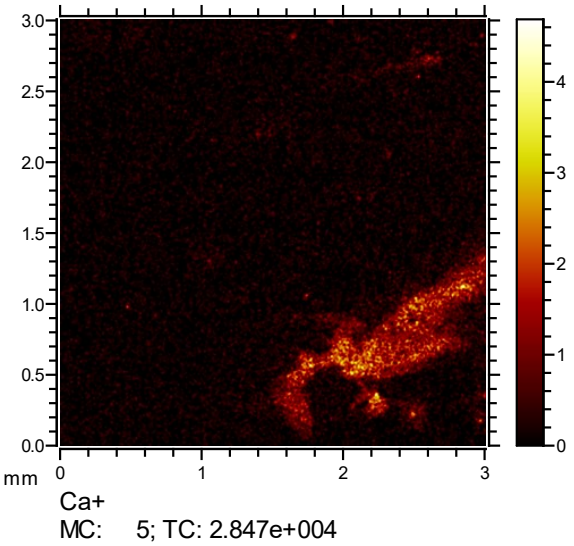

Figure 56: Chemical map of the surface of the functionalized film for calcium ions. The respective signal intensities (displayed in counts) for individual pixels are color-coded according to the key on the right of each image. MC: maximum counts per pixel. TC: total counts per image.

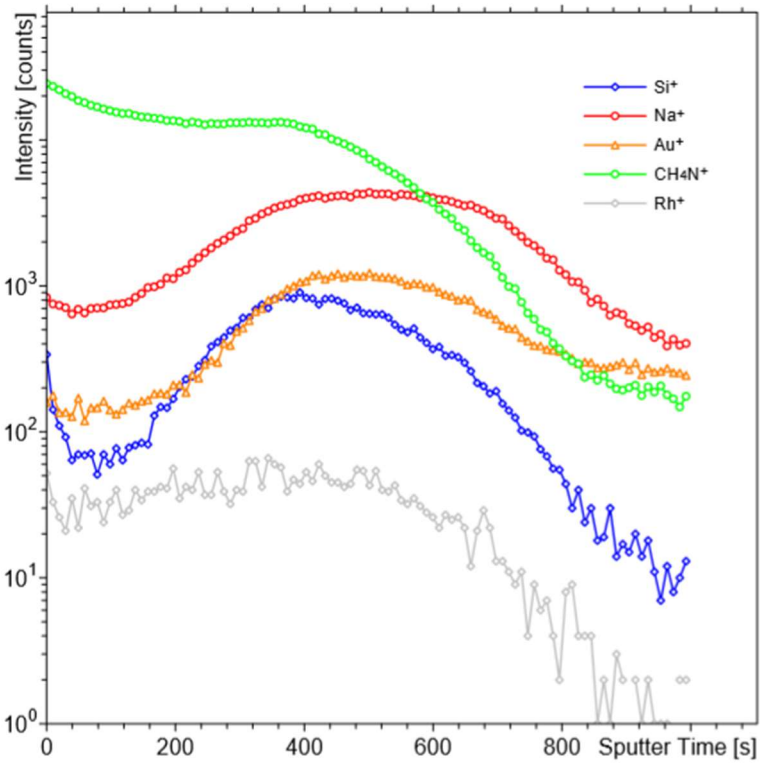

Figure 57: Dpeth profile of the PDA film with 2.5keV.

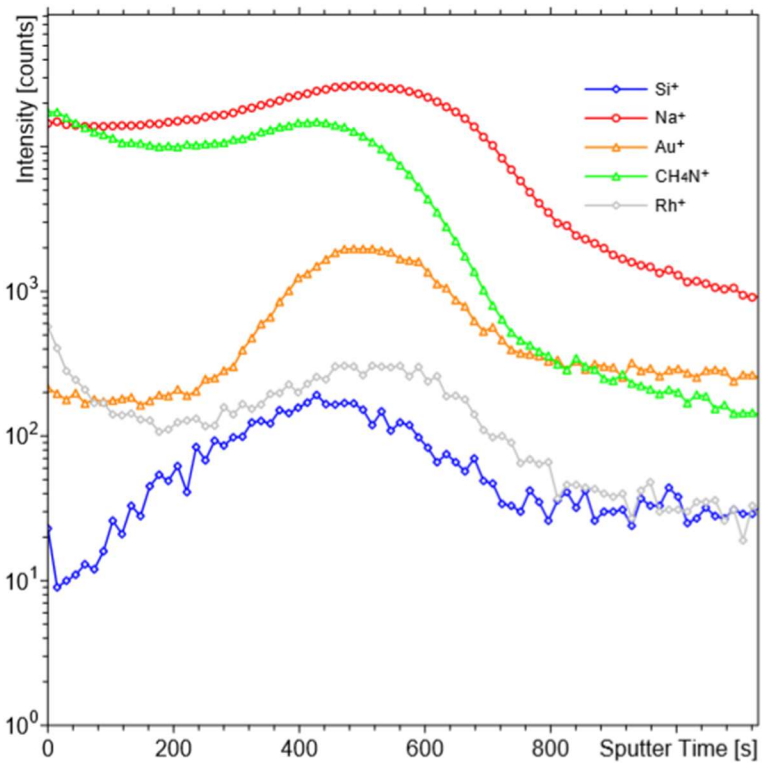

Figure 58: Depth profile of the functinalized fil with 2.5keV.

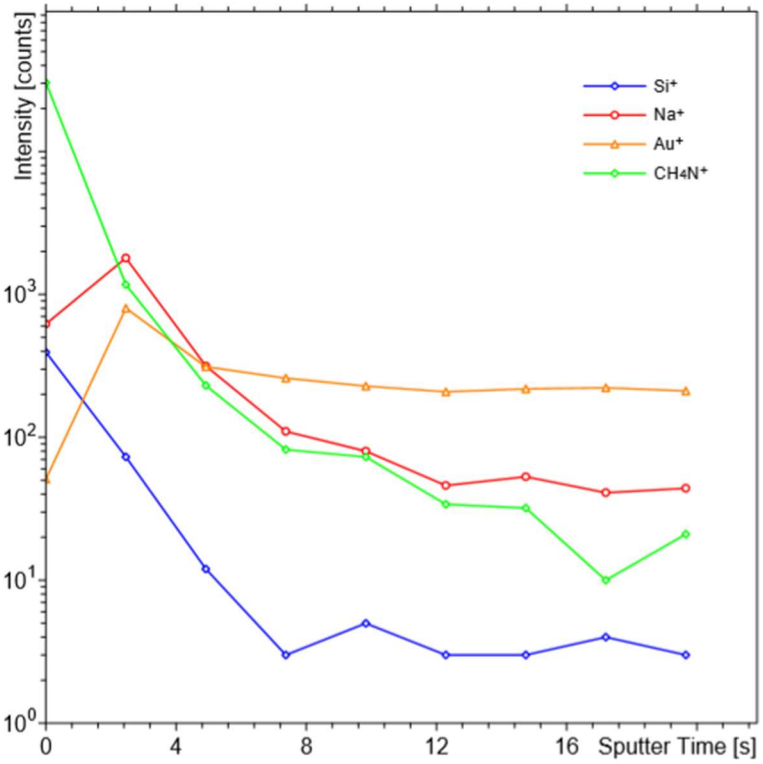

Figure 59: Depth profile of the PDA film with 10 keV.

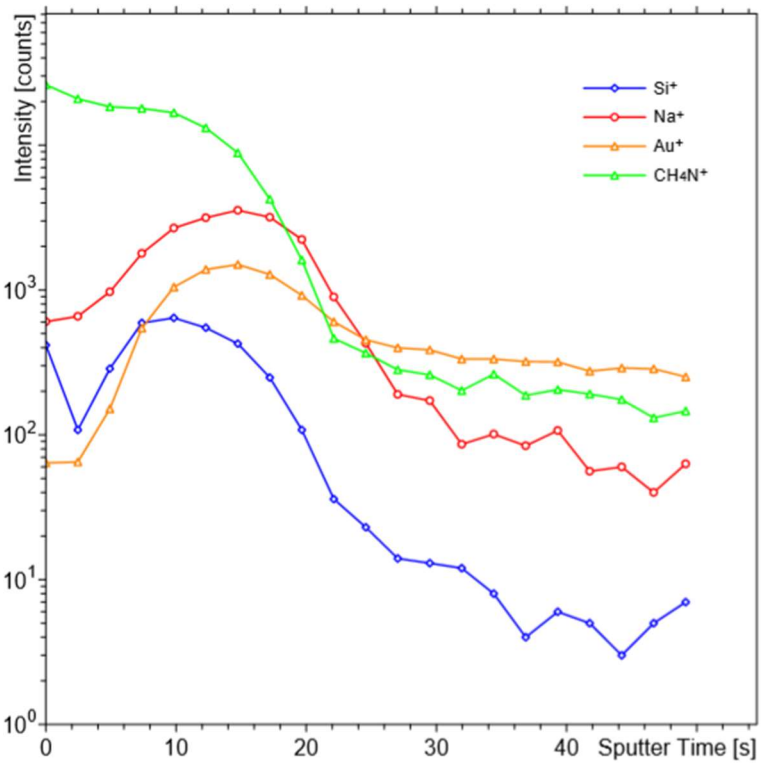

Figure 60: Depth profile of the PDA film with 5 keV.

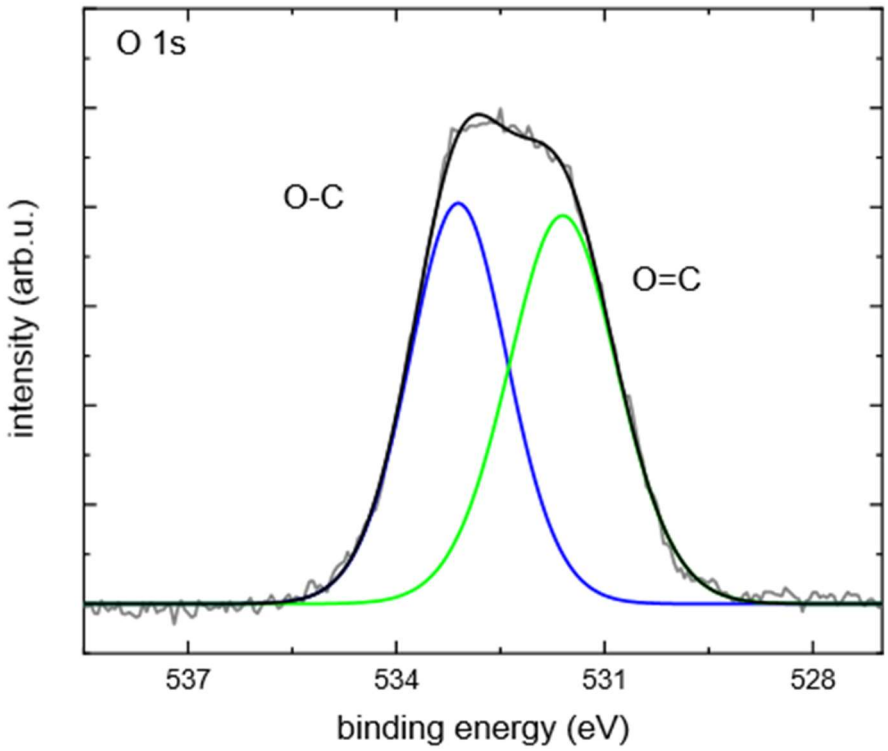

Figure 61: XPS spectra of the O 1s signal of the PDA film.

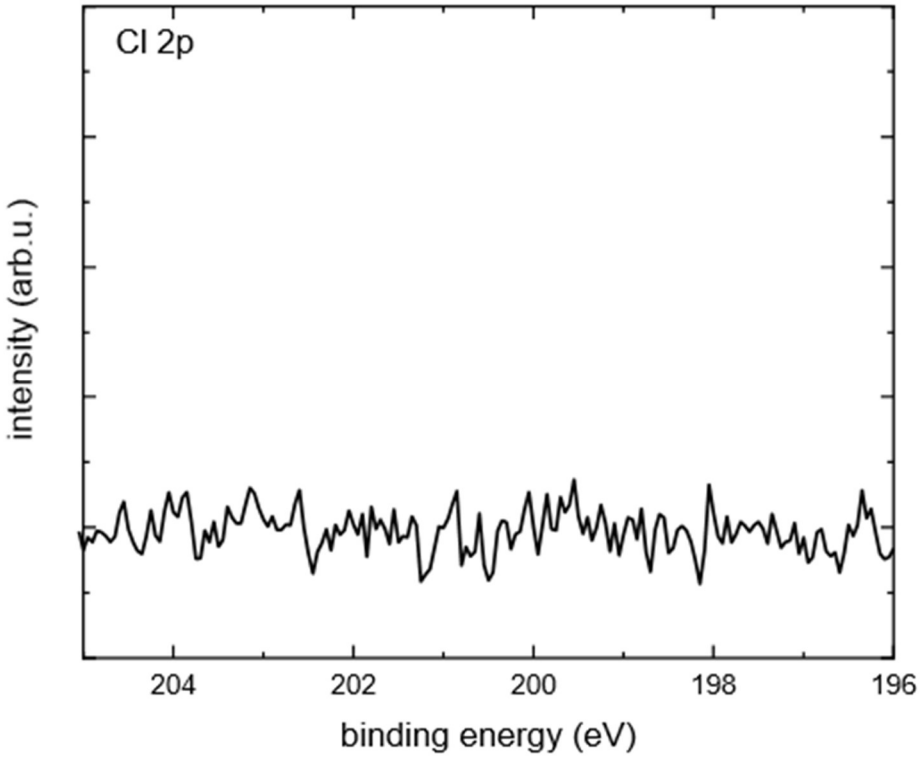

Figure 62: XPS spectra of the Cl 2p signal of the PDA film.

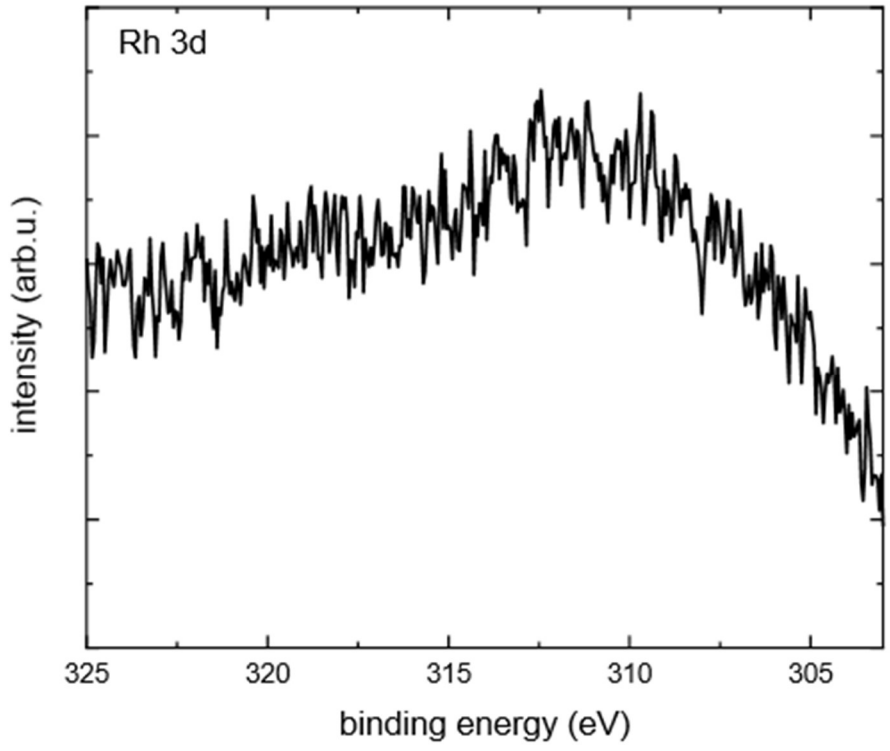

Figure 63: XPS spectra of the Rh 3d signal of the PDA film.

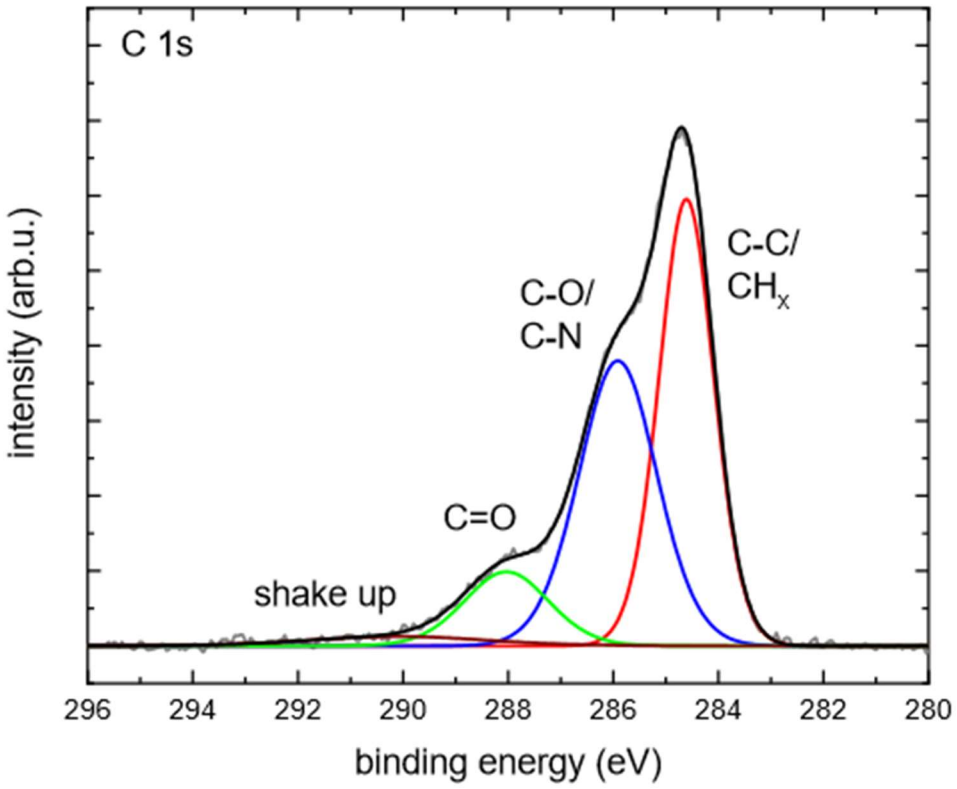

Figure 64: XPS spectra of the C 1s signal of the functionalized film after washing.

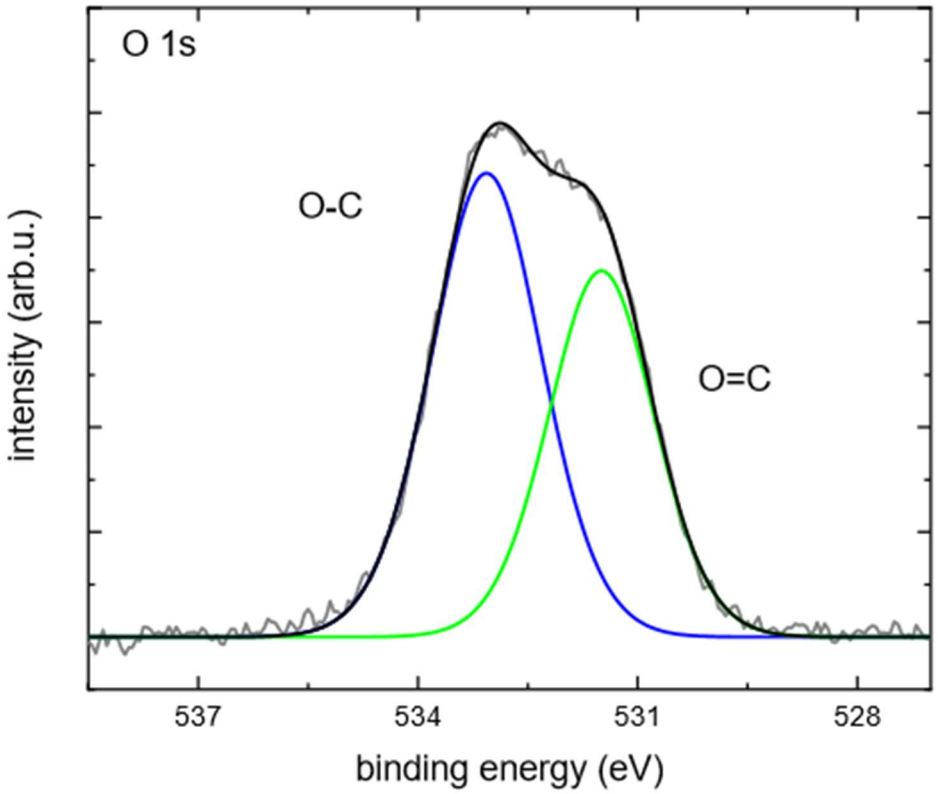

Figure 65: XPS spectra of the O 1s signal of the functionalized film after washing

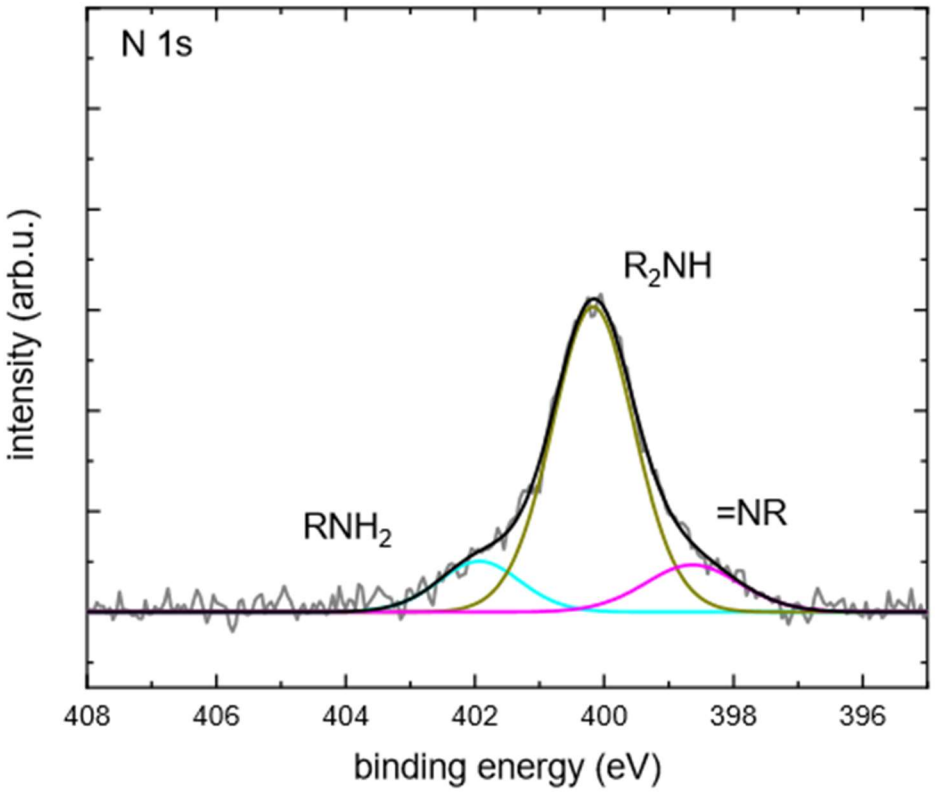

Figure 66: XPS spectra of the N 1s signal of the functionalized film after washing

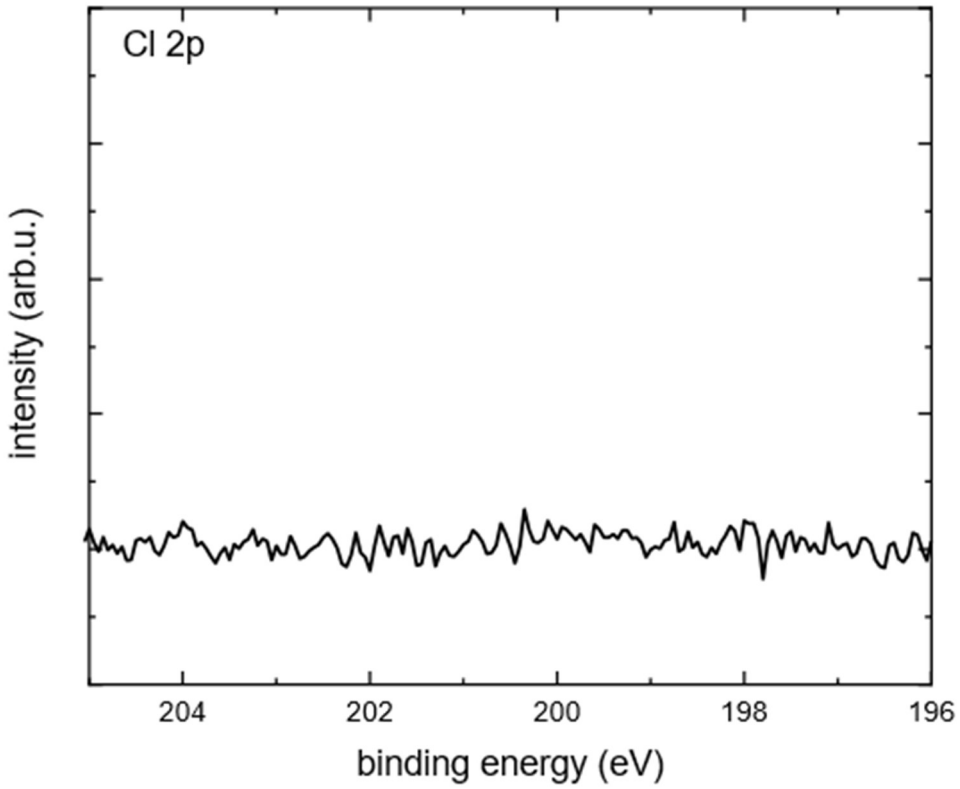

Figure 67: XPS spectra of the Cl 2p signal of the functionalized film after washing.

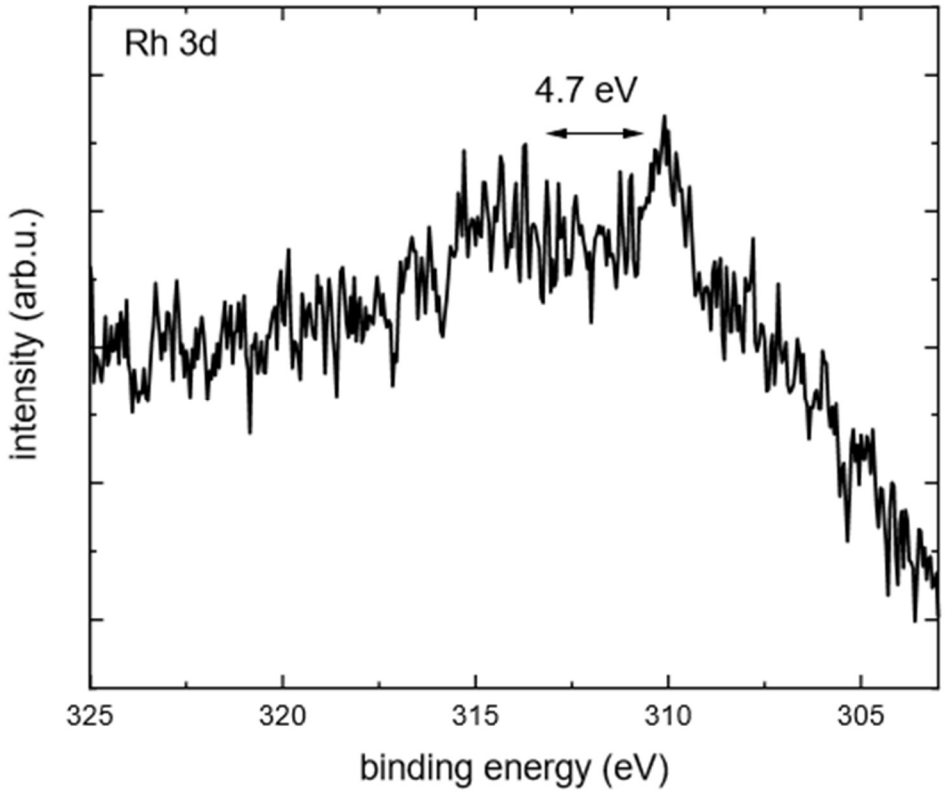

Figure 68: XPS spectra of the Rh 3d signal of the functionalized film after washing.

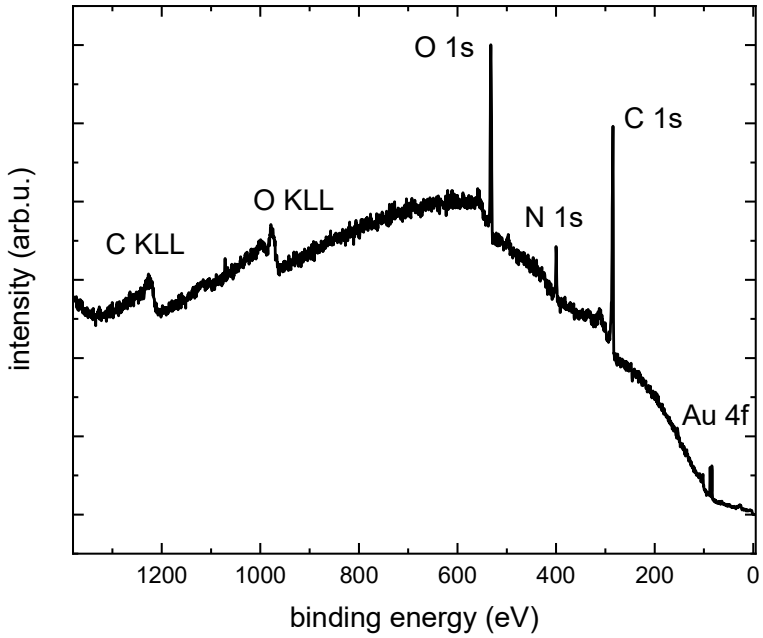

Figure 69: XPS spectra of the functionalized film without washing.

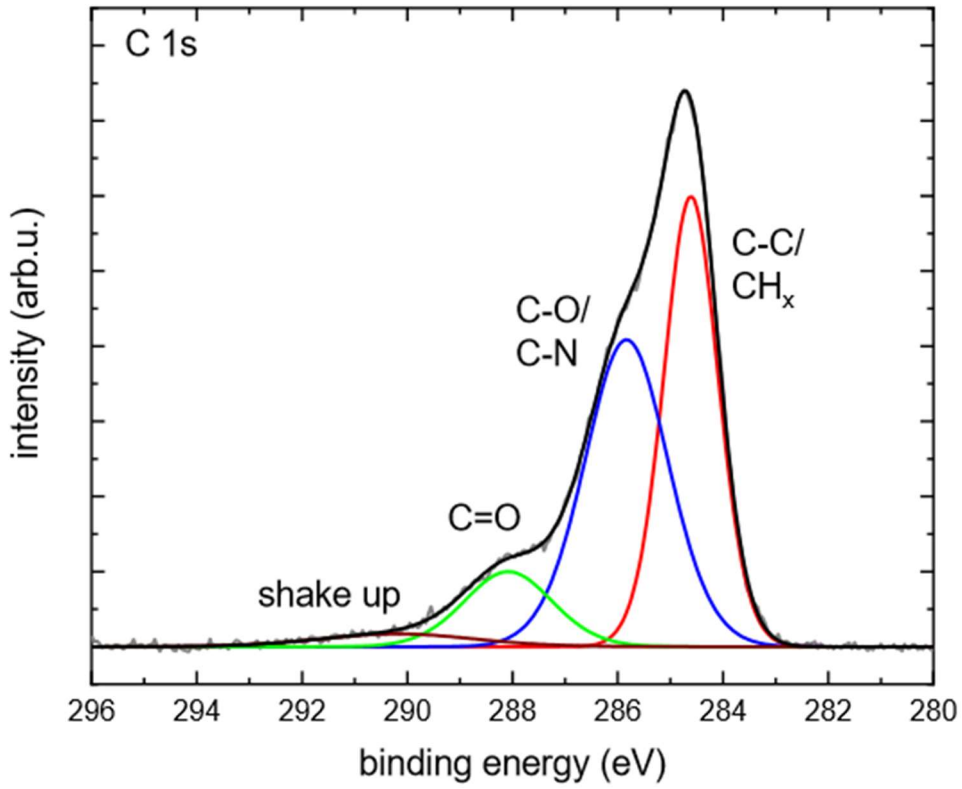

Figure 70: XPS spectra of the C 1s signal of the functionalized film without washing.

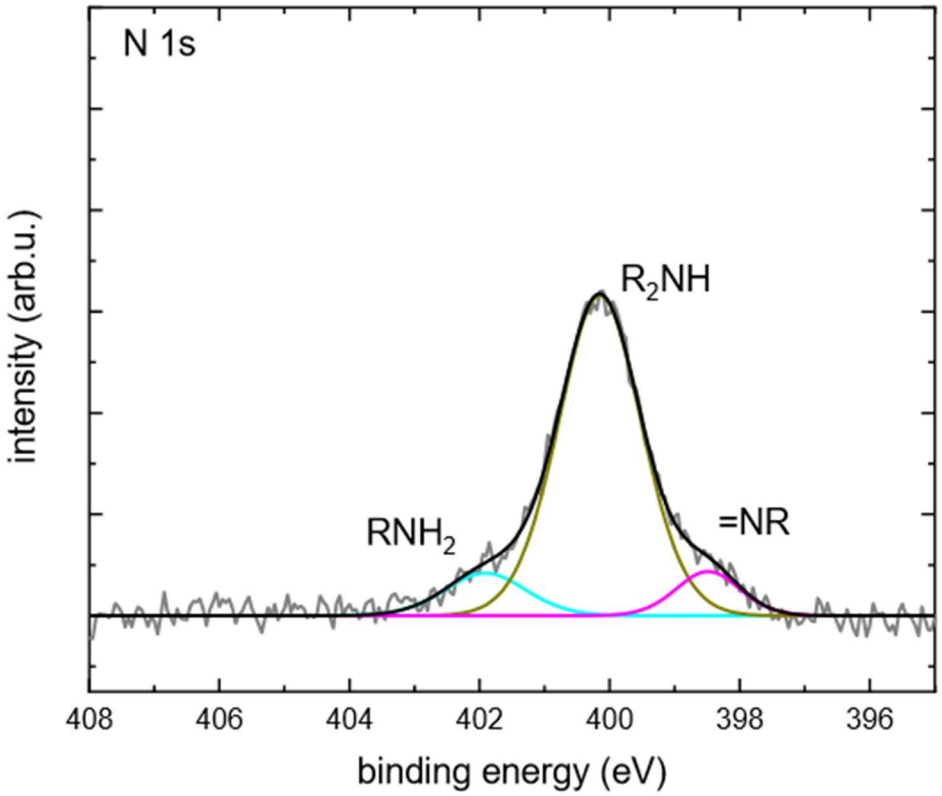

Figure 71: XPS spectra of the N 1s signal of the functionalized film without washing.

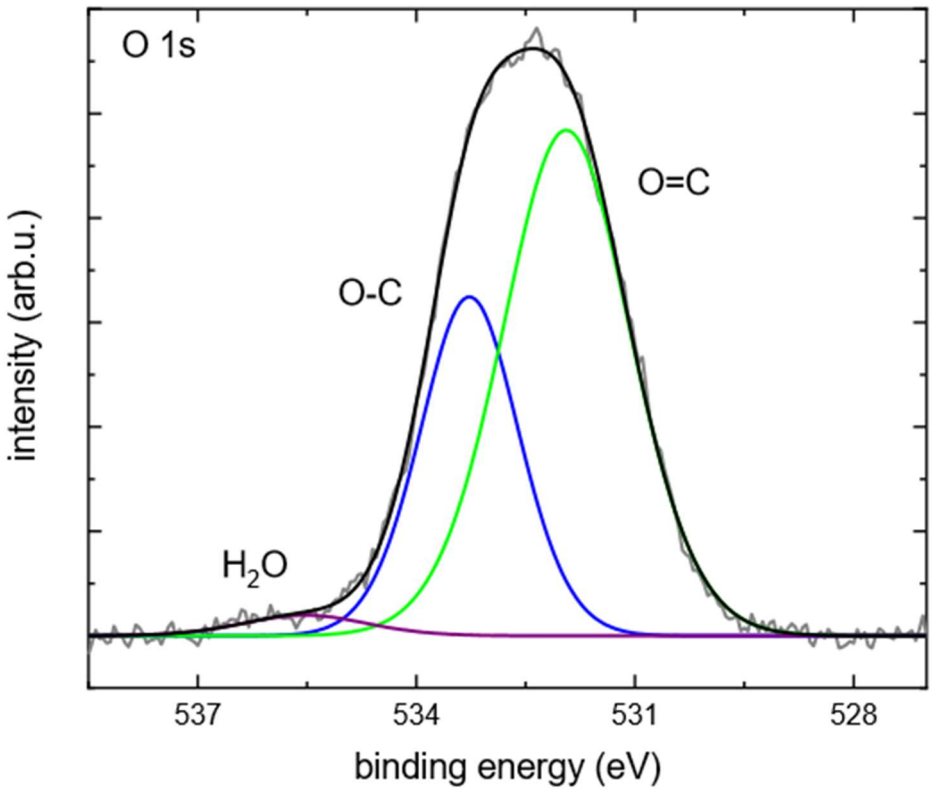

Figure 72: XPS spectra of the O 1s signal of the functionalized film without washing.

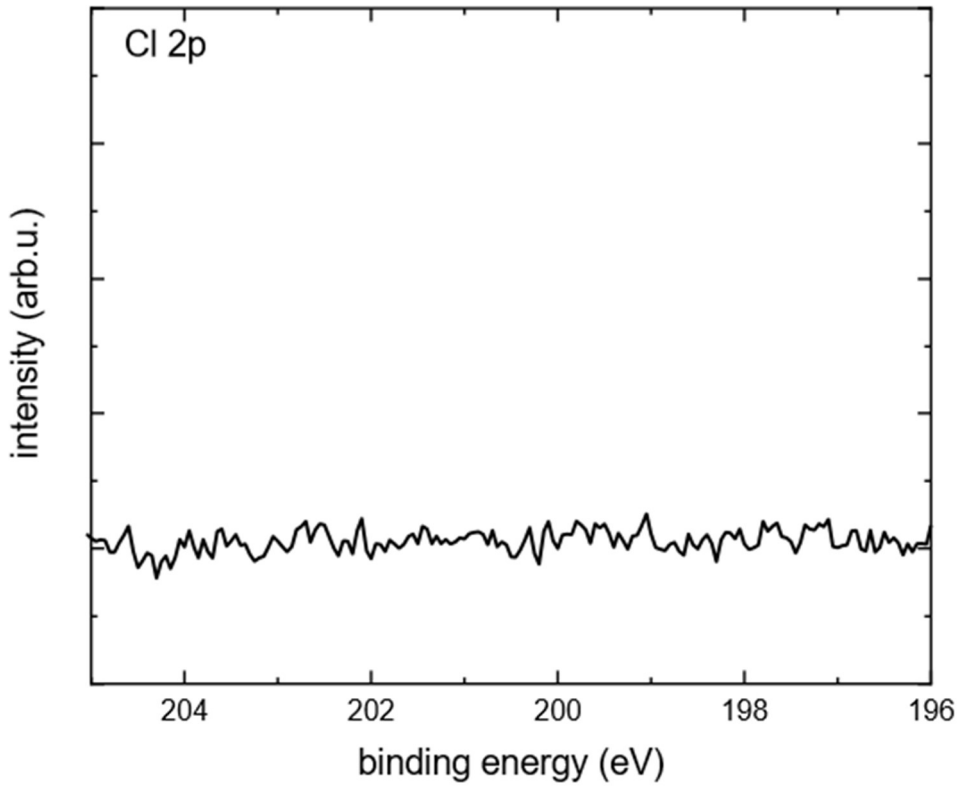

Figure 73: XPS spectra of the Cl 2p signal of the functionalized film without washing.

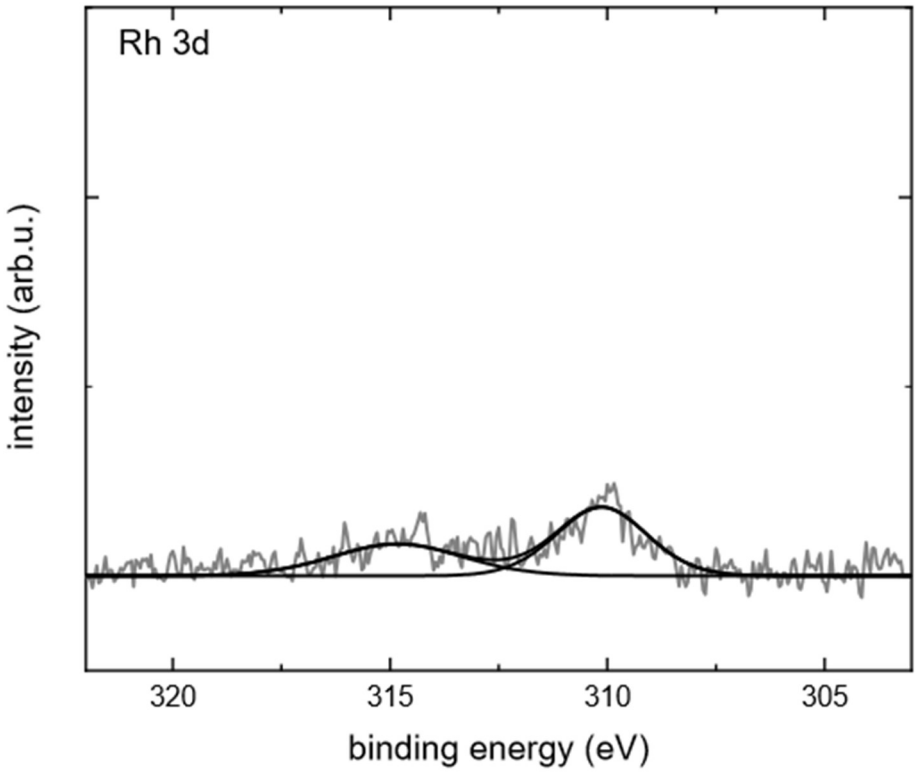

Figure 74: XPS spectra of the Rh 3d signal of the functionalized film without washing.

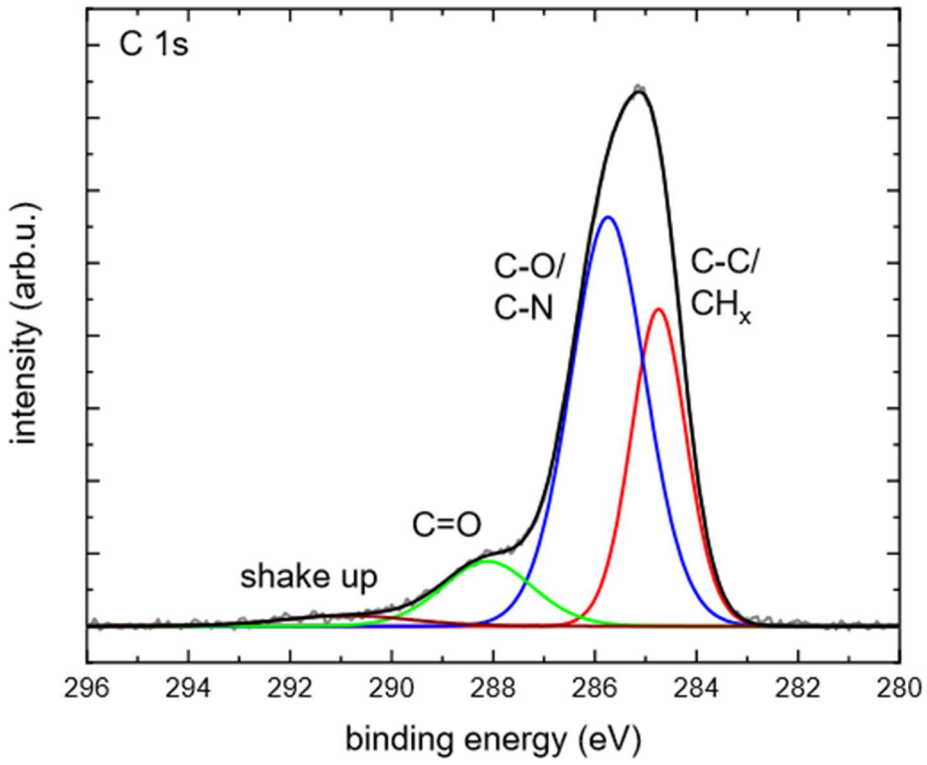

Figure 75: XPS spectra of the C 1s signal of the unwashed film functionalized with a ration of dissolved catalyst to phosphate buffer of 1:9.

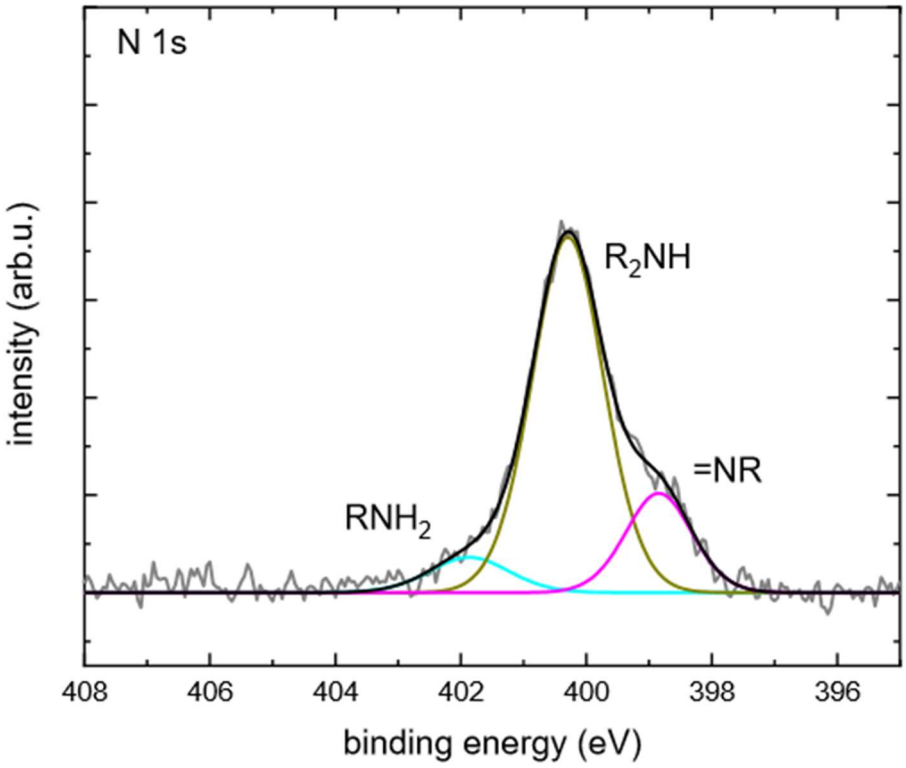

Figure 76: XPS spectra of the N 1s signal of the unwashed film functionalized with a ration of dissolved catalyst to phosphate buffer of 1:9.

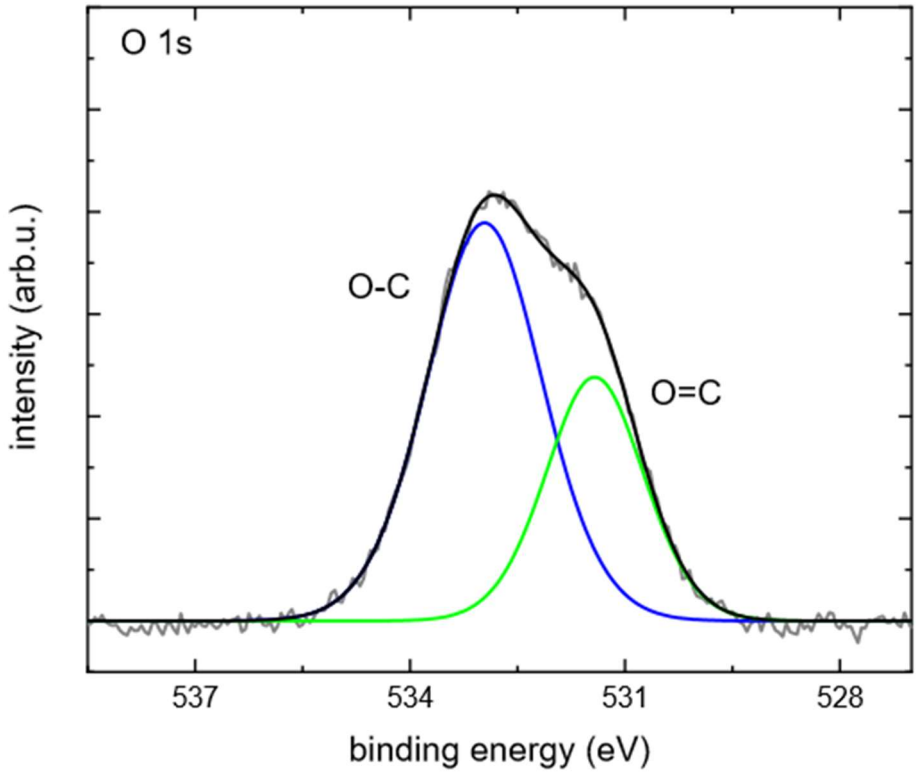

Figure 77: XPS spectra of the O 1s signal of the unwashed film functionalized with a ration of dissolved catalyst to phosphate buffer of 1:9.

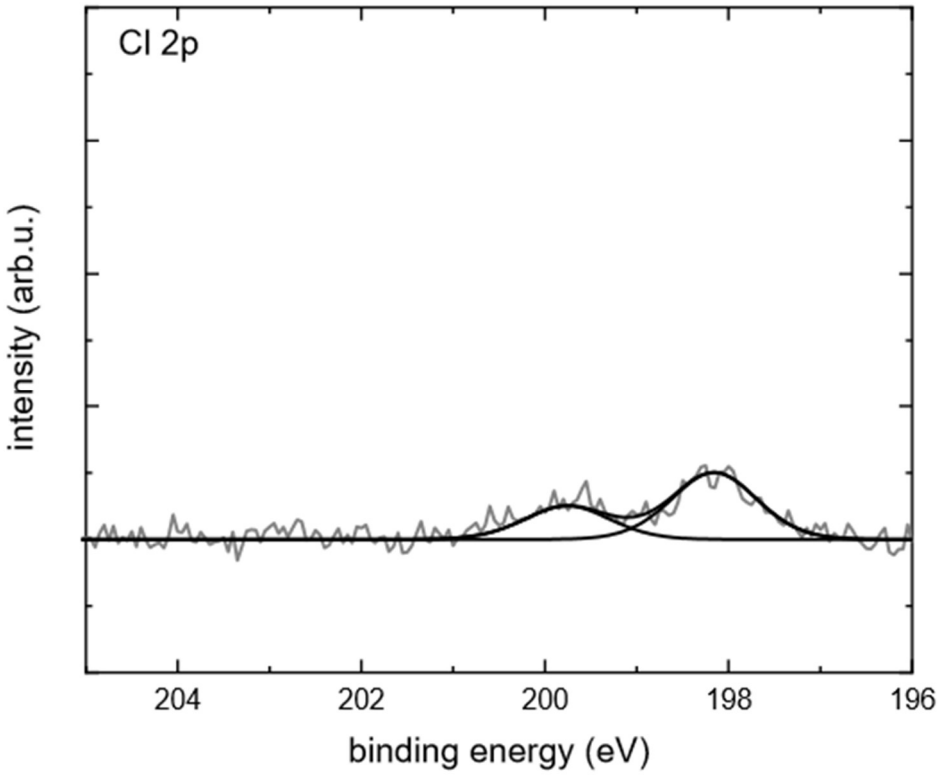

Figure 78: XPS spectra of the Cl 2p signal of the unwashed film functionalized with a ration of dissolved catalyst to phosphate buffer of 1:9.

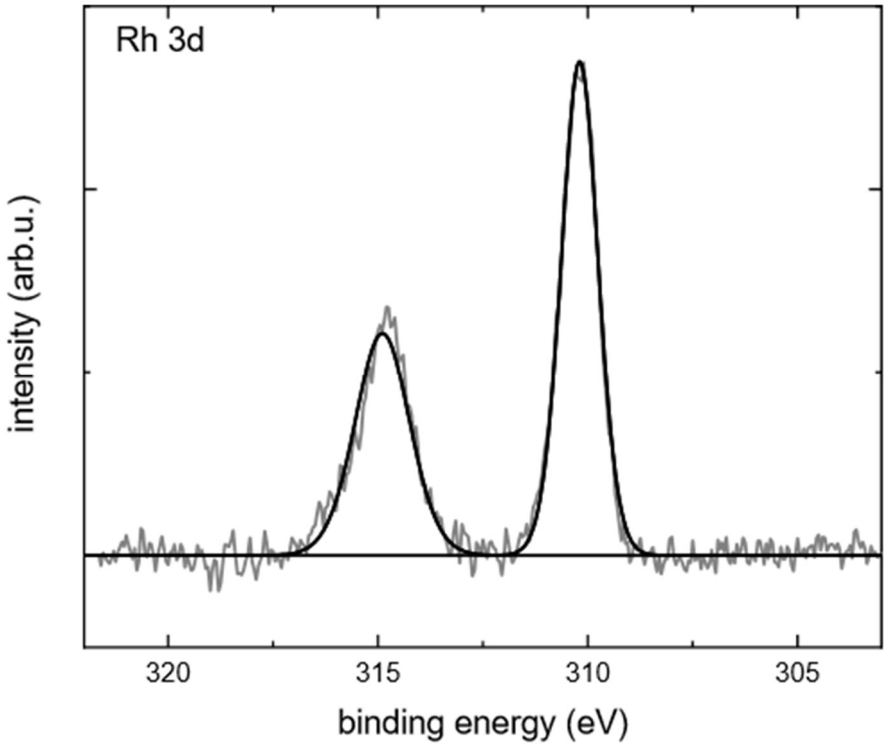

Figure 79: XPS spectra of the Rh 3d signal of the unwashed film functionalized with a ration of dissolved catalyst to phosphate buffer of 1:9.

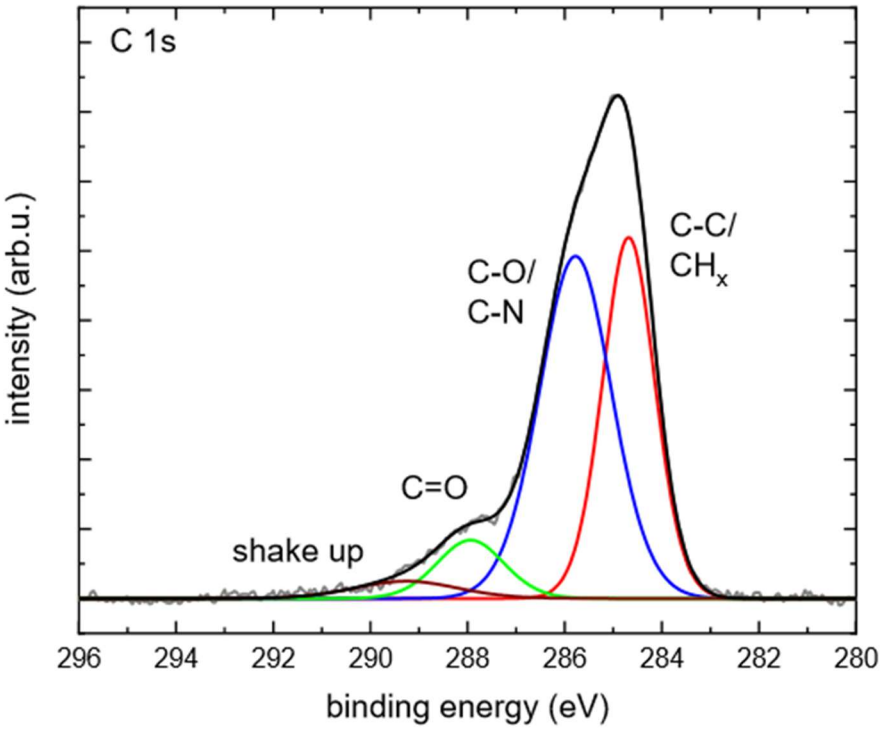

Figure 80: XPS spectra of the C 1s signal of the washed film functionalized with a ration of dissolved catalyst to phosphate buffer of 1:9.

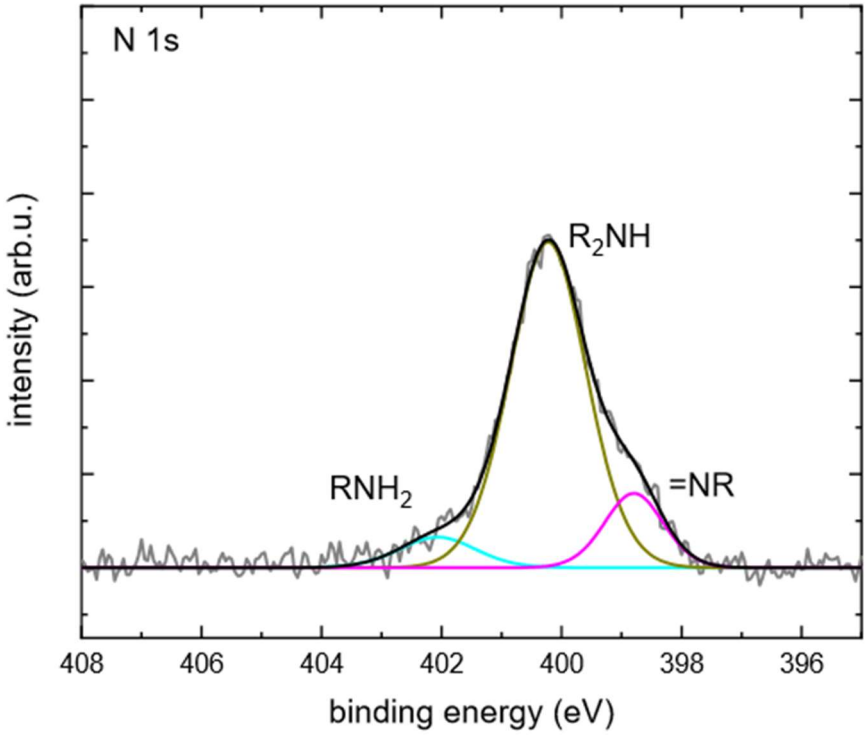

Figure 81: XPS spectra of the N 1s signal of the washed film functionalized with a ration of dissolved catalyst to phosphate buffer of 1:9.

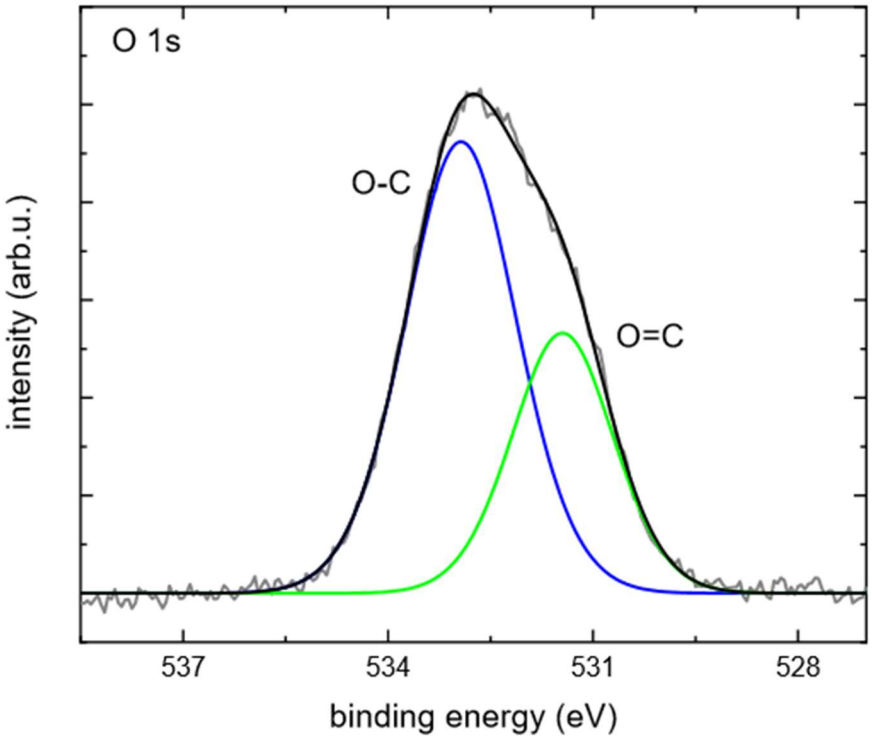

Figure 82: XPS spectra of the O 1s signal of the washed film functionalized with a ration of dissolved catalyst to phosphate buffer of 1:9.

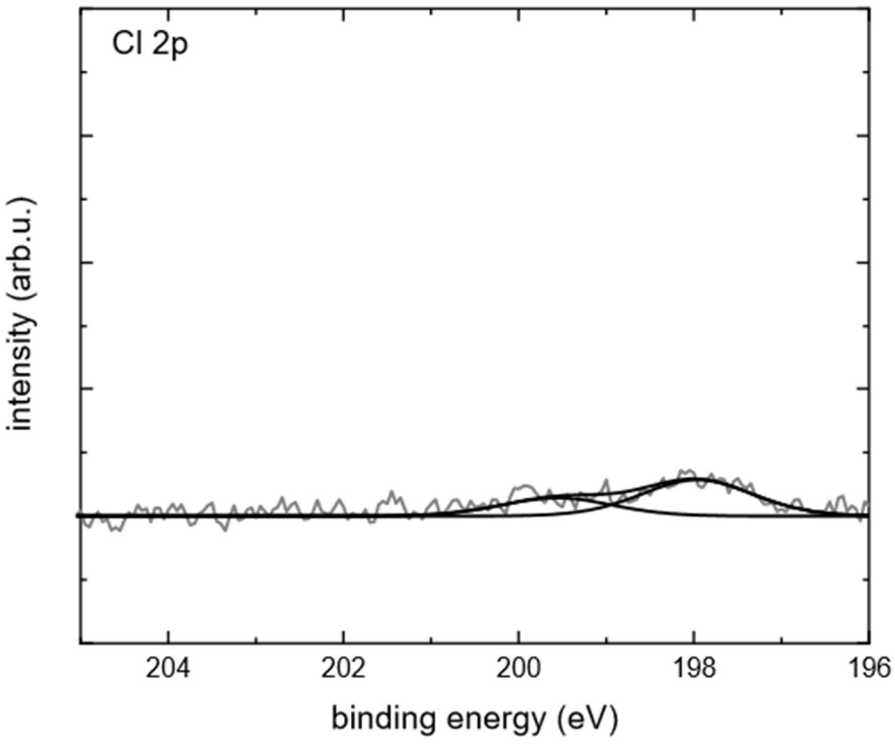

Figure 83: XPS spectra of the Cl 2p signal of the washed film functionalized with a ration of dissolved catalyst to phosphate buffer of 1:9.

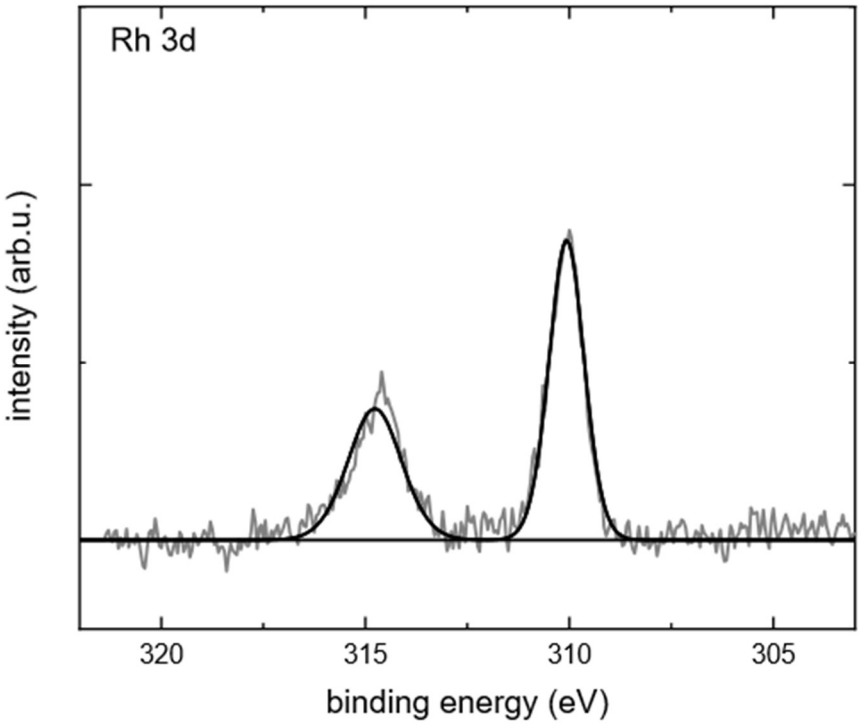

Figure 84: XPS spectra of the Rh 3d signal of the washed film functionalized with a ration of dissolved catalyst to phosphate buffer of 1:9.

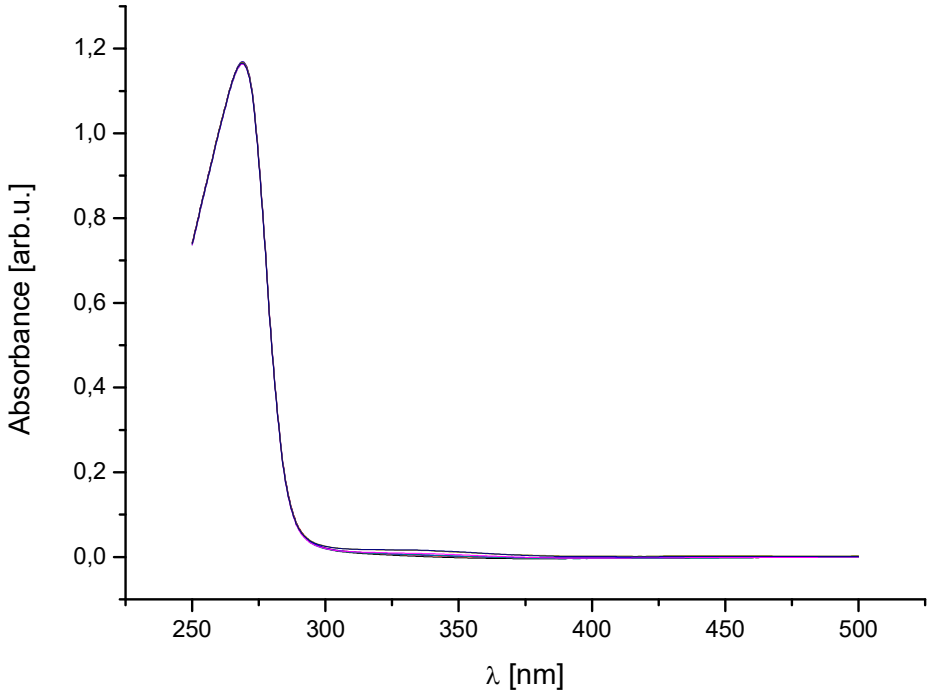

Figure 85: Absorption spectrum of the thermochemical reduction of NAD+ catalyzed by the functionalized film (high concentration) after 0 min (black), 10 min (red), 25 min (blue), 50 min (cyan), 75 min (magenta), 100 min (dark yellow) and 125 min (navy blue) of heating.

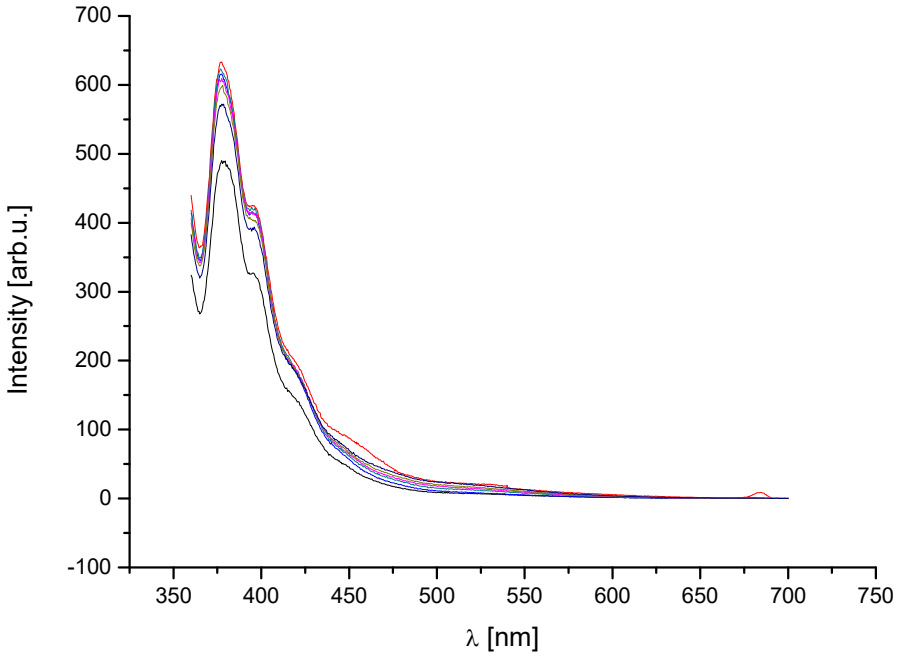

Figure 86: Emission spectrum of the thermochemical reduction of NAD^+ catalyzed by the functionalized film (low concentration) after 0 min (black), 10 min (red), 25 min (blue), 50 min (cyan), 75 min (magenta), 100 min (dark yellow) and 125 min (navy blue) of heating.

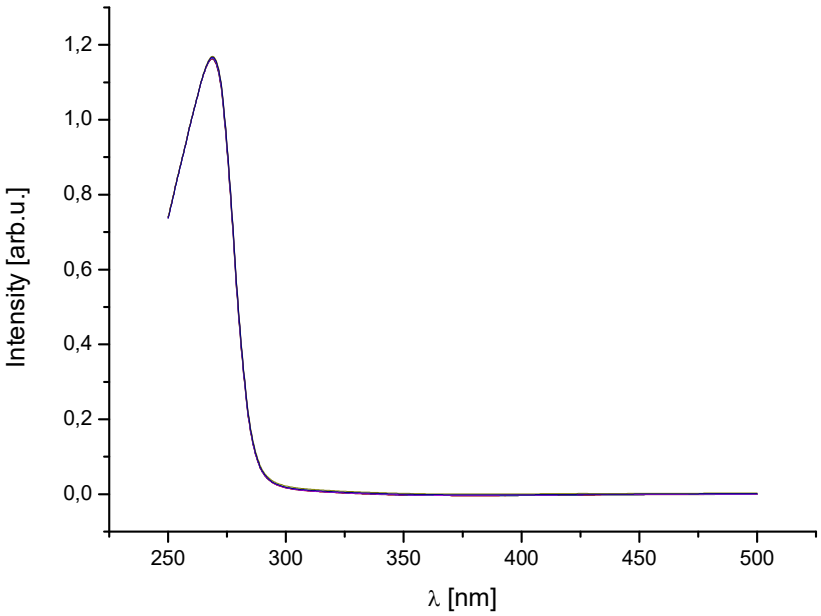

Figure 87: Absorption spectrum of the thermochemical reduction of NAD+ catalyzed by the functionalized film (low concentration) after 0 min (black), 10 min (red), 25 min (blue), 50 min (cyan), 75 min (magenta), 100 min (dark yellow) and 125 min (navy blue) of heating

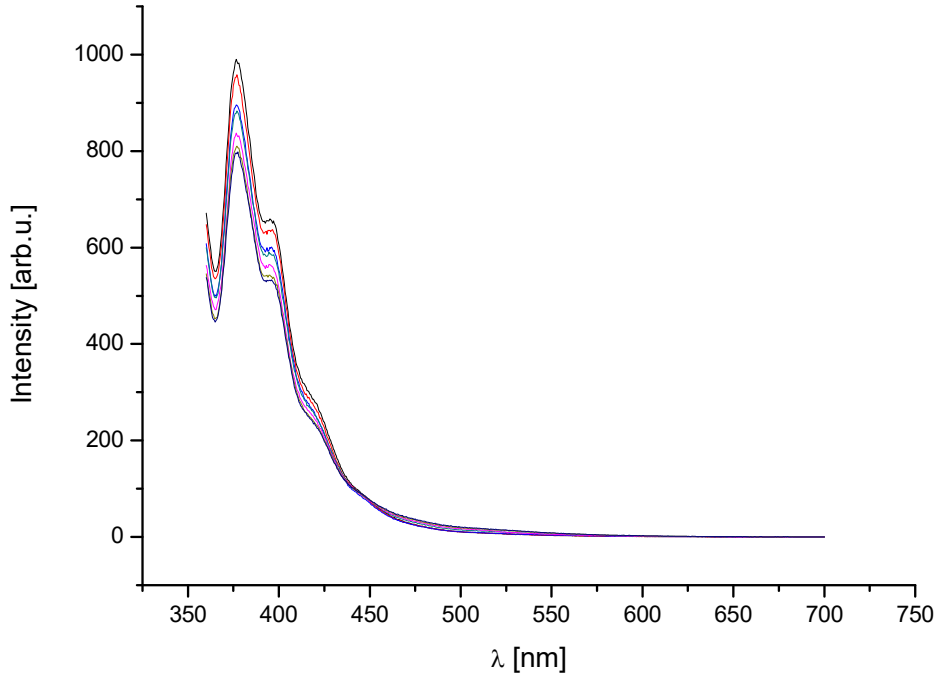

Figure 88: Emission spectrum of sodium formate with the functionalized film (high concentration) after 0 min (black), 10 min (red), 25 min (blue), 50 min (cyan), 75 min (magenta), 100 min (dark yellow) and 125 min (navy blue) of heating.

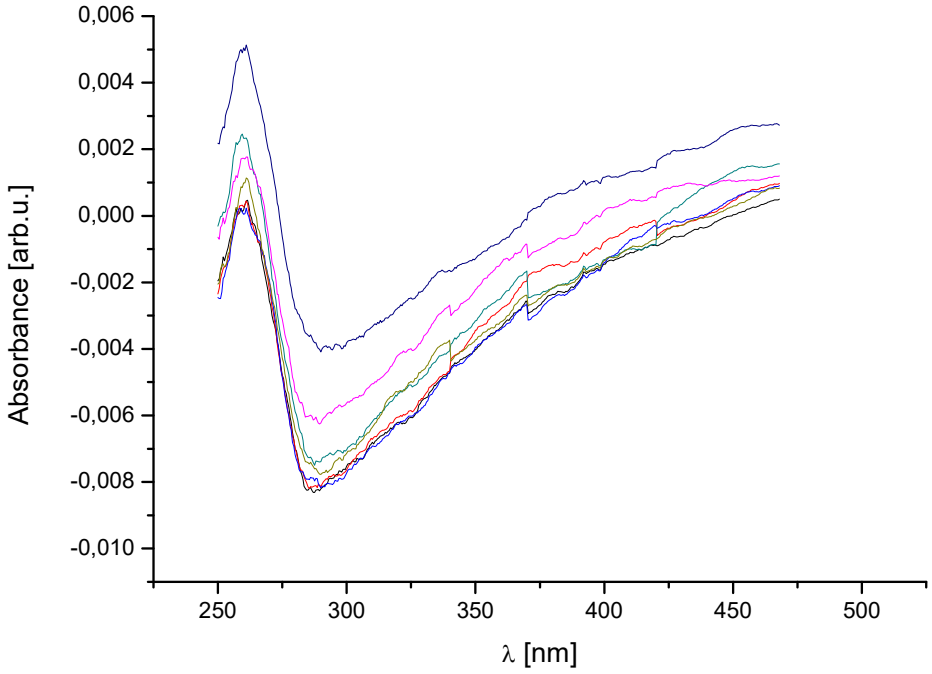

Figure 89: Absorption spectrum of sodium formate with the functionalized film (high concentration) after 0 min (black), 10 min (red), 25 min (blue), 50 min (cyan), 75 min (magenta), 100 min (dark yellow) and 125 min (navy blue) of heating.

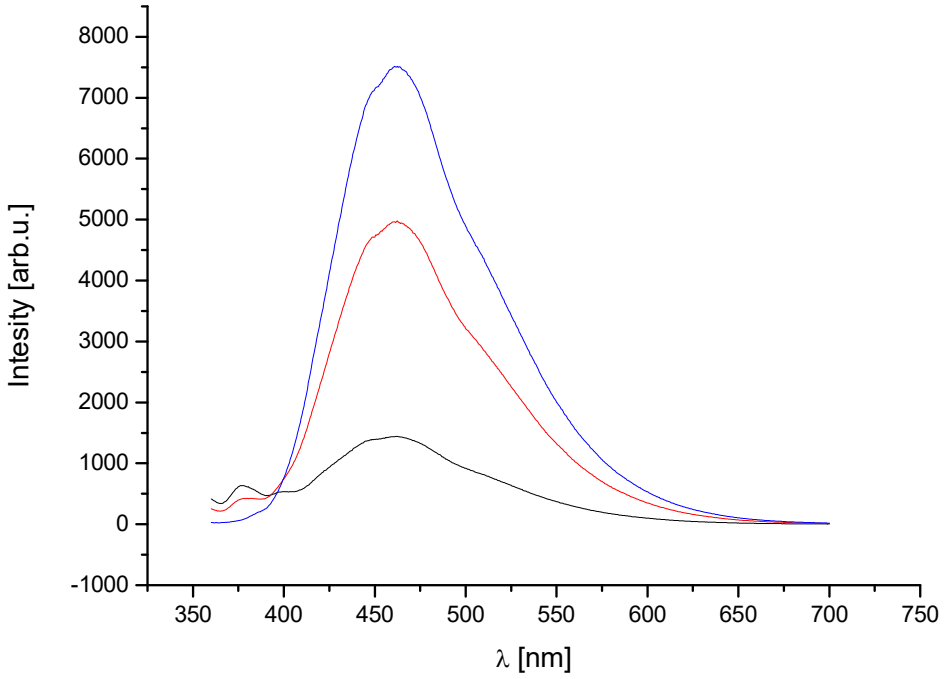

Figure 90: : Emission spectrum of the homogenous catalysis after 0 min (black), 10 min (red), 25 min (blue), 50 min (cyan), 75 min (magenta), 100 min (dark yellow) and 125 min (navy blue) of heating.

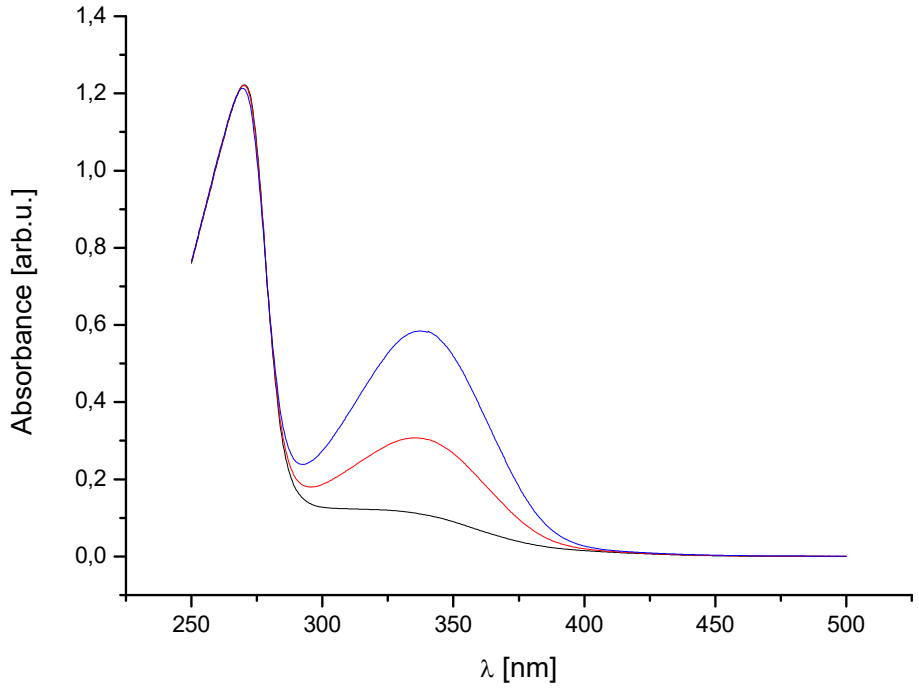

Figure 91: Emission spectrum of the homogenous catalysis after 0 min (black), 10 min (red), 25 min (blue), 50 min (cyan), 75 min (magenta), 100 min (dark yellow) and 125 min (navy blue) of heating.

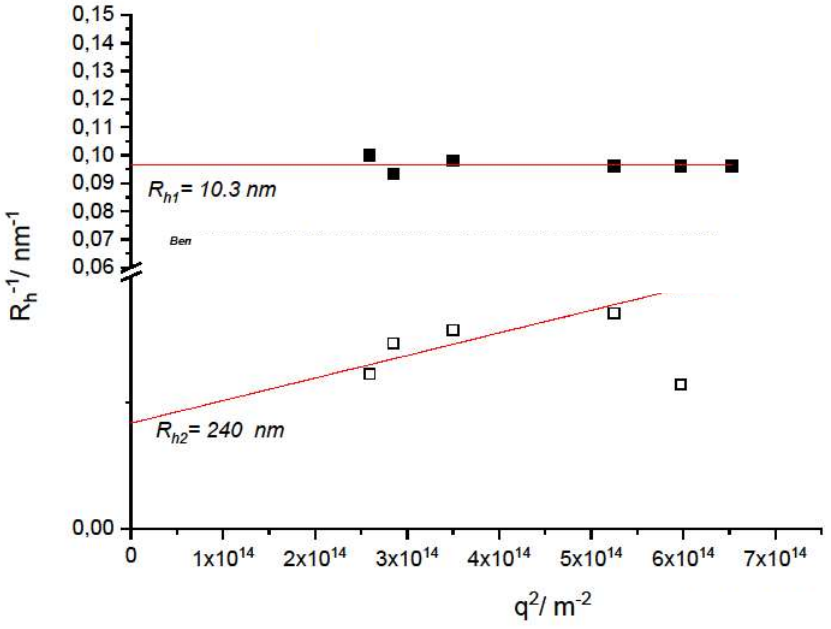

Figure 92: Hydrodynamic radius of the pure nanorods from DLS measurements.

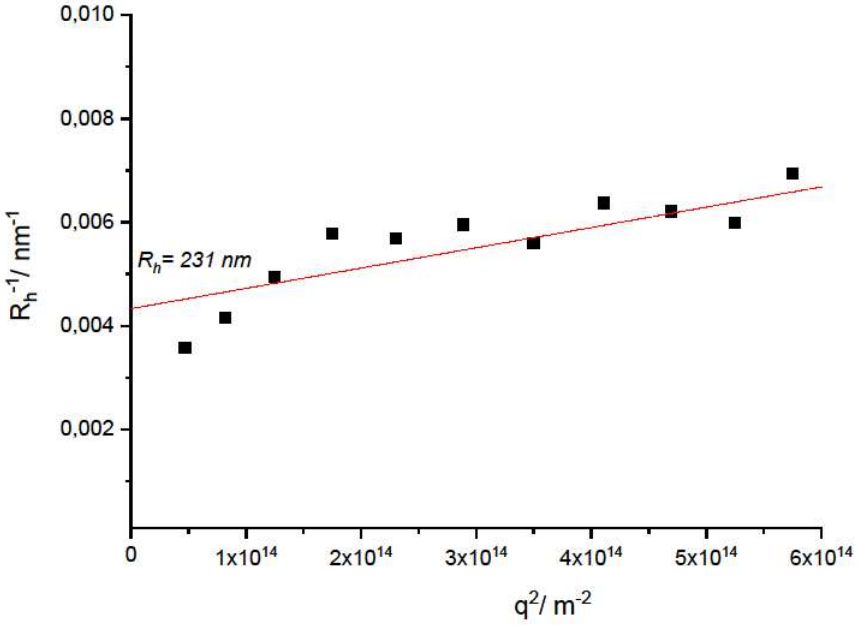

Figure 93: Hydrodynamic radius of the coated nanorods from DLS measurements.

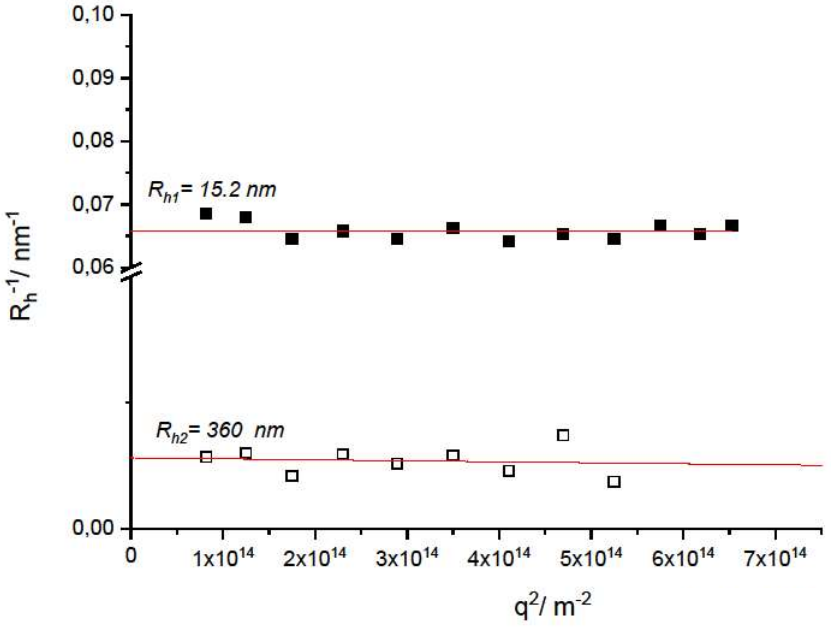

Figure 94: Hydrodynamic radius of the coated nanorods functionalized with PEG from DLS measurements.

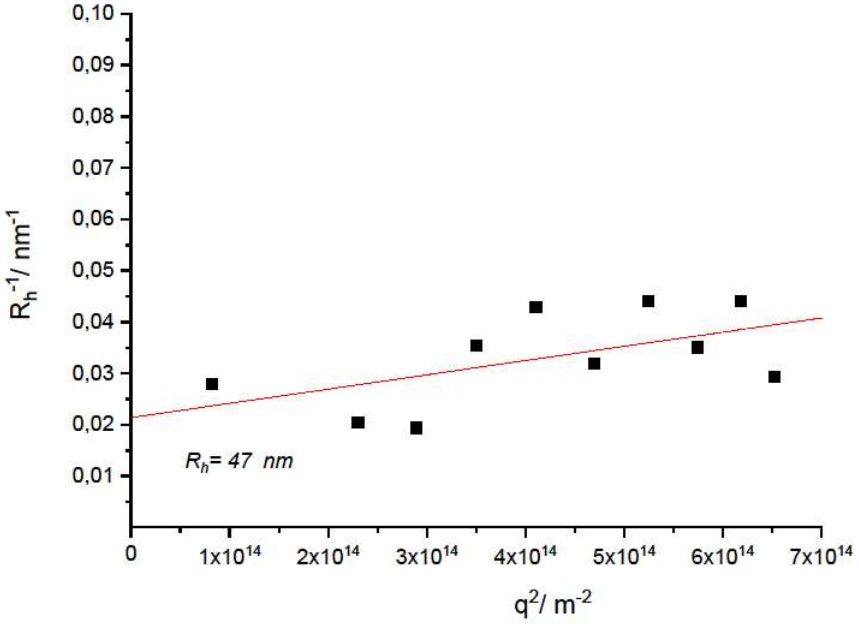

Figure 95: Hydrodynamic radius of the coated nanorods functionalized with PEG and catalyst from DLS measurements.

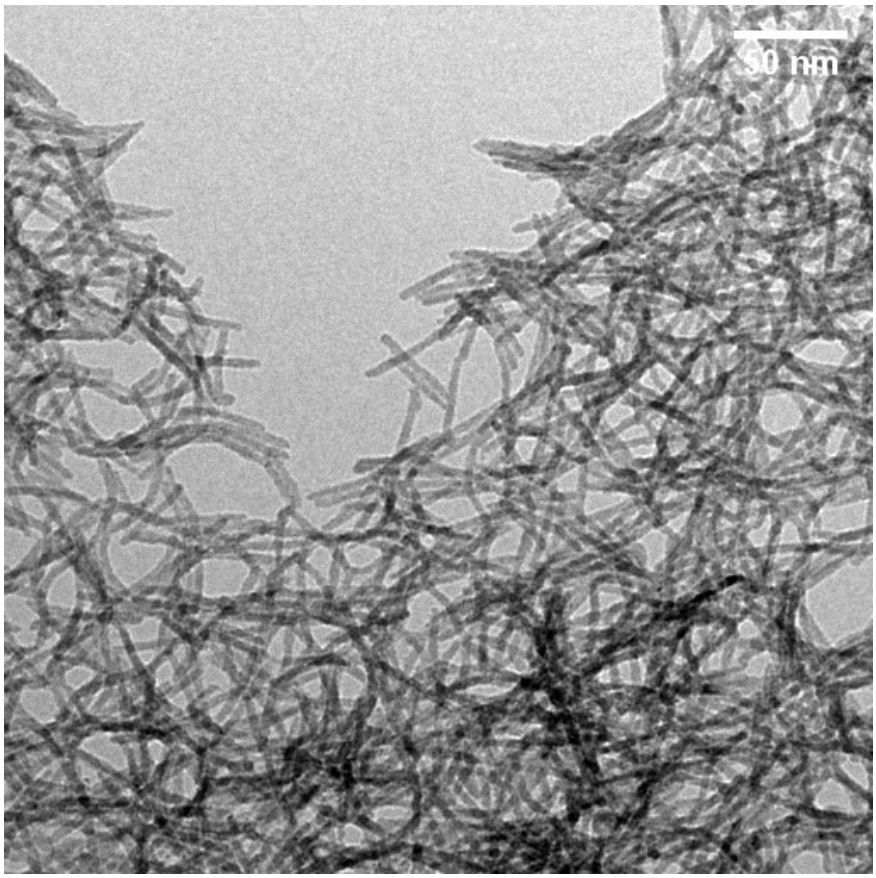

Figure 96: TEM picture of the PDA coated nanorods functionalized with PEG.

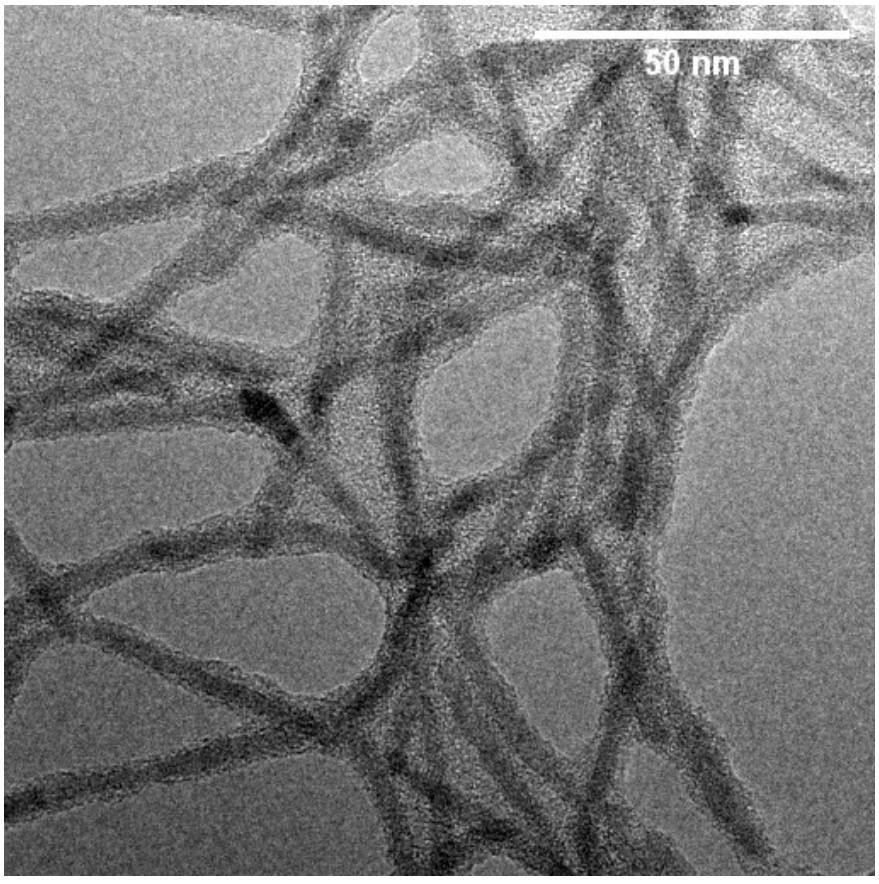

Figure 97: TEM image of the PDA coated nanorods functionalized with PEG and the catalyst.

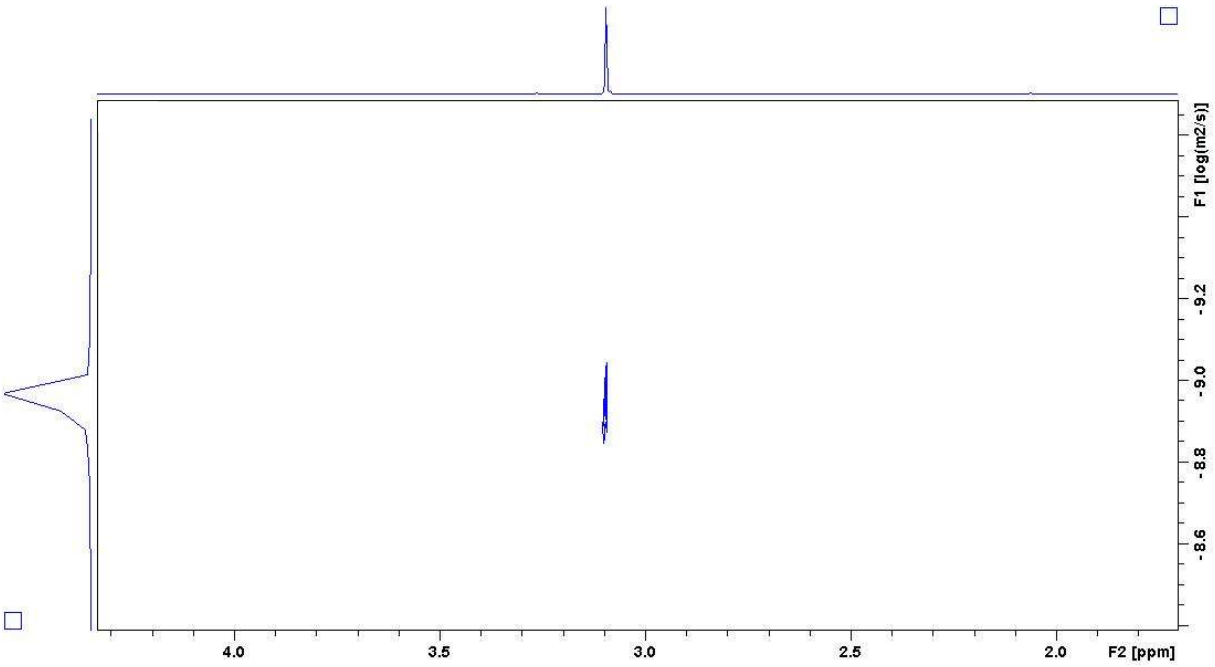

Figure 98: Dosy spetrum of the pure nanorods.

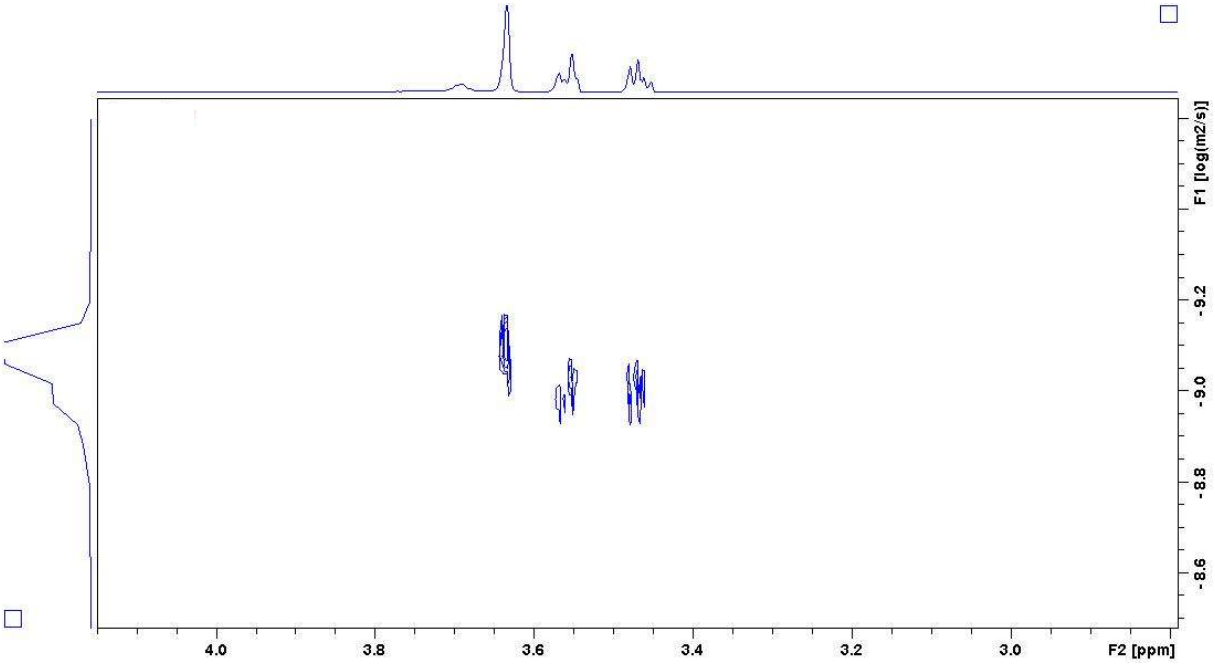

Figure 99:Dosy spectrum of the PDA coated nanorods.

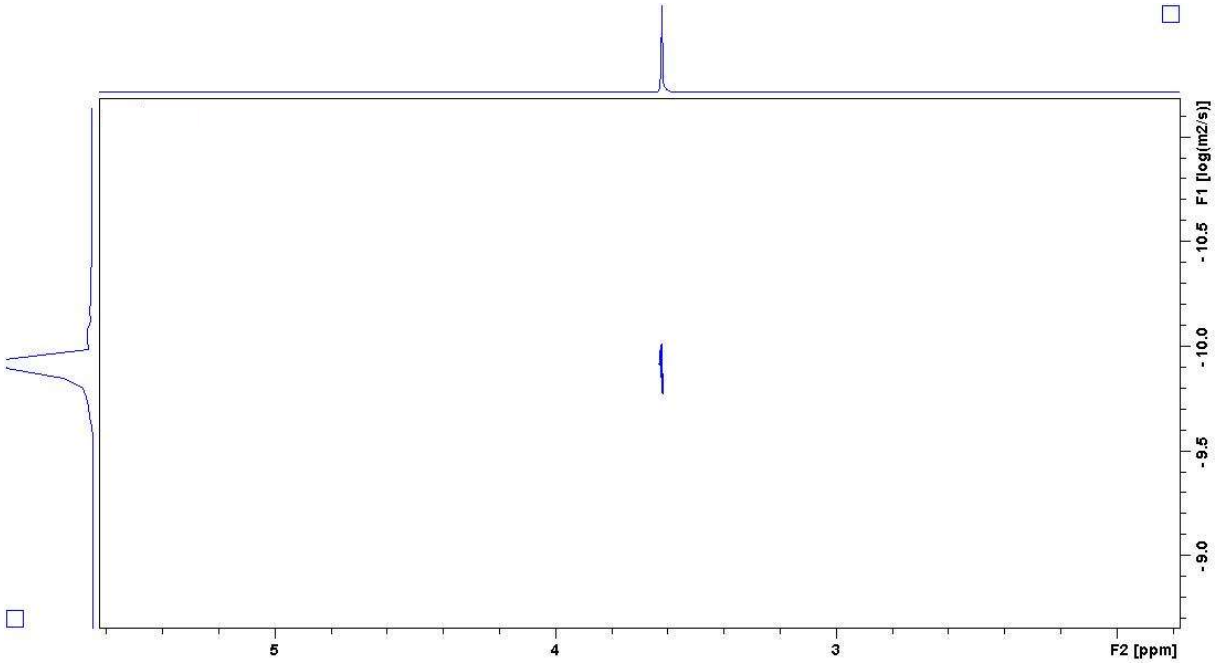

Figure 100: Dosy spectrum of the PDA coated nanorods functionalized with PEG.

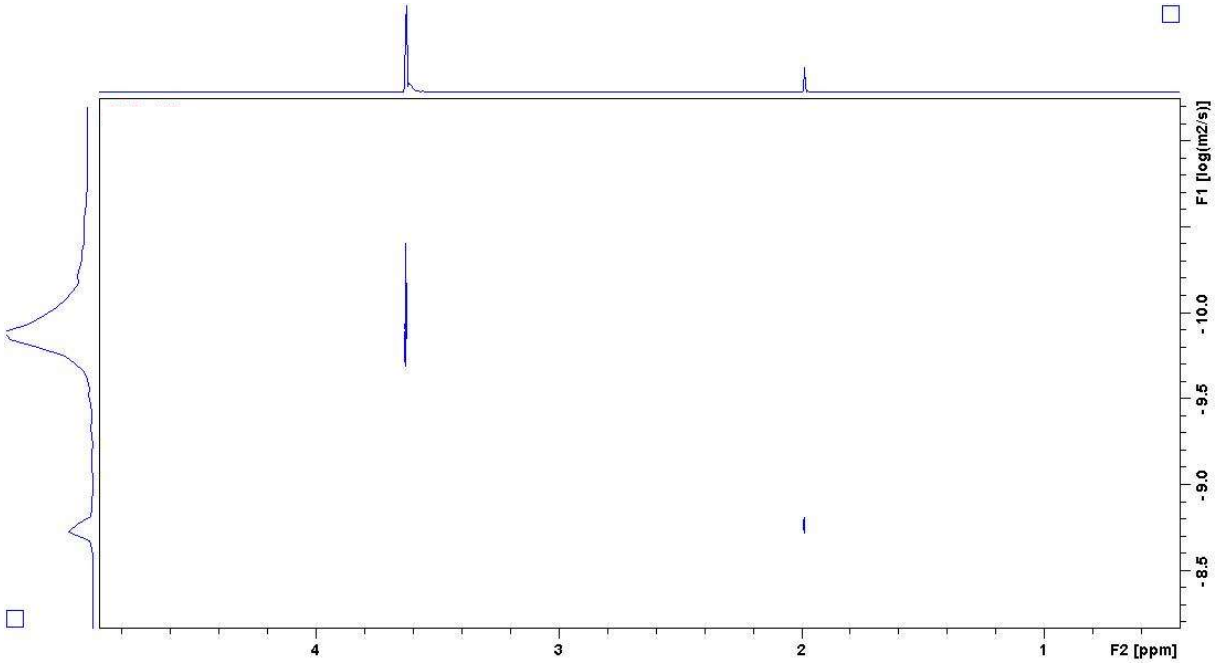

Figure 101: Dosy spectrum of the PDA coated nanorods functionalized with PEG and the catalyst.

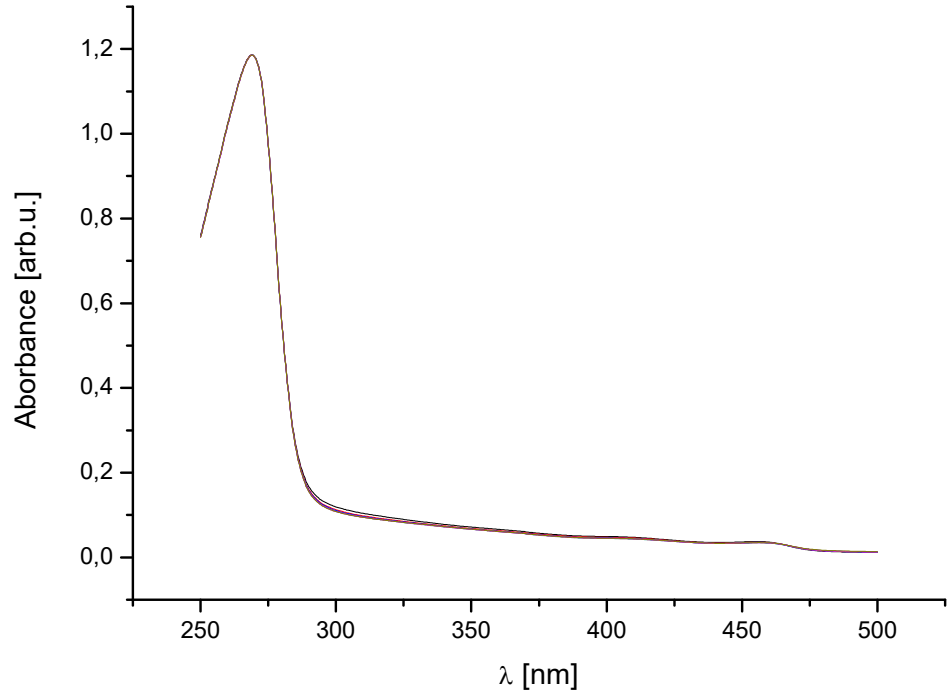

Figure 102: Absorption spectrum of the thermochemical reduction of NAD^+ with the functionalized nanorods after 0 min (black), 10 min (red), 20 min (blue), 30 min (cyan), 40 min (magenta) and 50 min (dark yellow) of heating at 40 °C.

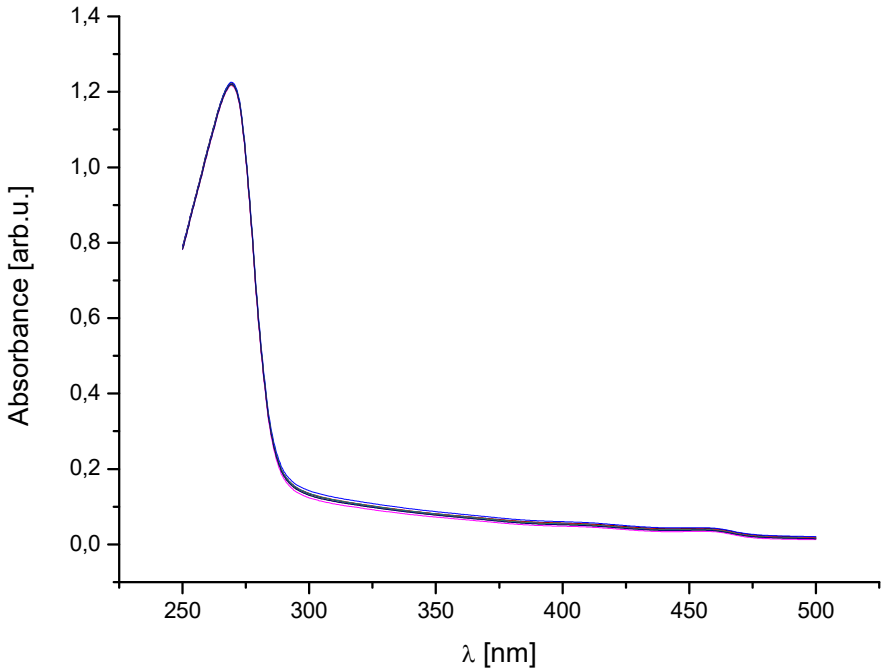

Figure 103: Absorption spectrum of the photocatalytic reduction of NAD^+ with the functionalized nanorods after 0 min (black), 10 min (red), 20 min (blue), 30 min (cyan), 40 min (magenta), 50 min (dark yellow) and 60 min (navy blue) of irradiation at wavelenght 465 nm.

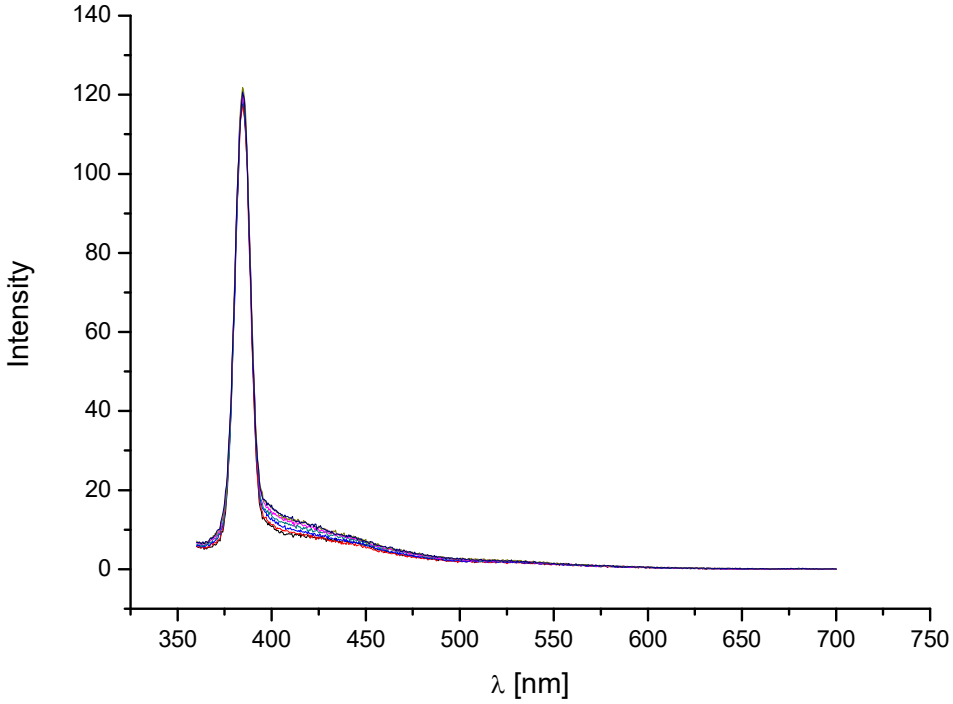

Figure 104: Emission spectrum of NAD^+ after 0 min (black), 10 min (red), 20 min (blue), 30 min (cyan), 40 min (magenta), 50 min (dark yellow) and 60 min (navy blue) of irradiation at wavelength 465 nm.

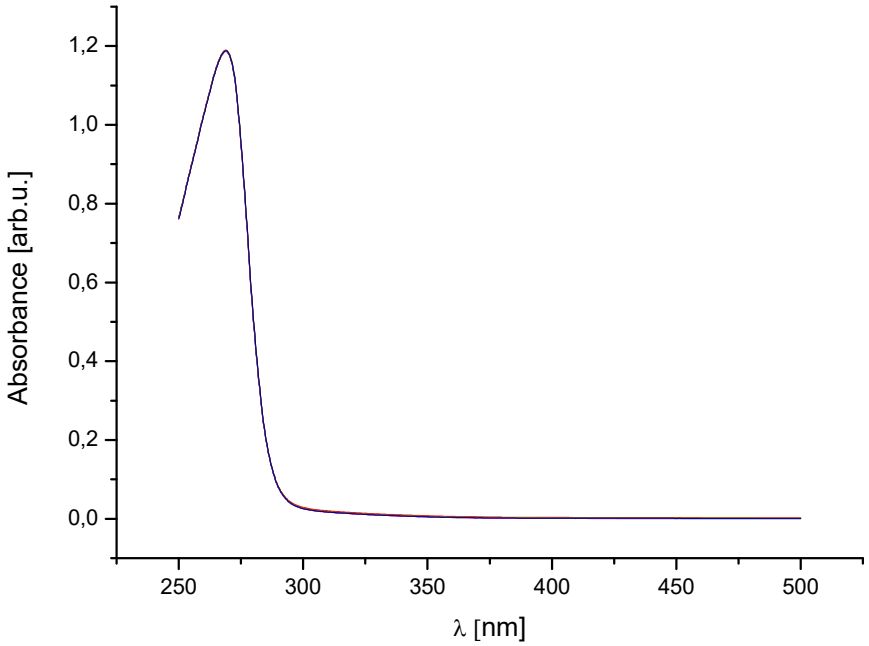

Figure 105: Absorption spectrum of NAD^+ after 0 min (black), 10 min (red), 20 min (blue), 30 min (cyan), 40 min (magenta), 50 min (dark yellow) and 60 min (navy blue) of irradiation at wavelength 465 nm.

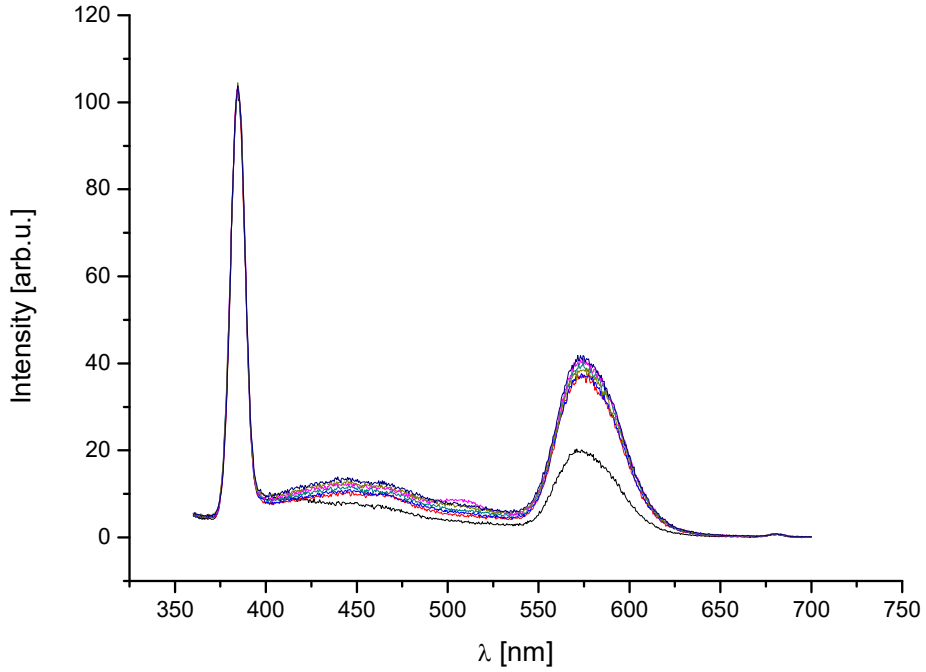

Figure 106: Emission spectrum of the functionalized nanorods used for the catalysis after 0 min (black), 10 min (red), 20 min (blue), 30 min (cyan), 40 min (magenta), 50 min (dark yellow) and 60 min (navy blue) of irradiation at wavelength 465 nm.

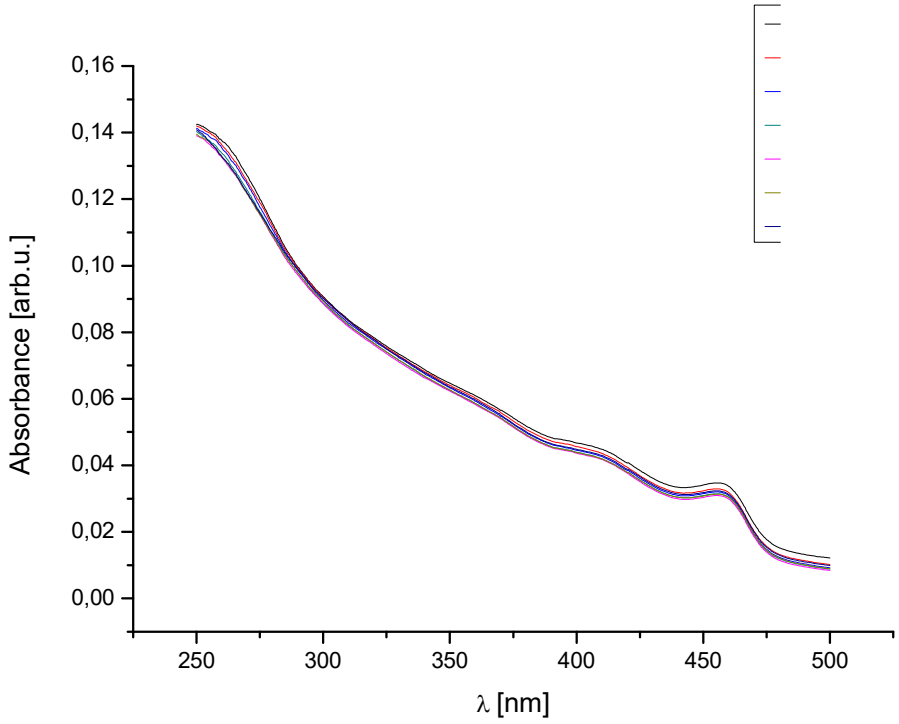

Figure 107: Absorption spectrum of the functionalized nanorods used for the catalysis after 0 min (black), 10 min (red), 20 min (blue), 30 min (cyan), 40 min (magenta), 50 min (dark yellow) and 60 min (navy blue) of irradiation at wavelength 465 nm.

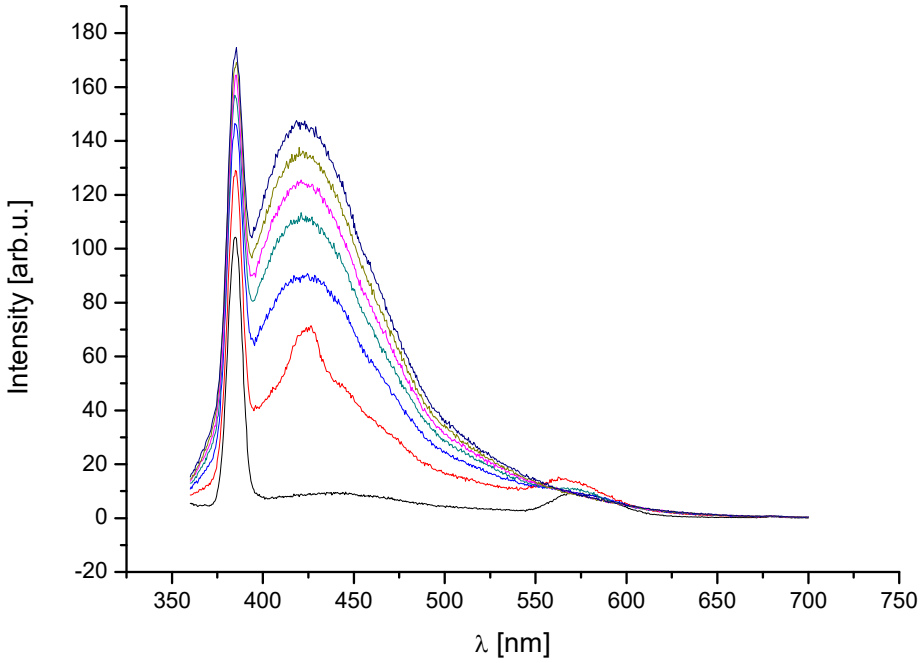

Figure 108: Emission spectrum of the photocatalytic reduction of NAD^+ in the presence of oxygen after 0 min (black), 10 min (red), 20 min (blue), 30 min (cyan), 40 min (magenta), 50 min (dark yellow) and 60 min (navy blue) of irradiation at wavelength 465 nm.

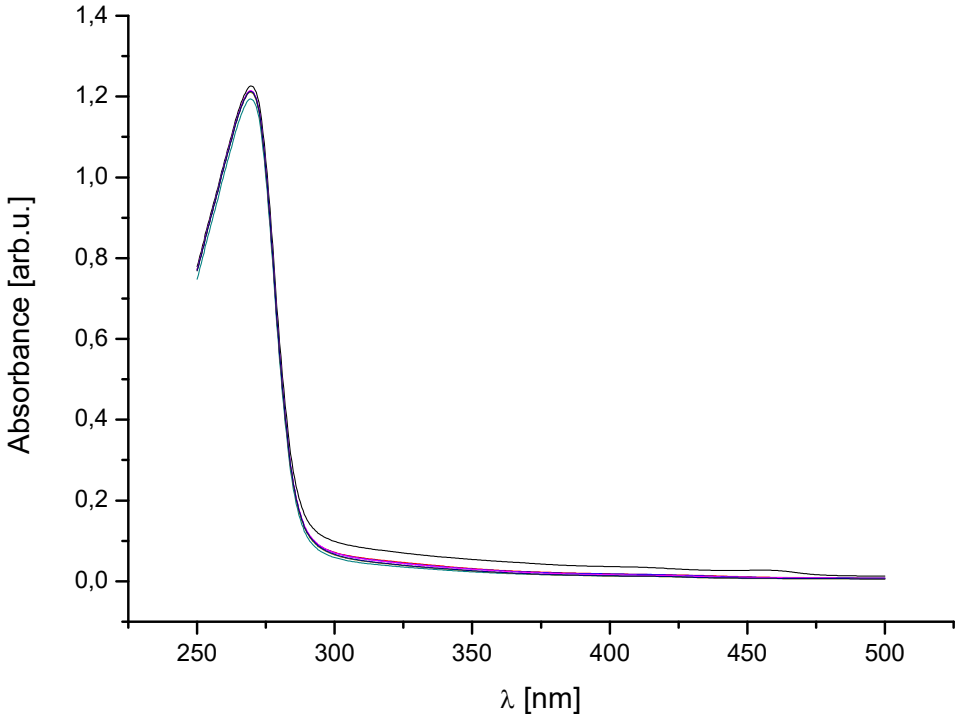

Figure 109: Absorption spectrum of the photocatalytic reduction of NAD^+ in the presence of oxygen after 0 min (black), 10 min (red), 20 min (blue), 30 min (cyan), 40 min (magenta), 50 min (dark yellow) and 60 min (navy blue) of irradiation at wavelength 465 nm.

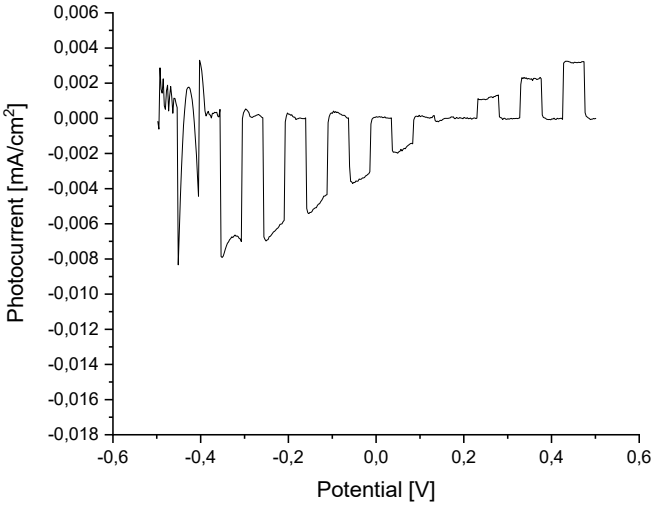

Figure 110: Photocurrent of the 5 cycle film at pH 2.6 with pulsed light.

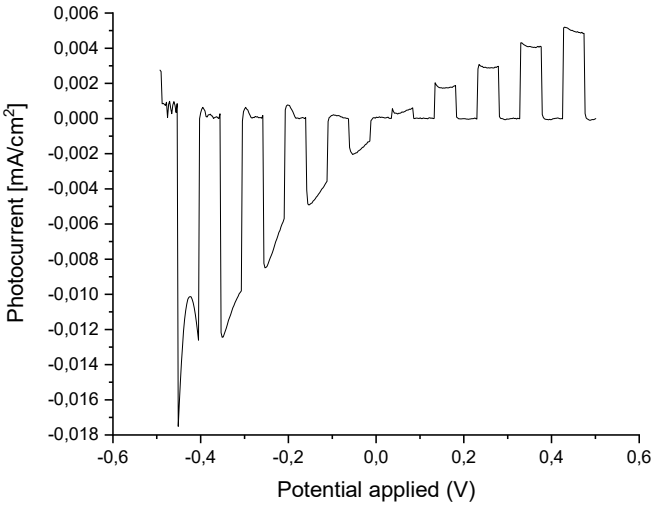

Figure 111: Photocurrent of the 5 cycle film at pH 5.46 with pulsed light.

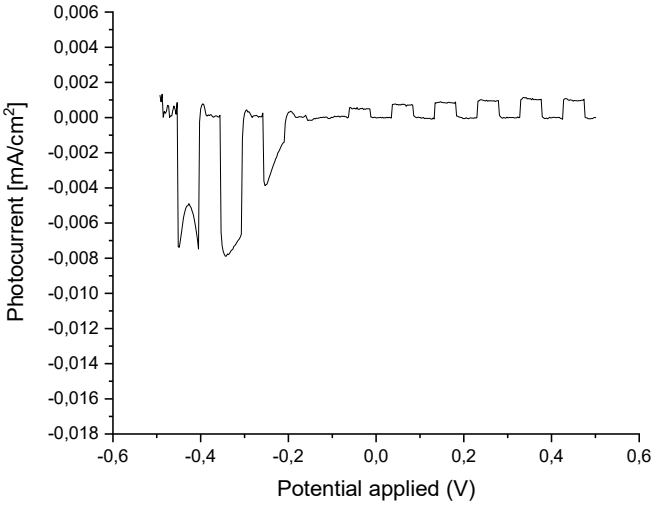

Figure 112: Photocurrent of the 5 cycle film at pH 7 with pulsed light.

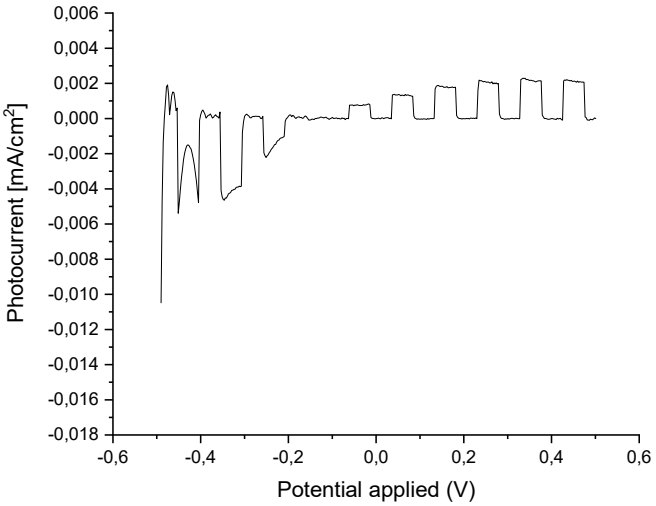

Figure 113: Photocurrent of the 5 cycle film at pH 7.98 with pulsed light.

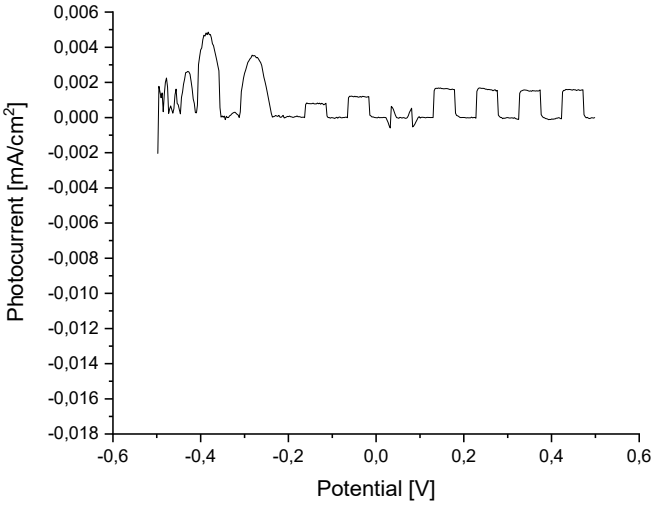

Figure 114: Photocurrent of the 5 cycle film at pH 10 with pulsed light.

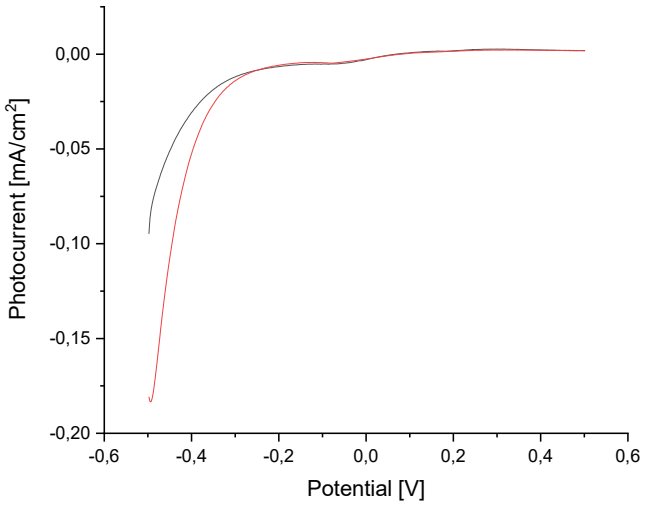

Figure 115: Photocurrent of ITO without light (black) and light (red) at pH 2.6.

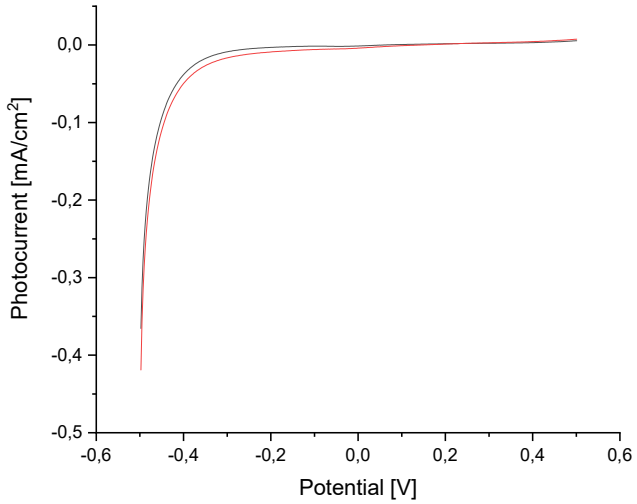

Figure 116: Photocurrent of the 5 cycle film without light (black) and light (red) at pH 2.6.

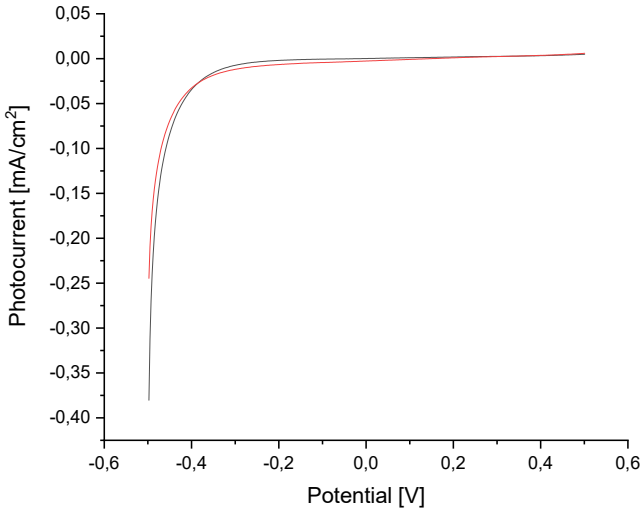

Figure 117: Photocurrent of the 15 cycle film without light (black) and light (red) at pH 2.6.

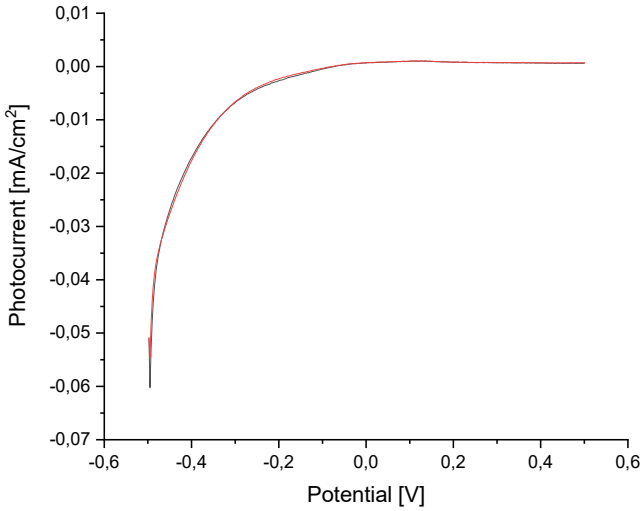

Figure 118: Photocurrent of ITO without light (black) and light (red) at pH 5.46.

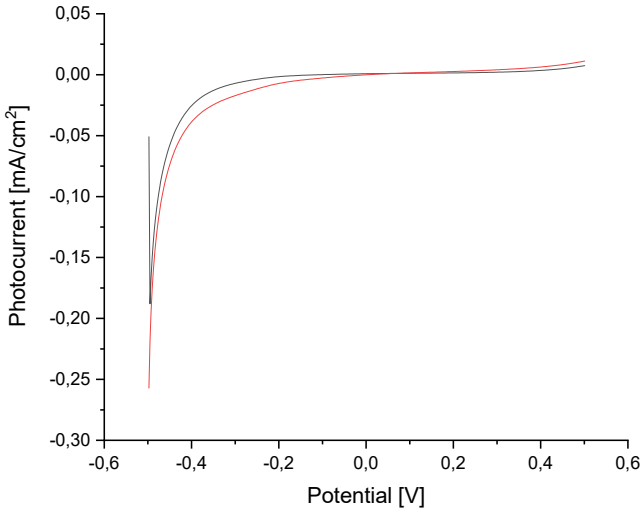

Figure 119: Photocurrent of the 5 cycle film without light (black) and light (red) at pH 5.46.

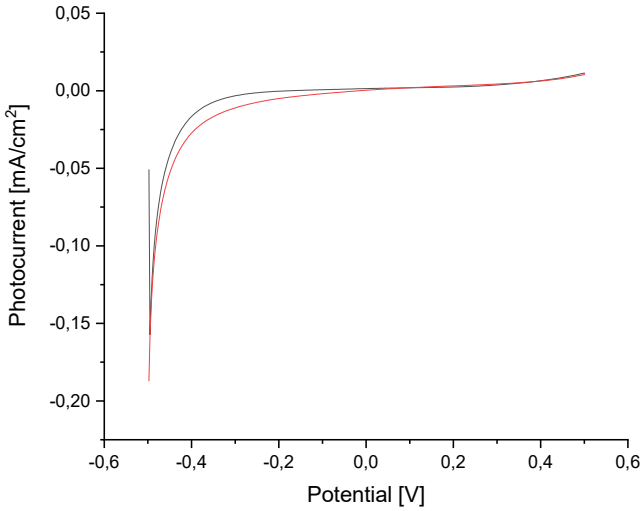

Figure 120: Photocurrent of the 5 cycle film without light (black) and light (red) at pH 5.46.

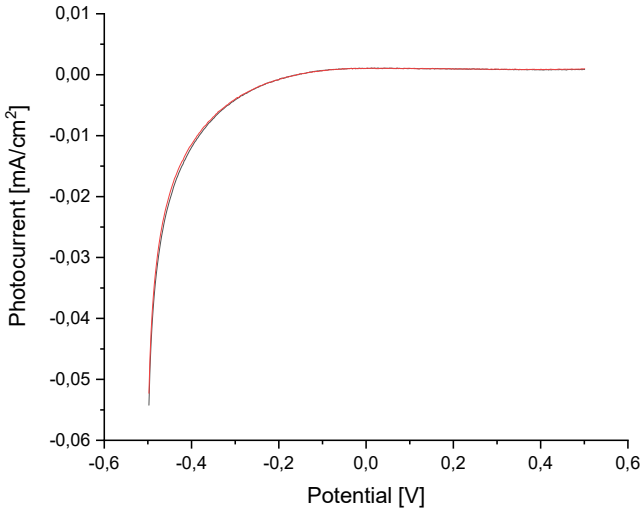

Figure 121: Photocurrent of ITO without light (black) and light (red) at pH 7.

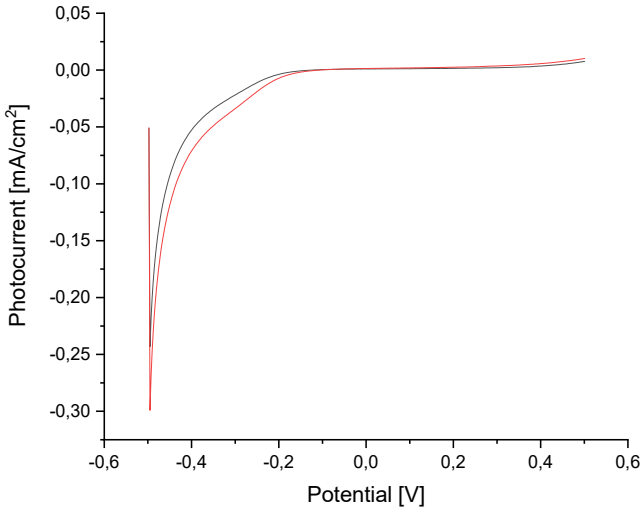

Figure 122: Photocurrent of the 5 cycle film without light (black) and light (red) at pH 7.

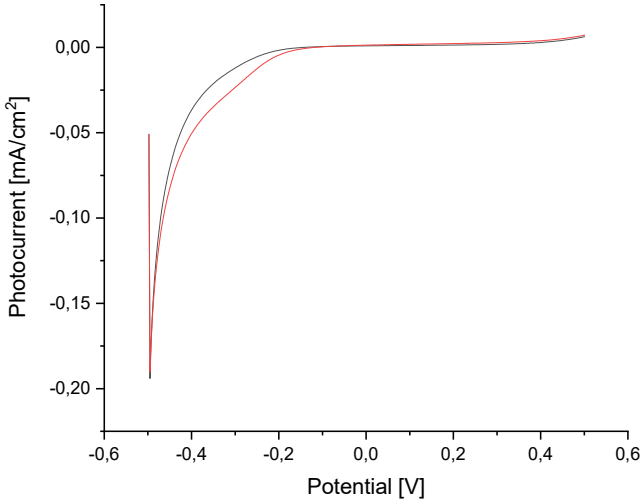

Figure 123: Photocurrent of the 15 cycle film without light (black) and light (red) at pH 7.

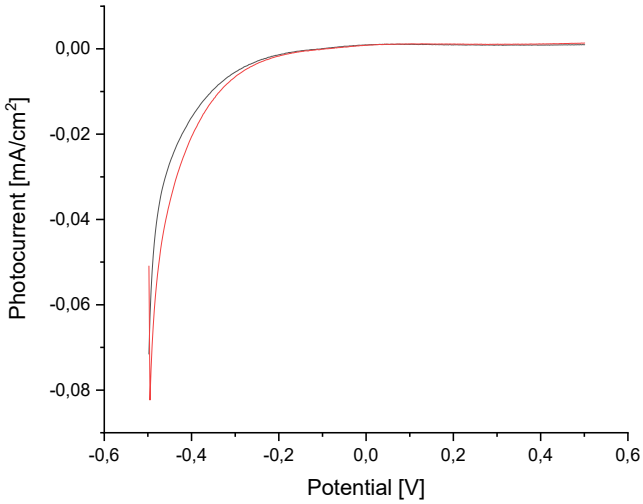

Figure 124: Photocurrent of ITO without light (black) and light (red) at pH 7.98.

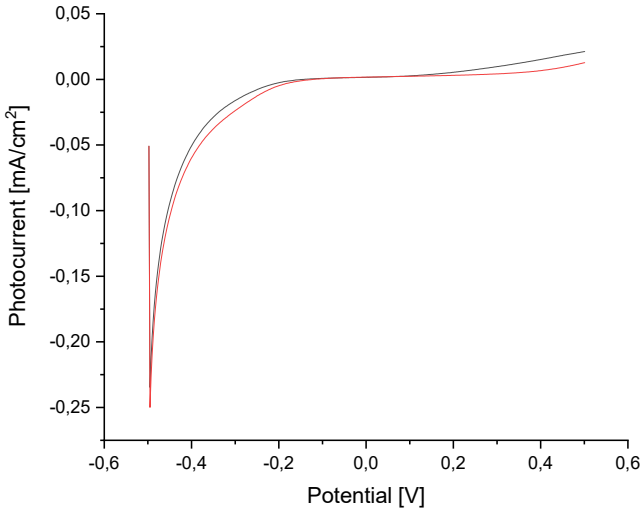

Figure 125: Photocurrent of the 5 cycle film without light (black) and light (red) at pH 7.98.

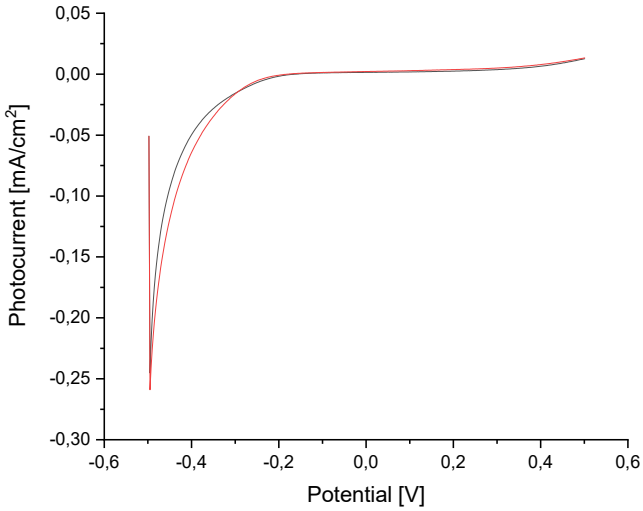

Figure 126: Photocurrent of the 15 cycle film without light (black) and light (red) at pH 7.98.

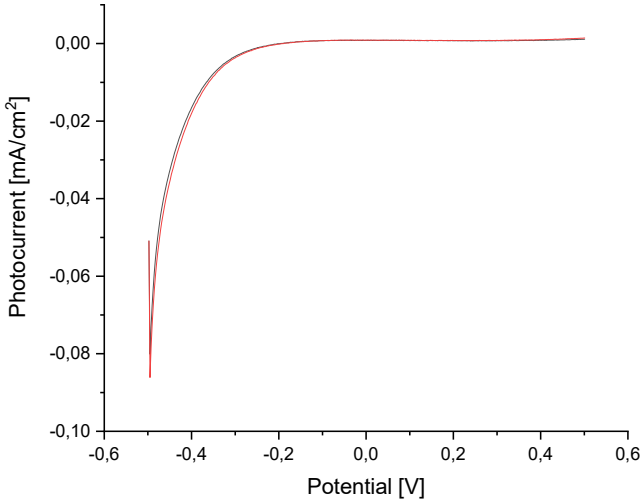

Figure 127: Photocurrent of ITO without light (black) and light (red) at pH 10.

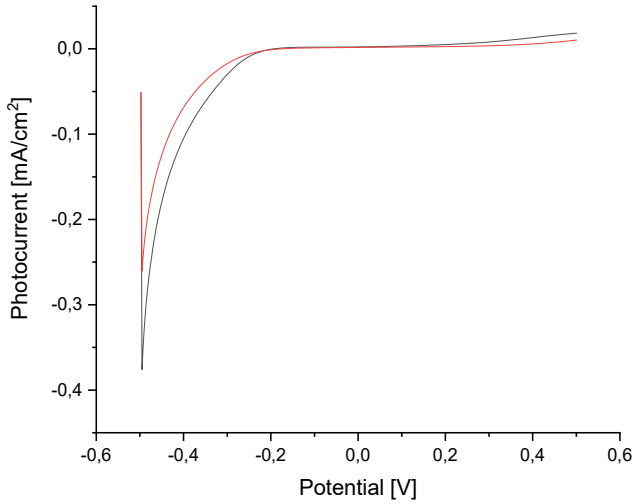

Figure 128: Photocurrent of the 5 cycle film without light (black) and light (red) at pH 10.

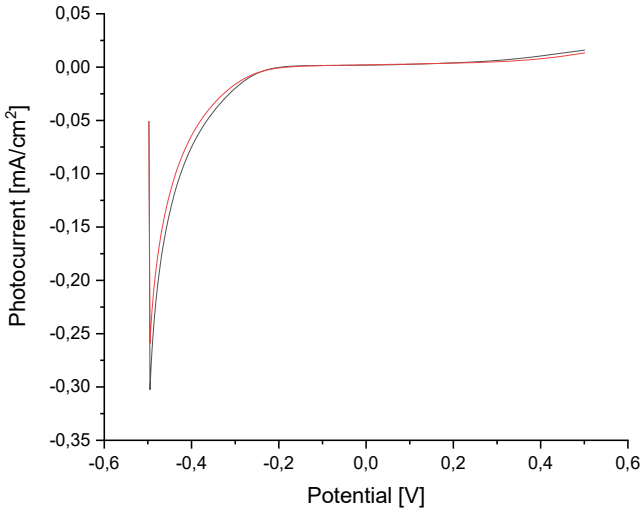

Figure 129: Photocurrent of the 15 cycle film without light (black) and light (red) at pH 10.

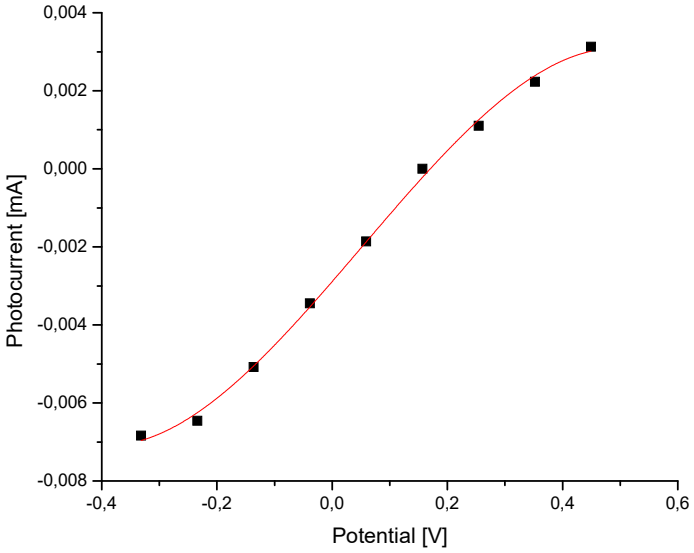

Figure 130: 3. polynomial regression of the average illuminated parts of the pulsed measurement of the 5 cycle film at pH 2.6.

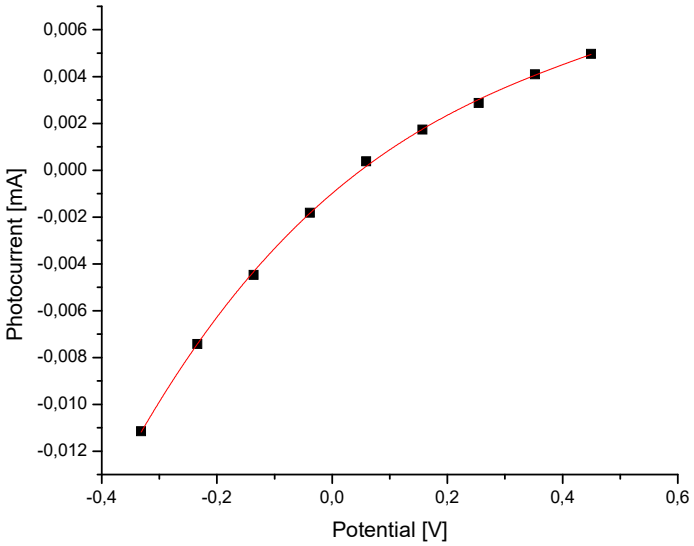

Figure 131: 3. polynomial regression of the average illuminated parts of the pulsed measurement of the 5 cycle film at pH 5.46.

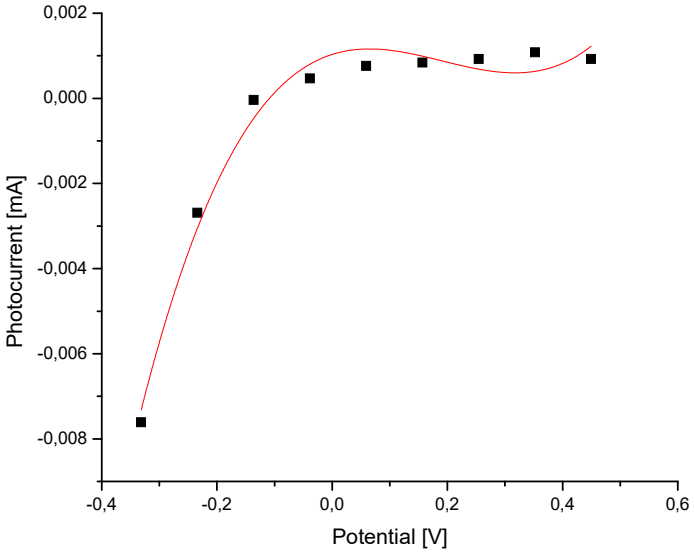

Figure 132: 3. polynomial regression of the average illuminated parts of the pulsed measurement of the 5 cycle film at pH 7.

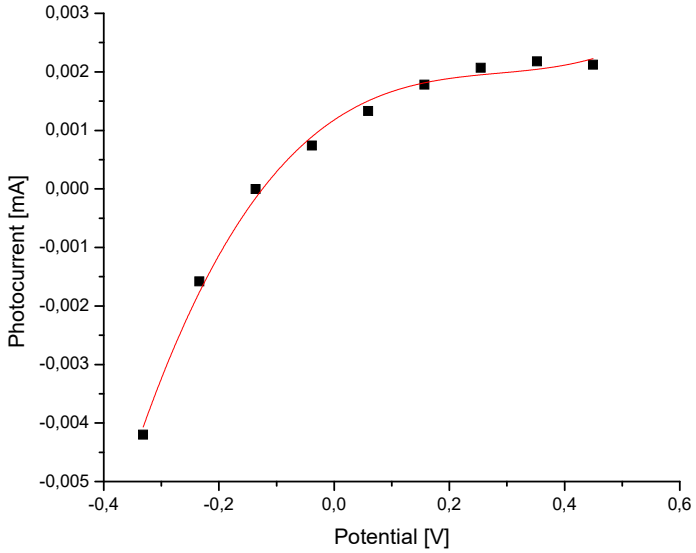

Figure 133: 3. polynomial regression of the average illuminated parts of the pulsed measurement of the 5 cycle film at pH 7.98.

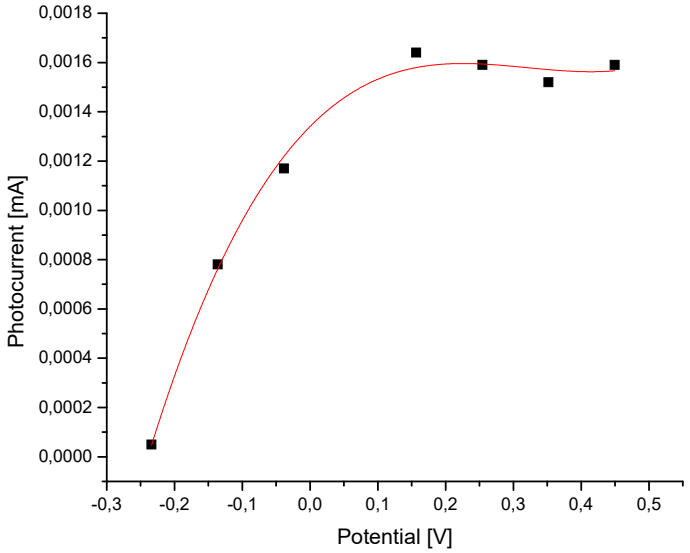

Figure 134: 3. polynomial regression of the average illuminated parts of the pulsed measurement of the 5 cycle film at pH 10.

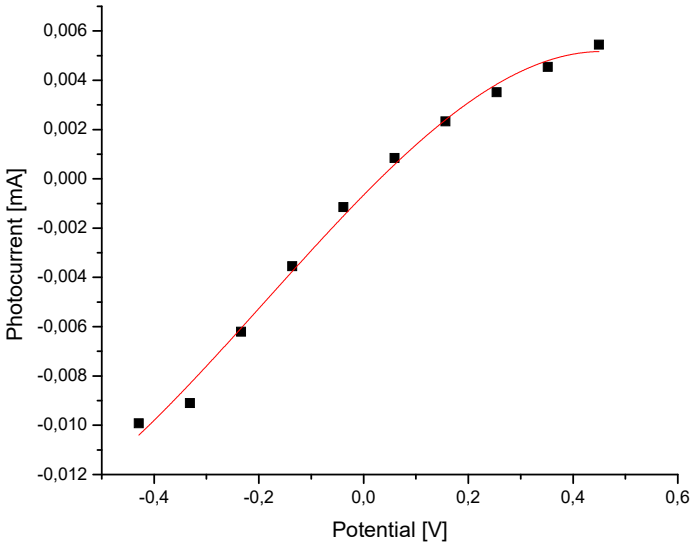

Figure 135: 3. polynomial regression of the average illuminated parts of the pulsed measurement of the 15 cycle film at pH 5.46.

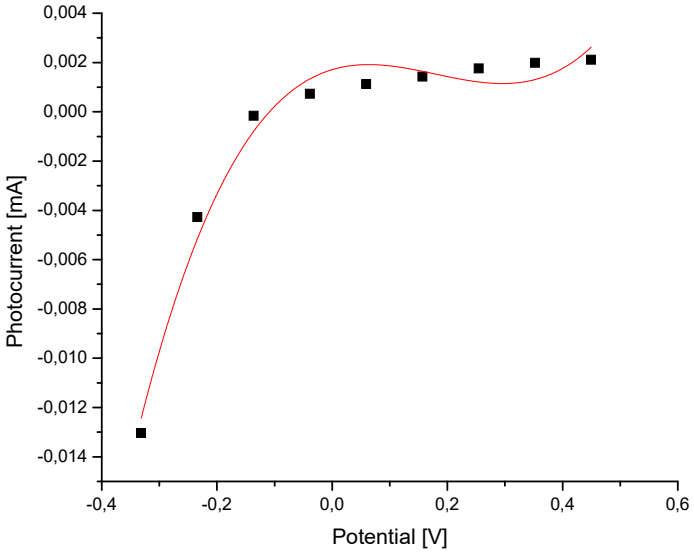

Figure 136: 3. polynomial regression of the average illuminated parts of the pulsed measurement of the 15 cycle film at pH 7.

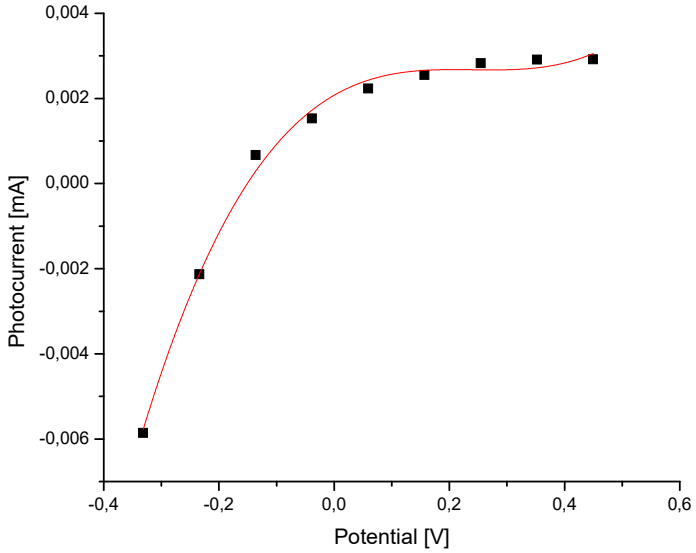

Figure 137: 3. polynomial regression of the average illuminated parts of the pulsed measurement of the 15 cycle film at pH 7.98.

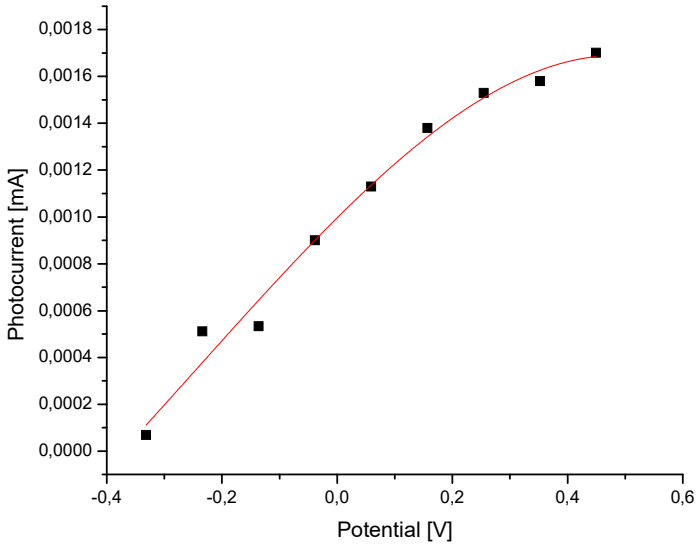

Figure 138: 3. polynomial regression of the average illuminated parts of the pulsed measurement of the 15 cycle film at pH 10.

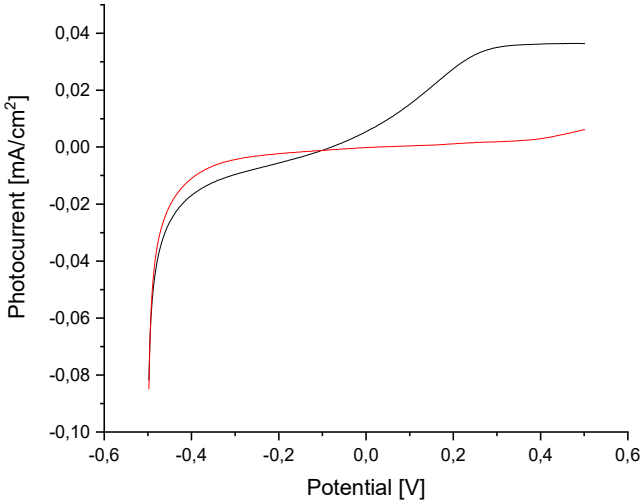

Figure 139: Dark (red) and continuous light (black) spectra of the coated nanorods at pH 2.6.

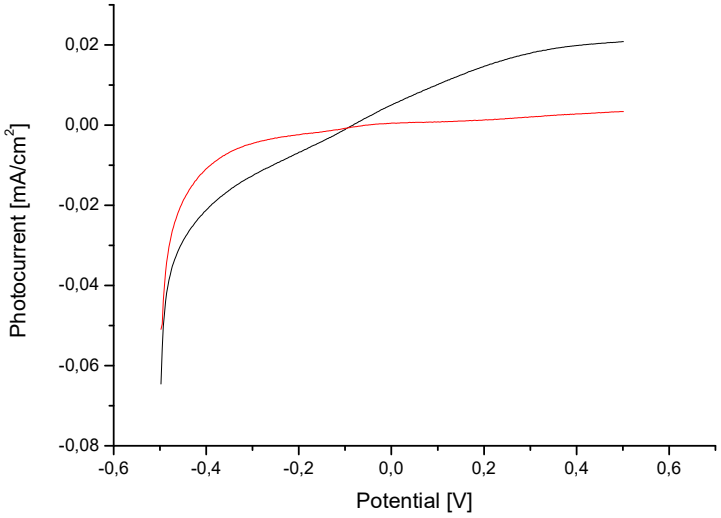

Figure 140: Dark (red) and continuous light (black) spectra of the coated nanorods at pH 5.46.

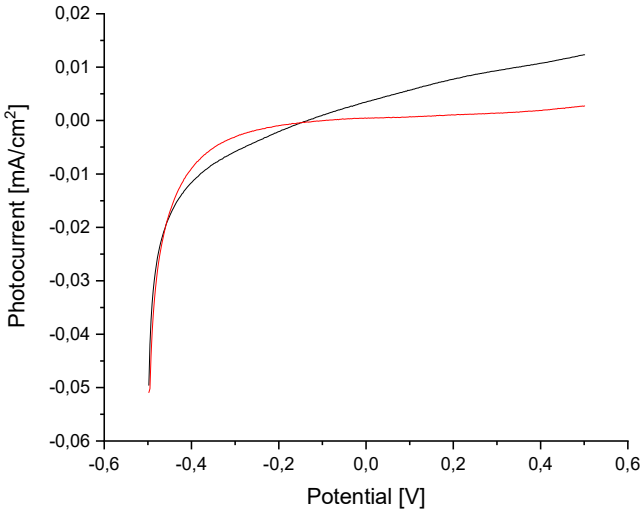

Figure 141: Dark (red) and continuous light (black) spectra of the coated nanorods at pH 7.

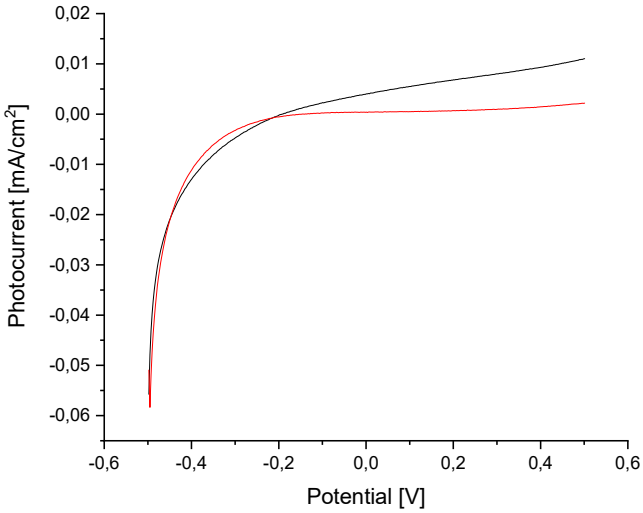

Figure 142: Dark (red) and continuous light (black) spectra of the coated nanorods at pH 7.98.

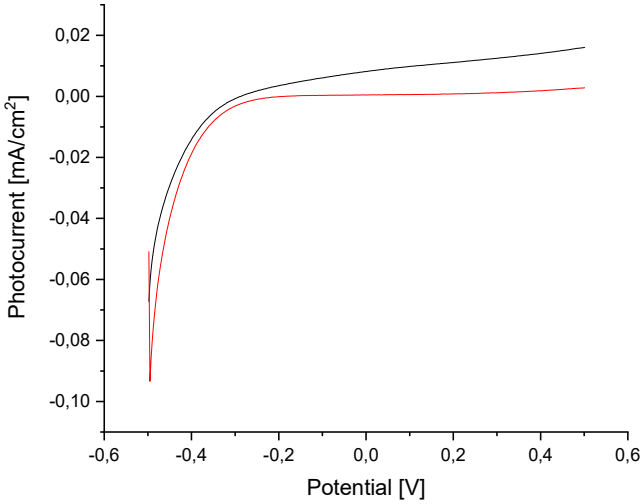

Figure 143: Dark (red) and continuous light (black) spectra of the coated nanorods at pH 10.

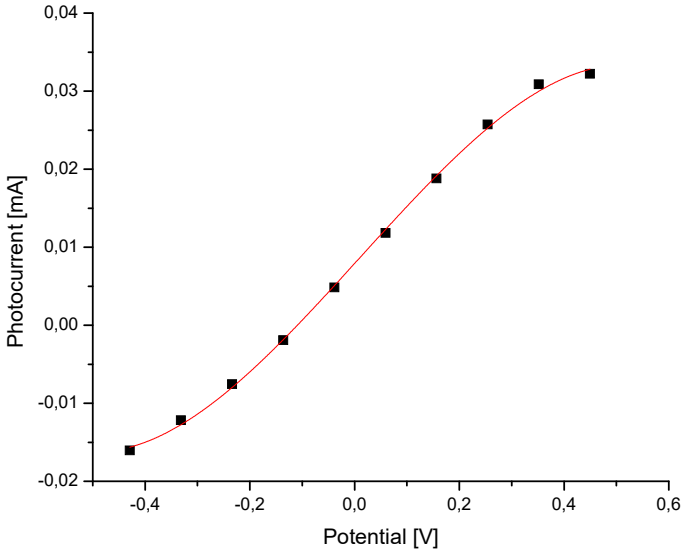

Figure 144: 3. polynomial regression of the average illuminated parts of the pulsed measurement of the coated nanorods at pH 5.46.

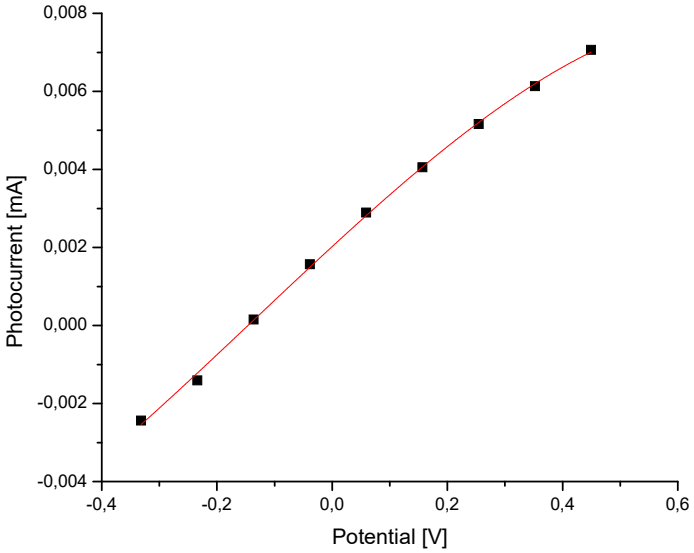

Figure 145: 3. polynomial regression of the average illuminated parts of the pulsed measurement of the coated nanorods at pH 7.

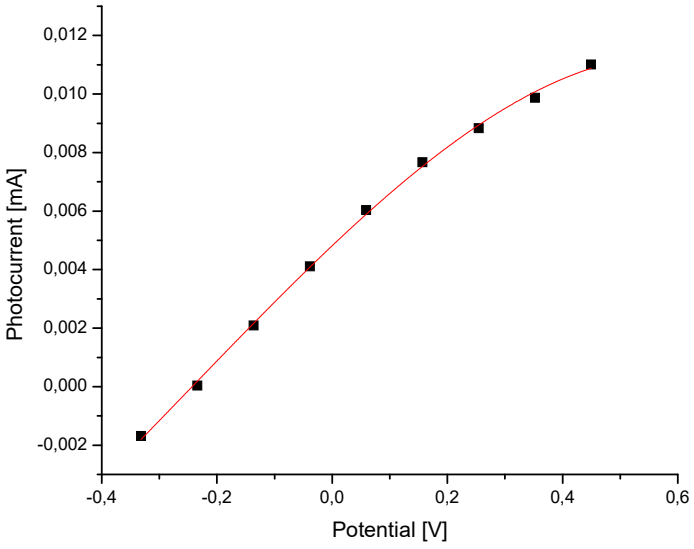

Figure 146: 3. polynomial regression of the average illuminated parts of the pulsed measurement of the coated nanorods at pH 7.98.

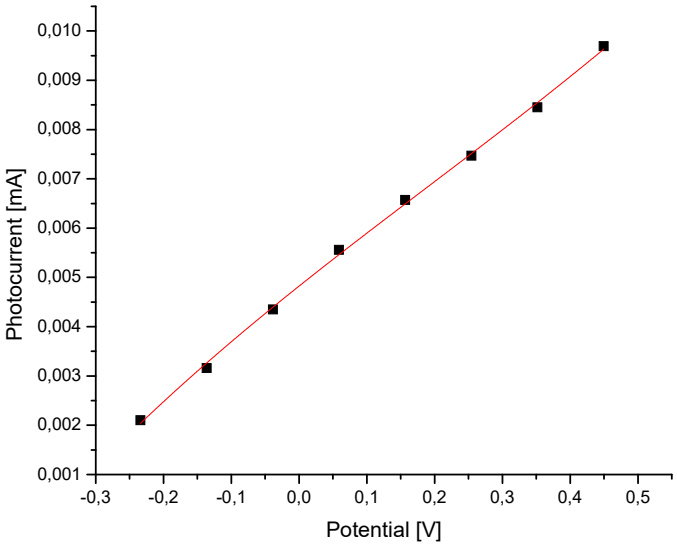

Figure 147: 3. polynomial regression of the average illuminated parts of the pulsed measurement of the coated nanorods at pH 10.